

**SURFACE TEXTURED PALM KERNEL ACTIVATED CARBON REINFORCED  
POLYMERIC COMPOSITE AS A POTENTIAL SELF-LUBRICATING BEARING**

**CHONG WEI SHENG**



**Faculty of Mechanical Engineering**

**UNIVERSITI TEKNIKAL MALAYSIA MELAKA**

**2018**

## DECLARATION

I declare that this thesis entitled “Surface Textured Palm Kernel Activated Carbon Reinforced Polymeric Composite as A Potential Self-lubricating Bearing” is the result of my own research except as cited in the references.



Signature : .....

Name : .....

Date : .....  
اونيورسيتي تيكنيكل مليسيا ملاك

UNIVERSITI TEKNIKAL MALAYSIA MELAKA

## APPROVAL

I hereby declare that I have read this project report and in my opinion this report is sufficient in terms of scope and quality for the award of the degree of the Bachelor of Mechanical Engineering.



Signature : .....

Name : .....

Date : .....  
اونيورسيتي تيكنيكل مليسيا ملاك

UNIVERSITI TEKNIKAL MALAYSIA MELAKA

## DEDICATION

To my loving father and mother



## ABSTRACT

A bearing is a device that controls all the relative motion to the desired motion while reduces operating friction. Self-lubricating bearings are plain bearings working without the need of any external lubrication. self-lubricating bearings are classified into two types. The first type is dry bearings which have solid lubricant such as graphite or polytetrafluoroethylene. The other type is bearing which has its own liquid lubricant reservoir such as porous metal structure which acts as a well for oil and dimples on surface which holds greases. Effect of speed and load on the tribological performance of surface textured palm kernel activated carbon reinforced polymeric composite (PKAC-E) need to be investigated. The performance of surface textured palm kernel activated carbon reinforced polymeric composite are compared to conventional bearing material. PKAC powder weighted at 60% are mixed with epoxy weighted at 40%. is then fabricated into disk specimen by hot press moulding. The PKAC epoxy composite disc specimen is patterned using a CO<sub>2</sub> laser surface patterning machine with pore diameter of 1000 μm with depth of 500 μm, contact ratio value of 0.21 and area density of 19%. The sliding experiments was performed with a ball-on-disc equipment in dry condition in room temperature. A microscope was then used to observe and analyse the morphology of wear tracks for both the ball bearing and discs. The wear track widths of the discs are also measured with the microscope at five different points and the average is calculated. Coefficient of friction of PKAC-E disk for textured and nontextured rises with sliding speed and applied load. Non-textured surface demonstrated a lower coefficient of friction at low speed and low load and at high speed and high load. Textured disc has a wider wear track on disc than nontextured disc which increases the wear of the material. Textured disc produced lower coefficient of friction at high speed and low load. PKAC has demonstrated to be the superior bearing material compared to SKD-II disc which is a conventional bearing material by producing lower coefficient of friction when tested at similar parameters.

## ABSTRAK

Galas ialah peranti yang mengawal semua gerakan relatif kepada gerakan yang dikehendaki sambil mengurangkan geseran operasi. Galas pelincir diri adalah galas biasa yang berfungsi tanpa memerlukan pelinciran luar. Galas pelincir diri dikelaskan kepada dua jenis. Jenis pertama adalah galas kering yang mempunyai pelincir pepejal. Jenis lain adalah bearing yang mempunyai takungan pelincir cecairnya sendiri seperti struktur logam berliang. Kesan kelajuan dan beban ke atas prestasi tribologi komposit polimer bertetulang kernel sawit diaktifkan karbon (PKAC-E) perlu disiasat. Prestaskomposit polimer bertetulang kernel sawit diaktifkan karbon berbanding bahan galas konvensional. Serbuk PKAC yang berwajaran 60% dicampur dengan epoxy wajaran pada 40%. Kemudian dituang ke dalam acuan dan menjalani pengacuan penekanan panas. Spesimen cakera epoxy komposit PKAC dibentuk menggunakan mesin penembusan permukaan laser CO<sub>2</sub> dengan diameter pori 1000 µm dengan kedalaman 500 µm, nilai nisbah sentuhan sebanyak 0.21 dan kepadatan kawasan sebanyak 19%. Eksperimen gelongsor dilakukan dengan peralatan bola-pada-cakera dalam keadaan kering dalam suhu bilik. Mikroskop kemudian diguna untuk memerhatikan dan menganalisis morfologi trek haus untuk bebola galas dan cakera. Lebar trek haus cakera juga diukur dengan mikroskop pada lima tempat yang berbeza dan purata dikira. Pekali geseran cakera PKAC-E untuk permukaan berstruktur dan rata meningkat dengan kelajuan gelongsor dan beban. Permukaan rata menunjukkan pekali geseran yang lebih rendah pada kelajuan rendah dan beban rendah serta pada kelajuan tinggi dan beban tinggi. Cakera permukaan berstruktur mempunyai kelebaran trek haus yang lebih luas pada cakera daripada cakera permukaan rata. Ini meningkatkan kadar haus cakera. Cakera permukaan berstruktur menghasilkan pekali geseran yang lebih rendah pada kelajuan tinggi dan beban rendah. PKAC adalah bahan galas yang lebih baik berbanding dengan cakera besi SKD-II yang merupakan bahan galas konvensional dengan menghasilkan pekali geseran yang lebih rendah apabila diuji pada parameter yang sama.

## ACKNOWLEDGEMENTS

First and foremost, I would like to take this opportunity to express my sincere acknowledgement to my supervisor Prof. Madya Dr Mohd. Fadzli Bin Abdollah from the Faculty of Mechanical Engineering Universiti Teknikal Malaysia Melaka (UTeM) for her essential supervision, support and encouragement towards the completion of this thesis.

I would also like to express my greatest gratitude to Mohmad Martini for her advice and suggestions throughout this entire project. Special thanks to my course mates for their advices and support.

Special thanks to all my peers, my mother, beloved father and siblings for their moral support in completing this degree. Lastly, thank you to everyone who had been to the crucial parts of realization of this project.

UNIVERSITI TEKNIKAL MALAYSIA MELAKA

## TABLE OF CONTENTS

	<b>PAGE</b>
<b>DECLARATION</b>	
<b>DEDICATION</b>	
<b>ABSTRACT</b>	<b>i</b>
<b>ABSTRAK</b>	<b>ii</b>
<b>ACKNOWLEDGEMENTS</b>	<b>iii</b>
<b>TABLE OF CONTENTS</b>	<b>iv</b>
<b>LIST OF TABLES</b>	<b>vii</b>
<b>LIST OF FIGURES</b>	<b>viii</b>
<b>LIST OF APPENDICES</b>	<b>xi</b>
<b>LIST OF ABBREVIATIONS</b>	<b>xii</b>
<b>LIST OF SYMBOLS</b>	<b>xiii</b>
<b>CHAPTER</b>	
<b>1. INTRODUCTION</b>	<b>1</b>
1.1 Background	1
1.2 Problem Statement	2
1.3 Objective	2
1.4 Scope of Project	3
<b>2. LITERATURE REVIEW</b>	<b>4</b>
2.1 Surface Texture	4
2.2 Fabrication of Surface Texture	4
2.2.1 Laser surface texturing	4
2.2.2 Micro-ball end milling	7
2.2.3 Micro-casting	10
2.2.4 Electrochemical machining	12
2.3 Application of Surface Texturization	17
2.3.1 Application of surface texturization in solar cells	17
2.3.2 Application of surface texturization in automotive component	18
2.3.3 Application of surface texturization in medical equipment	21

2.4	Self-lubricating Material Properties	25
2.5	Palm Kernel Activated Carbon (PKAC)	27
2.5.1	Tribological Properties of PKAC	27
2.5.2	Adsorption property of PKAC	28
<b>3.</b>	<b>MATERIALS AND METHODS/METHODOLOGY</b>	<b>29</b>
3.1	Sample Fabrication	30
3.2	Surface Roughness Measurements	30
3.3	Laser Surface Texturing	31
3.4	Sliding Tests	32
3.5	Hardness Measurements	32
3.6	Microscopic Observations and Measurements	33
<b>4.</b>	<b>RESULT AND ANALYSIS</b>	<b>34</b>
4.1	Physical-Mechanical properties	34
4.2	Effect of load on the coefficient of friction	35
4.3	Effect of sliding speed on PKAC-E disc	37
4.4	Wear track morphology of disc and ball bearing analysis	39
4.4.1	Wear track morphology of disc and ball bearing analysis for SKD-II disk	39
4.4.2	Wear track morphology of disc and ball bearing analysis for non-textured PKAC disk	40
4.4.3	Wear track morphology of disc and ball bearing analysis for textured PKAC disk	44
4.5	Effect of surface texturization on coefficient of friction for PKAC-E disc	49
4.6	Effect of surface texturization on wear of PKAC-E disc	57
4.7	Performance of SKD-II disc and PKAC-E disc as bearing material	59
<b>5.</b>	<b>CONCLUSION AND RECOMMENDATIONS</b>	<b>62</b>
5.1	Conclusion	62
5.2	Recommendation for future works	63

**REFERENCES**

**64**

**APPENDICES**

**70**



## LIST OF TABLES

<b>TABLE</b>	<b>TITLE</b>	<b>PAGE</b>
4.1	Mechanical properties of PKAC disc, ball bearing and SKD-II steel disc	34
4.2	Wear track hardness of different type of discs after sliding test under 5N at 200rpm	34
4.4	Tabulation of coefficient of friction based on their parameters	36
4.7	Tabulation of coefficient of friction based on their parameters	37
4.10	Tabulation of wear track morphology of ball bearing and disc of SKD-II disc	40
4.11	Tabulation of wear track morphology of ball bearing and disc of nontextured PKAC disc	42
4.12	Tabulation of wear track morphology of ball bearing and disc of textured PKAC disc	46
4.13	Tabulation of wear track width of different types of disc in $\mu\text{m}$ according to their tested parameters	48

## LIST OF FIGURES

FIGURE	TITLE	PAGE
2.1	Surface topography of a LST processed micro-dimple	7
2.2	Conventional Milling Process	8
2.3	Mechanism to form dimple with consistent depth of cut	9
2.4	Inclined ball end milling	10
2.5	Processes involved in micro casting metal	12
2.6	ECM principle and equipment	14
2.7	Through-mask electrochemical micromachining procedure with a textured dry film.	16
2.8	SEM image of frontal side of laser patterned multicrystalline silicon surface	18
2.9	Stribeck Curve for Textured and Untextured Surface	20
2.10	3D Image of Blended Dimple	24
2.11	3D Image of Regular Dimple	24
2.12	Friction force against time (a) for regular dimple (b) for blended dimple (c) respective phase	25
3.3	Structural parameter for patterned surface	31

FIGURE	TITLE	PAGE
3.4	Elementary components and principal on ball-on-disk tribometer	32
4.3	Hardness comparison between different type of discs	35
4.5	Coefficient of friction against load for non-textured disc	36
4.6	Coefficient of friction against load for textured disc	37
4.8	Coefficient of friction against sliding speed for nontextured disc	38
4.9	Coefficient of friction against sliding speed for textured disc	39
4.14	Coefficient of friction against load for 100rpm	49
4.15	Coefficient of friction against load for 150rpm	50
4.16	Coefficient of friction against load for 200rpm	51.
4.17	Carbon Transfer on Ball Bearing Surface Comparison for 5N at 200rpm	52
4.18	Carbon Transfer on Ball Bearing Surface Comparison for 5N at 150rpm	52
4.19	Carbon Transfer on Ball Bearing Surface Comparison for 15N at 150rpm	53
4.20	Carbon Transfer on Ball Bearing Surface Comparison for 5N at 100rpm	54
4.21	Carbon Transfer on Ball Bearing Surface Comparison for 10N at 200rpm	54
4.22	Carbon Transfer on Ball Bearing Surface Comparison for 10N at 150rpm	55

<b>FIGURE</b>	<b>TITLE</b>	<b>PAGE</b>
4.23	Carbon Transfer on Ball Bearing Surface Comparison for 10N at 150rpm	55
4.24	Carbon Transfer on Ball Bearing Surface Comparison for 15N at 200rpm	56
4.25	Carbon Transfer on Ball Bearing Surface Comparison for 15N at 100rpm	56
4.26	Trapping of Wear Debris on (i) Textured Surface (ii) Textured Surface	57
4.27	Disc Wear Track Width Against Sliding Speed for 5N	58
4.28	Disc Wear Track Width Against Sliding Speed for 10N	58
4.29	Disc Wear Track Width Against Sliding Speed for 15N	59
4.30	Coefficient of Friction Comparison Between Different Type Of Discs under 5N at 200rpm	60
4.31	Wear track width comparison between different type of discs under 5N at 200rpm	61

## LIST OF APPENDICES

APPENDIX	TITLE	PAGE
A	Data of Sliding Test	70
B	Microscopic Image of Wear Track of Disc and Ball Bearing	80



## LIST OF ABBERRATIONS

COF	Coefficient of Friction
ECM	Electrochemical Machining
IR	Infrared
LST	Laser Surface Texturing
PKAC	Palm Kernel Activated Carbon
PKAC-E	Palm Kernel Activated Carbon Epoxy
RPM	Revolution Per Minute
UV	Ultraviolet



اونيورسيتي تيكنيكل مليسيا ملاك  
UNIVERSITI TEKNIKAL MALAYSIA MELAKA

## LIST OF SYMBOLS

$D_s$  = Sliding distance

$F$  = Frictional force

$L$  = Applied load

$N$  = Rotation speed

$R_c$  = Contact ratio

$t$  = Rotating duration

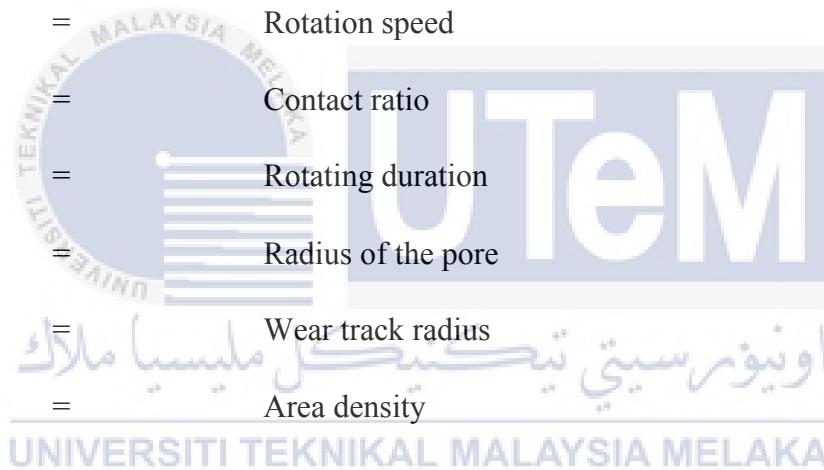
$r$  = Radius of the pore

$r_w$  = Wear track radius

$A_\rho$  = Area density

$\ell$  = Distance between dimples

$\mu$  = Coefficient of friction



# CHAPTER 1

## INTRODUCTION

### 1.1 BACKGROUND

A bearing is a device that controls all the relative motion to the desired motion while reduces operating friction. Self-lubricating bearings are plain bearings working without the need of any external lubrication. Plain bearings can only be classified as self-lubricating bearing due to its operating motion which is sliding. Other bearings such as rolling element bearing such as ball bearing and roller bearing and elastomeric bearing are not considered as self-lubricating bearing because they do not require lubrication to operate.

According to Evans (1981), self-lubricating bearings are classified into two types. The first type is dry bearings which have solid lubricant such as graphite or polytetrafluoroethylene. The other type is bearing which has its own liquid lubricant reservoir such as porous metal structure which acts as a well for oil and dimples on surface which holds greases.

Usage of self-lubricating bearings are most predominant when the conditions are:

- a) production of hydrodynamic oil layer is unable to take place due to the type of operation motion
- b) the external environment such as vacuum and low temperature inhibits the utilization of regular lubricants
- c) major simplification of devices or machines by removing lubrication supply

Solid lubrication is required in a rising amount of equipment especially in the aerospace field. This is because conventional fluid lubrication is insufficient in the elevated temperature and causes contamination in environment such as vacuum environment and sliding electrical contacts. Solid lubrication has the upper hand compared to fluid lubrication because fluid lubrication film has unpredictable life span and requires maintenance which can become costly and challenging. The most enticing substitute is to manufacture parts from material with self-lubricating property. Self-lubricating material can be described as a material that displays a little friction or abrasion in sliding motion even without the presence of an external lubrication. (Lancaster, 1967).

Since the last couple of years dry bearing material has pique the interest of engineers and researcher of linear motion bearings due to their special tribological characteristic and likelihood of removing grease-based lubrication. Due to pro-environmental purpose, engineers and equipment proprietor are obliged to replace conventional grease lubricated bearing components with self-lubricated bearings (Gawarkiewicz and Wasilczuk, 2006).

UNIVERSITI TEKNIKAL MALAYSIA MELAKA

## **1.2 PROBLEM STATEMENT**

As the world is ushering in an unprecedented level of environmental literacy, the current form of lubricant used needs to change because it is hazardous to the environment. Grease or oil-based lubricants are destructive to the environment especially when it is not disposed properly.

Almost all lubrication consumed by the automotive and production industry are oil or grease based. This form of lubrication is hazardous to the environment and non-biodegradable. A lot of pollutants can be introduced to the waste line when the lubrication

is disposed. In the long haul, the waste lubricants will amass and be destructive to the environment. This causes environmental government agency to continue implement strict regulations on the usage, storage and removal of oil and grease-based lubricants. This also rises the cost of disposal of conventional lubricants (Menezes et al., 2012).

### 1.3 OBJECTIVES

The objectives of the project are as follows:

- a) To investigate the effect of load-speed on tribological performance of surface textured palm kernel activated carbon reinforced polymeric composite
- b) To compare the performance of surface textured palm kernel activated carbon reinforced polymeric composite with conventional bearing material

### 1.4 SCOPES OF PROJECT

The scopes of project are as follows:

- a) The test samples are fabricated in only disc shape.
- b) The test samples are only experimented with ball-on-disc test in dry condition at room temperature.
- c) The max load used to test the test samples is 15N.
- d) The maximum speed used to test the test samples is 200rpm.
- e) The maximum sliding distance used to test the test samples is 1000m.

## CHAPTER 2

### LITERATURE REVIEW

#### 2.1 Surface Texture

Wear and friction of a surface can be decrease with the correct choice of surface engineering techniques. It can be achieved through modifying the components dimension, increasing hardness, applying surface coating, anti-friction additives, refine surface quality, creating definite surface configuration which is known as surface texturing (Sedlac̆ek and Podgornik, 2017). The primary benefit of surface texturing on the enhancement of tribological attributes is with microcavities functioning as lubricant reservoirs which then thicken the film layer between the joining parts. A resulting lift effect that deceases bearing surface contact is produced from the hydrostatic pressure generated from the increment in film thickness (Ibatan et al., 2015).

#### 2.2 Fabrication of Surface Texture

##### 2.2.1 Laser surface texturing

The most promising way employed currently to texture surfaces in engineering application is laser texturing (LT). It can be utilized on a wide variety of materials. It supports the formation of arrangements with minuscule attributes. For instance, attributes with depth of 200nm and radius of 10mm can be achieved in steel specimen by utilizing a femtosecond pulse laser. The utilization of more advanced optics can result in laser beam sizes lower than 5mm. Other way, depend on laser-induced periodic surface texturing,

utilized a femtosecond laser to form an array on concavities was not deterministic. Nevertheless, the utilization of LT display constraints. For starters, the cutting mechanism constantly prompt the generation of heightened features surrounding the pockets which comes from the expelled molten materials. These lateral rims are usually solid from the microstructural alterations as a result from the process could lead to harsh abrasive wear of the opposing surface. Therefore, these rims need to be eliminated via mechanical or laser polishing. This occurrence is essentially removed by utilizing very short pulse laser such as femtosecond laser. The secondary concern for LT is the texturing speed. The process comprises of ablation which alter the material state instantly from solid to gaseous with minimal metallurgical surface harm. The ablation fluence ranges for materials varying to soft metals to glasses and hard composites is within  $0.2$  to  $20\text{Jcm}^{-2}$ .<sup>29</sup> If the laser system is supplied with significantly high maximum pulse energy, a tiny concavity can be form by laser ablation using a fixed laser spot with size on par with the dimple and remove the necessity to conduct laser spot scanning as long as the laser influence is at least greater than the ablation fluence range for the specific material and then the depth of the concavity will be based on the number of pulses. The utilization of high pulse energies, miniscule spot diameters and very short pulse periods has enable material removal to be accomplished for a large variety of materials at higher texturing speeds. Nevertheless, since the patterns are usually formed in a serial sequence, the processing time for bigger parts can still be higher, especially lower cost LT equipment that utilized long pulse periods and big spot sized. Many parts the can have their performance enhance by surface texturing are affordable so they might need lower cost texturing ways to enhance of tribological performance accomplished by texturing to be economical (Costa and Hutchings, 2014).

For the last couple of years, laser surface texturing has been accounted as a productive and manageable way to fabricate texture of micro dimples by a rising amount of papers. By applying laser surface texturing, surface micro-textures can be fabricated on pretty much any materials. Laser is very quick and can manage the form and size of the micro dimple well. Processes of sublimation, melting and vaporization is generated by every laser pulse send to the surface, producing in a pore. The strong intensity of the laser beam pulse causes the area near to the dimple to also be subjected to melting and rapid re-solidification. This damage can be reduced by lowering the laser pulse duration (Vilhena et al., 2009).

Laser surface texturing (LST) is one of the most cutting-edge surface texturing approach in generating tiny concavities arrangements for sliding contacts. The laser utilized is remarkably quick which enables low processing duration and allows exceptional management of the form and dimension of the micro dimples that enables attainment of ideal design as shown in Figure 2.1. It can also be applied on a wide range of materials such as ceramics, hardened steel and polymers. The texturing process comprises of a concentrated pulsed laser to generate tiny concavities arrangements neighboring by a hardened melt rim. Melting and vaporization of material occur with laser surface texturing because of the intense energy usage. This causes heat affected area to be in a solidified melt rim state which transform the microstructure and mechanical characteristics. In order to reduce this effect, pulse energy and frequency need to be adjusted. CO<sub>2</sub> and Nd:YAG are the types of laser frequently used in laser surface texturing. Nd:YAG is more suitable to be used on metals due to Nd:YAG being inert gas which will improve the surface absorptivity hence resulting in a higher surface texture quality than CO<sub>2</sub> thickness (Ibatan, et al., 2015).

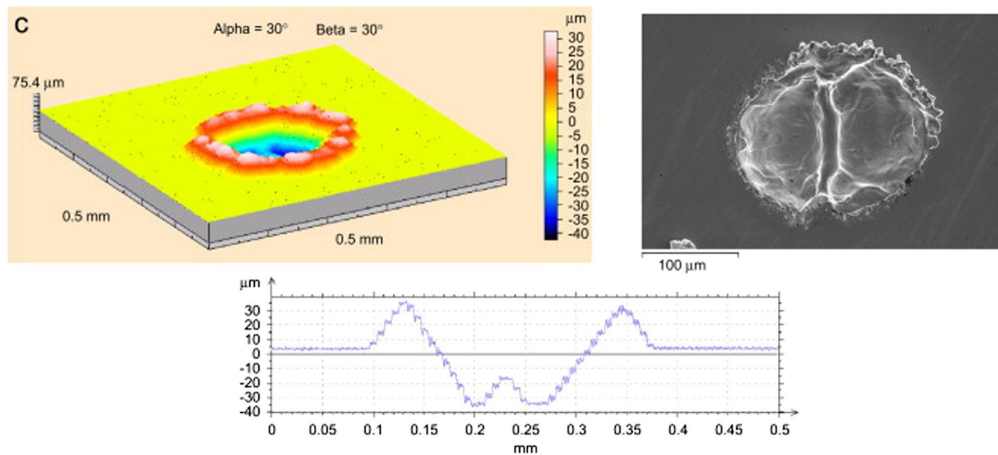


Figure 2.1: Surface topography of a LST processed micro-dimple (Ibatan, et al., 2015)

Development in laser surface texturing utilizing ultraviolet (UV) light lately has enable new prospects for tribological surface geographical alteration. It is currently feasible to generate micron-sized concavities on the surface of rigid ceramic coatings via pin-point modulation over location, size, depth and surface density. Solid condition pulsed UV laser surface texturing is affordable, quick and contributes a significant diminution in neighboring surface overheating compared to infrared (IR) lasers. Laser surface texturing process was studied for hydrodynamic lubrication modulation and may be employed to generate solid lubricant well that are optimal in depth, geometry and surface density. Besides that, laser processing can be sectionally administer to the surface of hard ceramic layers to produce an ideal abrasion resistance and load support with least influence on the surface fatigue life in aerospace systems (Voevodin and Zabinski, 2006).

### 2.2.2 Micro-ball end milling

Micro mechanical machining is considered as an alternative to fabricate texture surface. Press load is manipulated to obtain the desired size of dimple. Production of micro dimples by pellet pressing was effortless and inexpensive. Majority of the mechanical

processes for micro texturing was conducted on even surfaces. The surface texturing was also needed on curved surfaces. (Matsumura and Takahashi, 2012)

Physical characteristic will be altered by forming small concavity on the surface such as lubrication, aerodynamic and thermodynamic property. Typical milling process to produce tiny indentations arrangements on a metal surface requires the translation of cutting device in a horizontal and vertical motion as shown in Figure 2.2. This traditional milling technique consumes a lot of time. Besides that, the irregular motion of the cutting device constantly declines the precision of the cutting process. An effective approach to form concavity on the metal surface utilizing the milling technique is presented by the authors. The presented approach is described accordingly. Assume the inclined ball-end mill is translated solely in horizontal orientation with an immensely high feed rate and low depth of cut. Figure 2.3 shows the trochoid curve of the cutting boundary that is simulated with dotted line. This shows the approach is able to produce concavities on the surface. This approach needs seamless motion of the device only in horizontal translation. Hence, the formation of concavity can be executed in a significantly brief time period. On top of that, the seamless motion of the device enhances the precision of the cutting process (Kogusu et al., 2008).

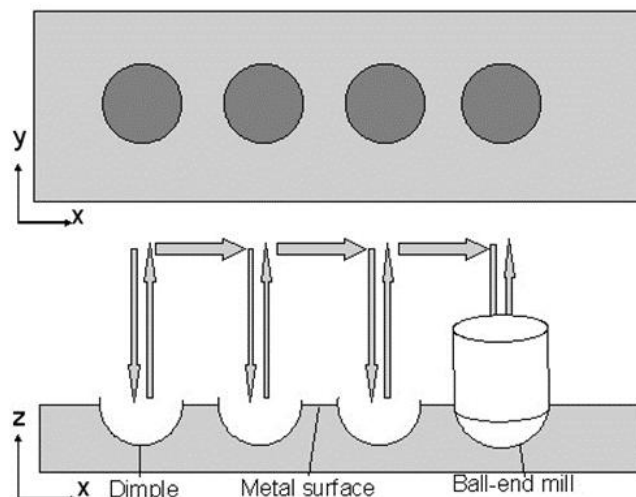


Figure 2.2: Conventional Milling Process (Kogusu et al., 2008)

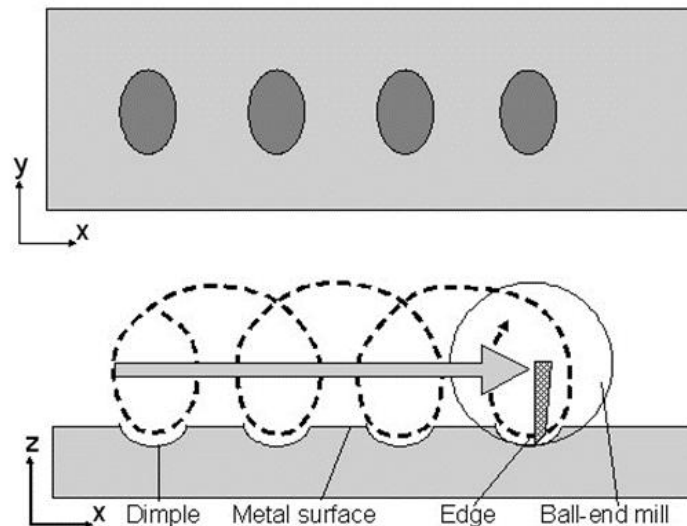


Figure 2.3: Mechanism to form dimple with consistent depth of cut (Kogusu et al., 2008)

Although the popularity and benefits presented by the laser surface texturing, applying it on a populace commercial magnitude may demonstrate to be challenging because of the tremendous measure of energy needed to generate an accurate tiny-indented surface. Mechanical process is proven to be superior over laser surface texturing in generating tiny concavities. Micro-ball end milling has been employed to produce micro-texture on a surface lately because of their special cutting mechanism. The processes of micro-ball end milling as tiny concavities are formed on a surface as shown in Figure 2.4. The approach can generate patterns on even and complicated surfaces. Some materials such as glass and brass has been utilized on forming tiny concavities on surfaces. This approach has a favorable prospect compared with other excessive energy consuming surface texturing approaches, but more studies are required to be carry out to resolve concerns such as ploughing consequences due to material removal waste, periodic forces and damping to extent device lifespan and mechanics for more accurate machining of surface attributes (Ibatan et al., 2015).

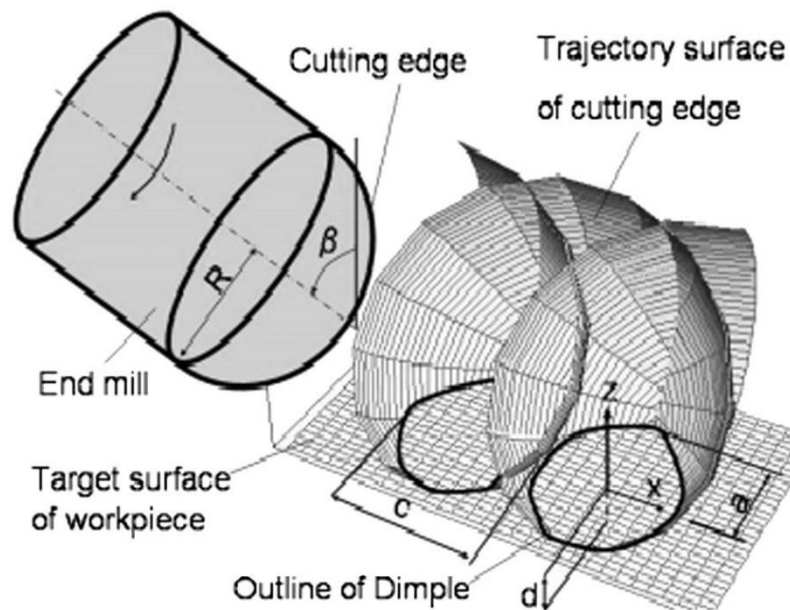


Figure 2.4: Inclined Ball End Milling (Ibatan et al., 2015)

### 2.2.3 Micro-casting

Metal microstructures and nanostructures are suitable as production molds for nanoimprint lithography (NIL) because they can be repeatedly utilized more than silicon or quartz. Publicize journals outlines that production of metal submillimeter, micro- and nanostructures by forging, electroplating and casting. Forging is capable of generating small-scale structures in ductile material. In a single presentation of metal forging process, a silicon carbide (SiC) cast template fabricated grooves with width of 40mm into detached aluminum thin layer at raised temperature. Likewise, aluminum film on silicon is embossed with a 300nm grooves. A separate research stated a thick nickel film is etched with grooves of sub-10nm by utilizing a diamond cast template. Despite lacking the compressive strength of SiC or diamond, silicon can be utilized as a cast for metal forging. Hence, silicon cast template function at a reduced forging pressures and more ductile metals. For instant, a tall structure with width of 250nm and height of  $1\mu\text{m}$  was fabricated into even gold and silver by utilizing silicon cast. The silicon was forfeited in the lost cast process. One of the issues surfaced when utilizing these metals is surface oxidation. Forfeiting of silicon could be avoided by demolding a silicon cast template following

fabricating structures of  $50\mu\text{m}$  into a fine film of aluminum on a silicon substrate. By conducting molecular dynamics (MD) simulations of small-scale forging, accumulation of excessive material is imminent and decreasing metal film thickness increases forging pressure are known. Microscale metal electroplating eliminates accumulation of excessive material and is more affordable than forging. However, it is more time-consuming and sample size is restricted. Some latest studies report that flexible nickel sheets could be electroplated onto a polymer constructed with NIL subsequent to sputtering a seed layer onto the constructed polymer. After liquefying the polymer in the lost mold process, that nickel could be enveloped around a roller that can etch a continuous sheet of polymer with holes with a width of  $1\mu\text{m}$  and a depth of  $250\text{nm}$ . Mg–Cu–Y bulk metallic glass can be etched with electroplated Ni-Co. The metallic glass can then be utilized to etch polymethylmethacrylate (PMMA) micro lenses. There have been reports of lesser work required to produce metal microstructures by molding. An approach for submillimeter molding for aluminum-bronze or gold alloy is to mold into little plaster casts that are cast from injection-molded PMMA gears. Another way for microscale metal casting for unidimensional structures is to mold microstructures into wax then mold ceramic into wax followed by curing ceramic in a lost wax process and finally mold metal into the microstructured ceramic. These latest methods can only fabricate metal microstructures that is even in a thin film form. Hence, there exists a necessity for affordable parallel processes to fabricate metal microstructure on curved surfaces. Therefore, Figure 2.5 demonstrates the process of casting. The process has been modified from an earlier method to fabricate microstructures on curved ceramics (Cannon and King, 2009).

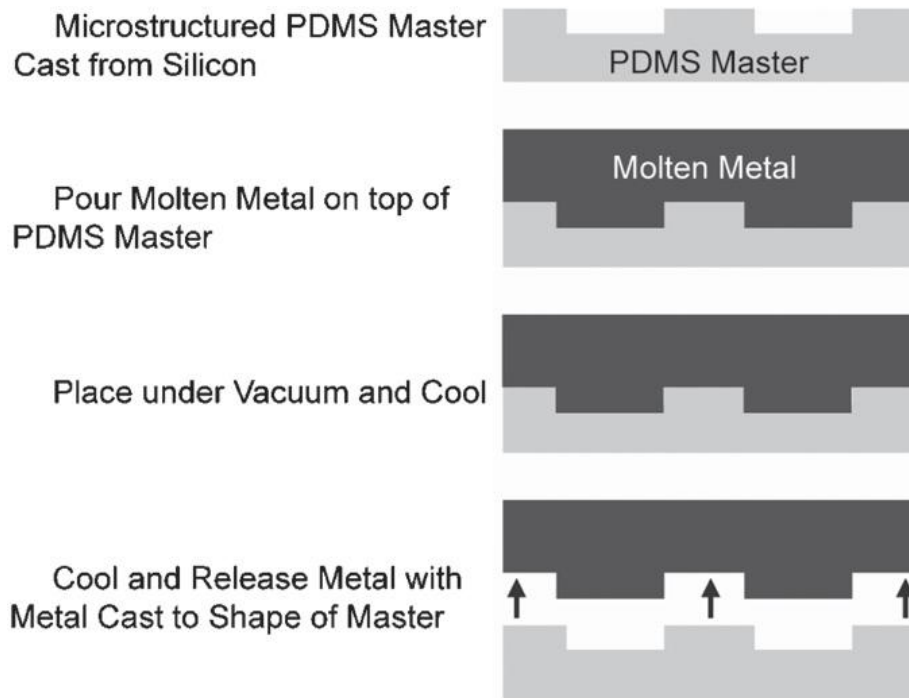


Figure 2.5: Processes involved in micro casting metal (Cannon and King, 2009)

#### 2.2.4 Electrochemical machining

Electrochemical machining (ECM) is an anodic electrochemical dissolution approach. Its fundamental concept and elementary equipment are shown in Figure 2.6. ECM presents a lot of superiority over conventional machining in terms of its usability irrespective to the hardness of material, zero tool abrasion, tremendous material removal pace, flat and bright surface and fabrication of complicated structure parts. ECM appeals to industries such as aerospace, automotive, defense and medical industry as a productive way to fabricate a wide range of components. Furthermore, recent development in machining precision and accuracy has allowed the electronic manufacturers to start micro-machine parts with ECM. ECM supplied with pulsed direct current voltage provide better accuracy governance. The integration of ECM with different machining method has exhibited better performance compared to that accomplished by solitary methods. ECM and its pulse system are discovering new utilizations in finishing cast for numerous industrial parts. By combining with different permitting technologies, ECM is discovering

wider utilization and rising approval in diverse of other industries. Regardless of these developments, study is still required on some respect of electrochemical machining. Present fields requiring concern comprise of design of device, monitoring and modulation of process, electrolyte processing, removal of machining wastes (known as sludge) and precision. The intricacy of ECM method causes the theoretical estimation and on-line supervise the interelectrode space size to be challenging which tremendously influence the ECM performance. Absence of competent ways of process modulation obstruct the combination of ECM tools inside the current manufacturing environment. Design of equipment is generally a expensive experimental step instead of an precise science. Extensive experience and professional expertise are needed to favorably conduct the process. Furthermore, ECM produces a lot of waste, primarily metal hydroxide sludge. The processing and disposal of the sludge could comprise of heavy metal originating from workpiece material will be intricated and expensive. ECM remain to be considered as a revolutionary machining method due to its immanent attributes and the necessity for thorough way to the issues discussed above. The latest and arising enabling technologies for identifying, supervising and regulating, equipment design software, sludge depletion, processing and disposal need to be combined with ECM to enhance the process accuracy, efficiency, reliability, self-regulatory and eco-friendliness (Rajurkar et al.,1999).

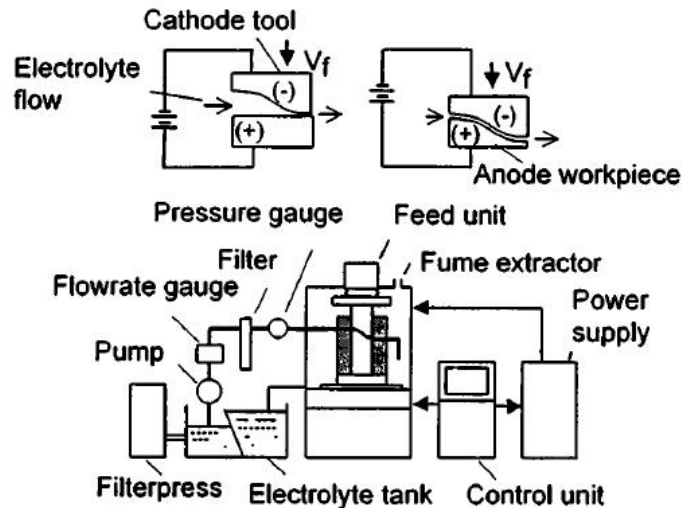


Figure 2.6: ECM principle and equipment (Rajurkar et al.,1999)

The metal-based workpiece (anode) is connected to the positive terminal of a power source and the device (cathode) to the negative terminal in electrochemical machining. Anodic liquification take place at the metallic workpiece. The liquefaction pace at the anodic areas that is nearer to the device is greater due to the ohmic decline in the solution is lesser. Therefore, the device shape is duplicated truly into the workpiece. ECM was favorably employed to form difficult to machine components since 1950s. ECM was utilized as a viable way to pattern surfaces in the 1970s but the patents designating the utilization of ECM to pattern surfaces was registered in the late 1980s. The primary disadvantage with the conventional method is the necessity to mask every workpiece to be patterned that increases cost and processing duration. Some study was geared on an alternate approach of utilizing ECM to pattern surfaces. This method comprises of identifying the electrical insulation which restrains the machining operation at the surface of the cathodic equipment rather than administering mask to every workpiece. Solely a single masking action is needed on the equipment that enable the patterning of multiple workpiece continuously due to lack of disintegration occurrence at the cathode. A few researchers have delved into this idea. Nonetheless, the current works vary from those ways in some vital attributes. The reasons for the variation in method utilized in the current

work are the insulation stays above the conductive surface and the electrolyte stream through tiny openings on the patterned device that determine the texture to be transmitted, securing productive cleaning of the equipment during machining. The amount of electrolyte utilized to machine each workpiece is relatively low and the entire equipment is rather elementary. On top of that, the operation happens at a one area instead of over a lot of locations in parallel. (Costa and Hutchings, 2008)

ECM is a favorable machining process with benefits like high machining effectiveness, liberty of material hardness and toughness, the lack of a heat influenced layer, an absence of remaining stresses, cracks, equipment abrasion and burrs and small fabrication expenditure. The production of tiny indentation pattern via ECM can comprise of maskless or through-mask material extraction. This way of machining is elementary compared to photolithographic technique. However, it requires lengthy time due to the production of indentation being point by point. Through-mask electrochemical micromachining (TMEMM) is a generally employed ECM technique for fabrication of tiny indentation pattern. TMEMM utilizes photolithography to fabricate micro-texture on photoresist-coated substrates by the process comprising of a soft bake to dehydrate the solvent subsequently to spin coating, subjection to ultraviolet (UV) ray, a post-exposure bake and photoresist maturing. The metal is subsequently dissolve discriminately from exposed areas. Nonetheless, the setup of micro indentation patterns on non-flat surface continue to be an issue because it is challenging to utilize on these surfaces. Tiny indentations patterns need to be fabricated on the external and internal surface of a hollow cylinder. Dry-film photoresists (acrylate-based photopolymers) was utilized as masks for powder blasting to outline microfluidic paths and as electroplating molds used in the LIGA process. One of the characteristic of these films is great flexibility and research stated that this trait is capitalized by utilizing dry-film photoresists to enclose the internal surface of the cylinder

and function as a mask during production of a tiny indentation pattern on the surface via electrochemical micromachining. The subsequent procedure as shown in Figure 2.7 was utilized to set up the dry film with tiny through-cavities:

- 1) Firstly, O<sub>2</sub> plasma treatment was utilized to clean the substrate for 3 minutes.
- 2) The substrate was laminated with the dry film
- 3) The dry film was bare through a photomask by utilizing a UV oven
- 4) The dry film was then immersed in an aqueous sodium potassium carbonate solution with concentration of 1% by weight and temperature of 30°C for a duration of 60 seconds to be developed
- 5) At last, the textured dry film was stripped from the substrate and employed to the surface of the workpiece

(Ningsonget al., 2013)

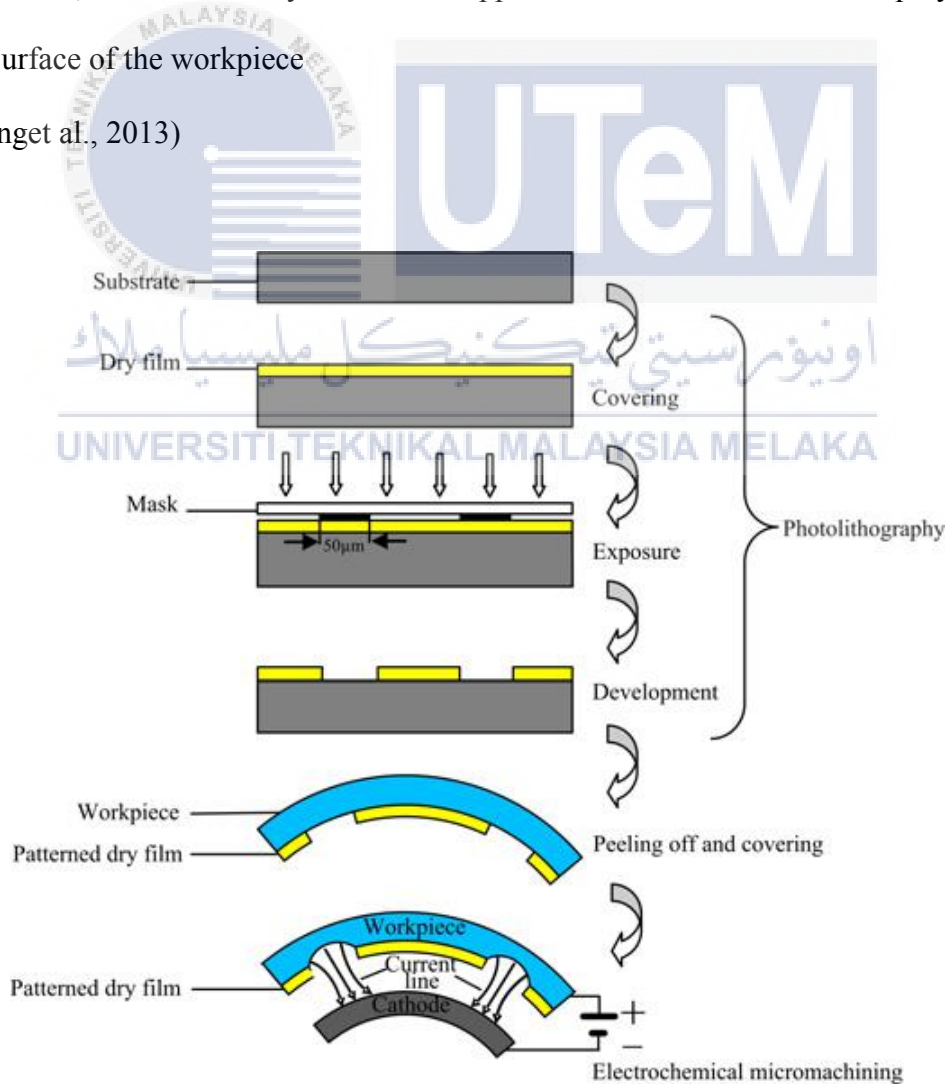


Figure 2.7: Through-mask electrochemical micromachining procedure with a textured dry film (Ningsonget al., 2013)

## 2.3 Application of Surface Texturization

### 2.3.1 Application of surface texturization in solar cells

This journal reports the feasible application of laser technique in patterning multicrystalline silicon photovoltaic cells as shown in Figure 2.8. Patterning improves the absorption of light ray by the subsequent situation:

- Increased likelihood of absorption of light beam which lowered the reflection by reflecting light from an angled surface as a result of texturization and hitting other surfaces
- Light beams are absorbed nearer to the junction because of the refraction of light beam inside the angled silicon propagate which is quicker than this process happening on a flat surface that is predominantly relevant in material diffusing at lengths about the thickness the cell.
- Photons with long wavelength might meet an angled silicon surface after being reflected from the rear surface to the front. This increases the likelihood of it being internally reflected at the glass surface or silicon interface and aiding the following absorption possibility.

The final occurrence is known as light trapping and provide an enhanced reaction particularly to infrared beam. In the past, improving light absorption of monocrystalline silicone photovoltaic cells by surface patterning has been achieved via fabrication of arbitrary arranged pyramids by alkaline chemical etching but this arbitrary attribute of the crystal arrangement of multicrystalline silicon wafers renders such method ineffective for this material due to the fact that only minimal part of grains share similar crystal arrangement at the top surface. On top of that, undesired steps and cavities formed between grains from alkaline etching that cause ineffective structural of the patterned surface (Dobrzański et al., 2007).

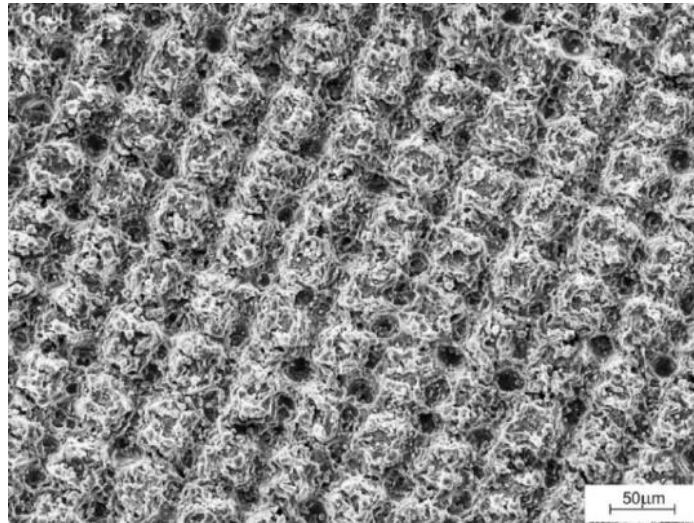


Figure 2.8: SEM image of frontal side of laser patterned multicrystalline silicon surface (Dobrzański et al., 2007)

### 2.3.2 Application of surface texturization in automotive components

A model was cultivated to show the capability of lowering friction losses via surface patterning in shapes of numerous spherical micro-openings in reciprocating system. An elementary ‘cylinder and piston’ system with steady external normal force was studied shown hydrodynamic effects could be produced through surface texturization surface texturing even for so-called parallel matching surfaces. The time deviation for clearance and frictional force at any designated working constraints were attained through determining the Reynolds equation and dynamic equation concurrently. The primary criterions of the issue were known, and a thorough parametric examination was conducted.

The subsequent conclusions sum up the result of the examination:

1. The interaction between neighboring openings is important and its influence on the hydrodynamic pressure dissemination must be consider.
2. The largest deviation of the fluid film clearance per cycle is low, only less than 30% of the opening depth. Therefore, the deviation in frictional force with angle of crank is primarily because of deviation in sliding speed

3. A deviation of area density of the opening falls in the range of 5% to 20% alters the frictional force by lower than 7%.
4. The impact of inertia due to the piston rings is insignificant. Altering the inertia variable by 3 orders of magnitude only result in 2% modification of mean frictional force.
5. Lowering the frictional force drastically by raising the number of openings (up to number of openings = 12) over the axial length. Above 12, decrement in frictional force develop into a modest pace.
6. An ideal depth of opening over diameter ratio was obtained which results in a minimal frictional force. This ratio ranges from 0.1 to 0.18 for all related criterions of the issue.
7. Despite not being to conduct a direct comparison between the model and a system that does not comprise of openings, it is obvious that a decrement in frictional forces by 30% and even more is attainable with patterned surfaces.

(Ronen et al., 2001)

Tribological impacts of micro-indenting on 30NiCrMo12 nitriding steel were examined by determining the friction coefficients by utilizing a pin-on-disc equipment. In constant working constraints, patterning was discovered to lower friction coefficient and wear compared to nonpatterned surface. When applied with a single drop lubrication, normal loads exceeding 3N, friction coefficient decreases by 75 percent from nonpatterned to patterned surface (approximately from 0.8 to 0.2). Stribeck curve as shown in Figure 2.9 sums up the evaluation of friction for nonpatterned and patterned surfaces showing that textured surfaces elude from transitioning hydrodynamic lubrication to mixed and boundary lubrication regime. For any loads and speeds experimented with, the system

remains working in hydrodynamic regime. Long sliding condition examination discovered that micro indentations ensure same and small friction coefficient for a lengthy duration. With dry contact condition, for normal load of 1N, friction coefficient is lowered to approximately 10 percent from nonpatterned to patterned surface. Debris were seen in contact area of pin and disc. The debris was deposited into the dimples in the textured surfaces and this incident helps enhanced the tribological performance of these surfaces. Debris in nonpatterned surfaces raises the friction coefficient and quicken wear. In short, positive outcomes are achieved in single drop lubrication can propose the concept of substituting intermediary materials for engine parts operating in constant working constraints with metal-to-metal contacts administered with laser surface texturing method (Borghi et al., 2008).

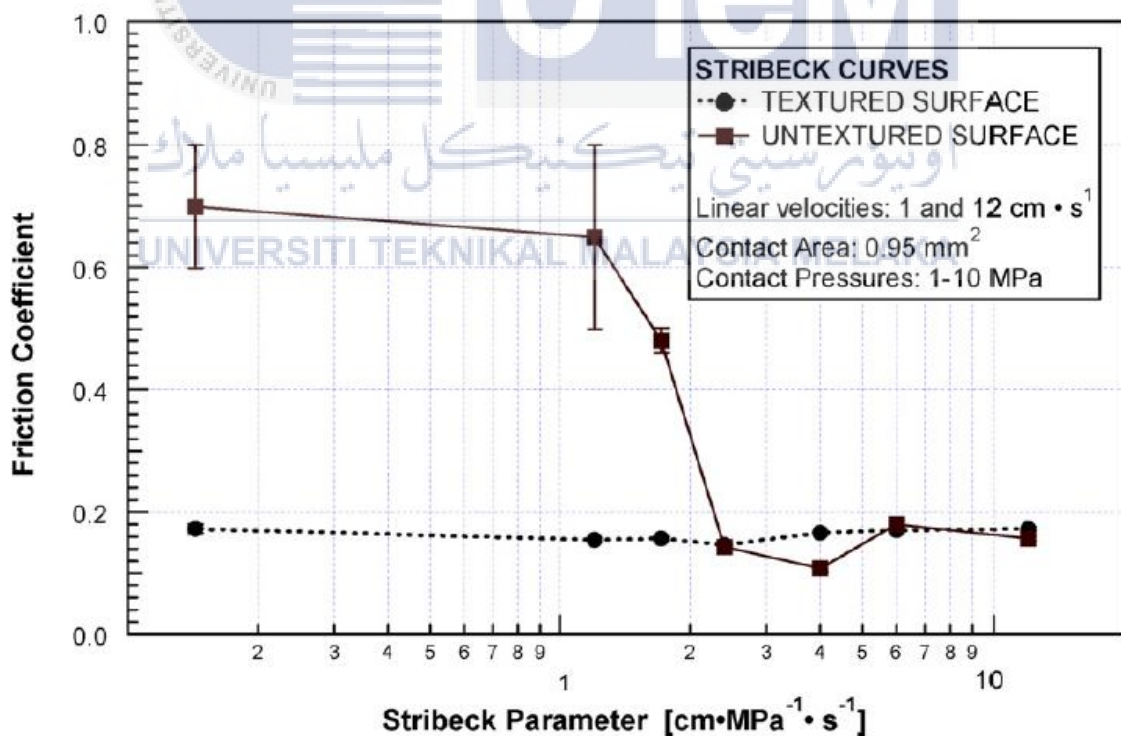


Figure 2.9: Stribeck Curve for Textured and Untextured Surfaces (Borghi et al., 2008)

Decrement in frictional forces in cylindrical face piston rings by partial laser surface texturing (LST) was studied on a reciprocating test rig by measurement of

frictional forces between cylinder liner compartments. The outcomes were compared with untextured barrel face piston ring. It was shown that in the range of test rig speed, frictional forces lowered by up to 25 percent can be achieved by partial LST cylindrical face rings. Several initial actual engine examinations with manufacture barrel formed piston rings and cylindrical liners did not demonstrate similar level of frictional force reduction. More study is needed with a firing engine using ideal partial LST cylindrical face rings (Ryk et al., 2006).

### **2.3.3 Application of laser texturing in medical equipment**

A model for laser surface texturing of medical needles was created. Micro-pathways with varying sizes, densities and position were fabricated on the needle. Impact of surface pattern on frictional forces between phantom tissue and needle were investigated by conducting friction examinations. It was demonstrated that friction rises during the event of needle insertion due to the surface pattern produced by LST. Micro-pathways with tinier sizes and higher area density generate greater friction because these parameters cause increased contacting boundary between patterned surfaces and soft tissue. Needles equipped with micro-pathways across the lateral orientation demonstrated a higher friction rise compared to needles equipped with micro-pathways across the axial orientation. Finite element simulation was done to show the interaction between patterned solid surface and phantom tissue. The outcome of the simulation displayed that stress heighten close to the edges and that phantom tissue tailored to the structure of the pattern. Pattern with blended edges are predicted to lower patient irritation and entry forces during percutaneous operations (Han et al., 2013).

In times of rising attention on the progress of minute tools and steady and operationally enhanced bioimplants, lasers are predicted to be an important part of surface

engineering and managing these devices. The utilization will comprise from laser cutting in stents to laser coatings and patterning of bioimplants. The emergence of laser based operation with lower wavelengths and shorter pulses with lowered heat input and smaller beam diameters will introduce new chances for future biomaterial utilization. New progress such as laser induced forward transfer(LIFT) and matrix-assisted pulsed laser evaporation direct write (MAPLE) are predicted to hold a important part in the processing of biomaterials in the most beneficial method for microscale to nanoscale surface topography. One of the primary objectives of bioimplants was the complete osteointegration into a bioenvironment. In order to achieve this, a thorough comprehension of cell attachment into patterned surface is needed. In times of rising attention into progress of a hierarchically dominated micro to nanopatterned surfaces, superior manufacturing procedure are needed to fabricate complicated texture continuously. Nevertheless, surface alterations such as patterning at any scale prone to cause modification in surface on the macro to atomic level. These impacts cannot be simply evaluated, and it may proceed to affect biological response. Out of all the surface engineering method tested, laser is the most suitable due to its specialties such as zero contact micromachining that result in immense level of purity, tremendous accuracy coherent energy ray, processing various materials and fast speed. A deep comprehension of thermodynamics and phase transformations during laser treatment to improve the performance of laser-improved coatings is to be obtained. Issues related with laser treatments such as microcracks and heat affected areas need to be reduced. Complete positioned supervision and regulating of the laser surface texturing need to include in the setup for productive feedback inspection of the operation (Kurella et al., 2005).

A laser surface texturing technique for fabricating micro-structure on echogenic needles was created. A rasterizing path was used to form circumferential pathways across the needle axial orientation and a triangular path and layer per layer scanning technique were used to fabricate corner-cube-like concavities on needle. On top of that, regulating overlapping in the feed direction was suggested to blend the edges of micro-pathways and micro concavities.

The outcomes of the test demonstrated that altering the pulse overlap could cause varying pathway depths or concavity and to produce blended patterns with varying fillet radius. The fillet radius impact was prominent when compared with typical pathways or concavities. Friction examinations were performed to investigate the impact of blended patterns on the friction behavior between needle and phantom tissue. It was shown that the micro-pathways fabricated with LST heighten the frictional force in the preliminary full contact phase because of the accumulation of stress developed at the sharp pathway rims. Blended pathway patterns have demonstrated decrement in friction soaring pace by a up to 89.3 percent. The decrement in friction in needles patterned having blended pathways in Phase 3 was more prominent because of the increase of percentage by up to 80.3%. Furthermore, needles having blended corner-cube-like-dimples as shown in Figure 2.10 have demonstrated a more prominent decrement of frictional force compared to needles having regular concavities as shown in Figure 2.11. Blended patterned needles typically function exceptionally in friction behavior as shown 2.12 because of the decrement of stress accumulation at the pathway or concavity rim. In the case of micro-patterns on echogenic needles, patterns with blended textures could be utilized to lower entry forces in percutaneous operation (Wang et al., 2016).

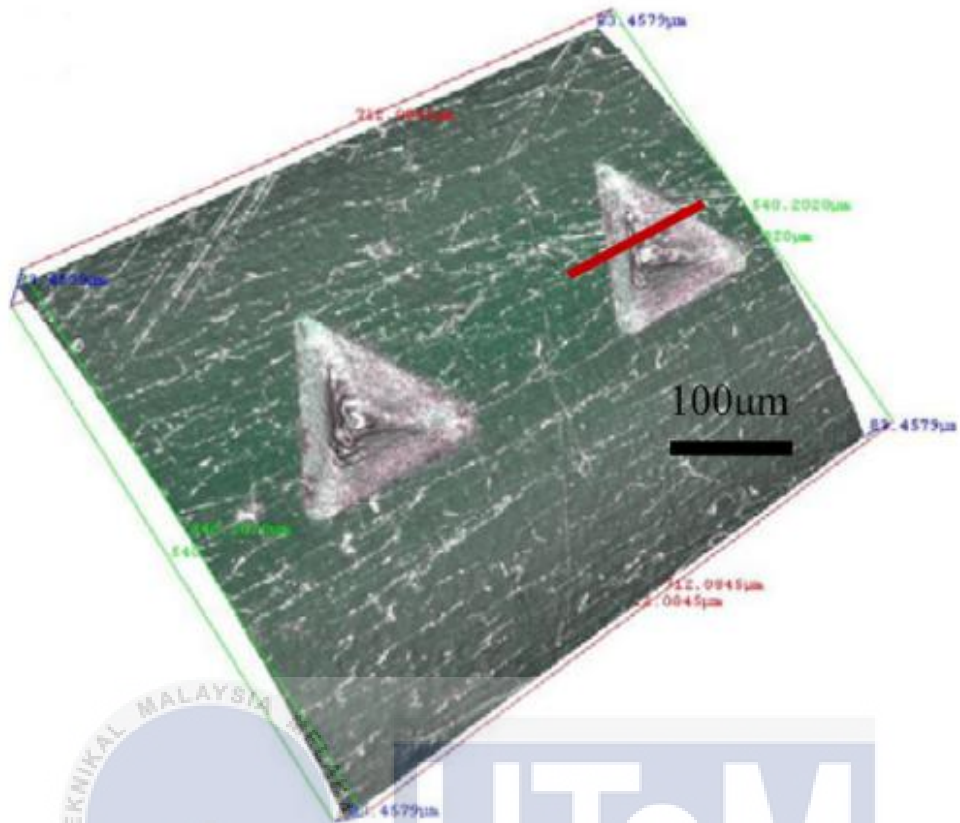


Figure 2.10: 3D Image of Blended Dimple (Wang et al., 2016)

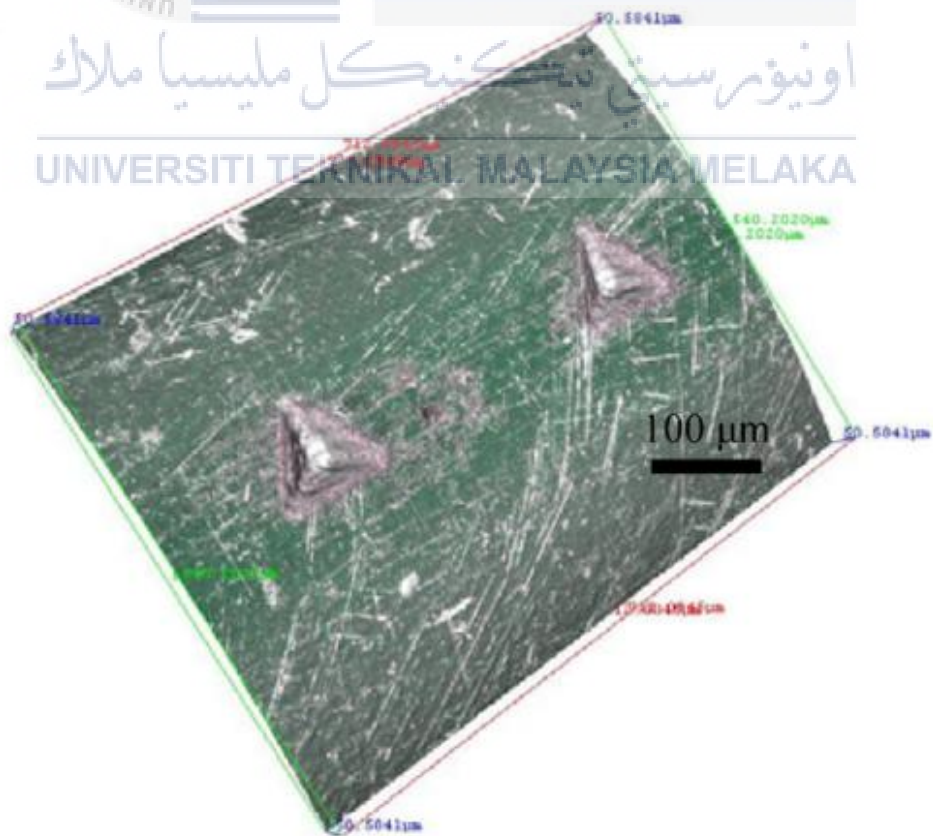


Figure 2.11: 3D Image of Regular Dimple (Wang et al., 2016)

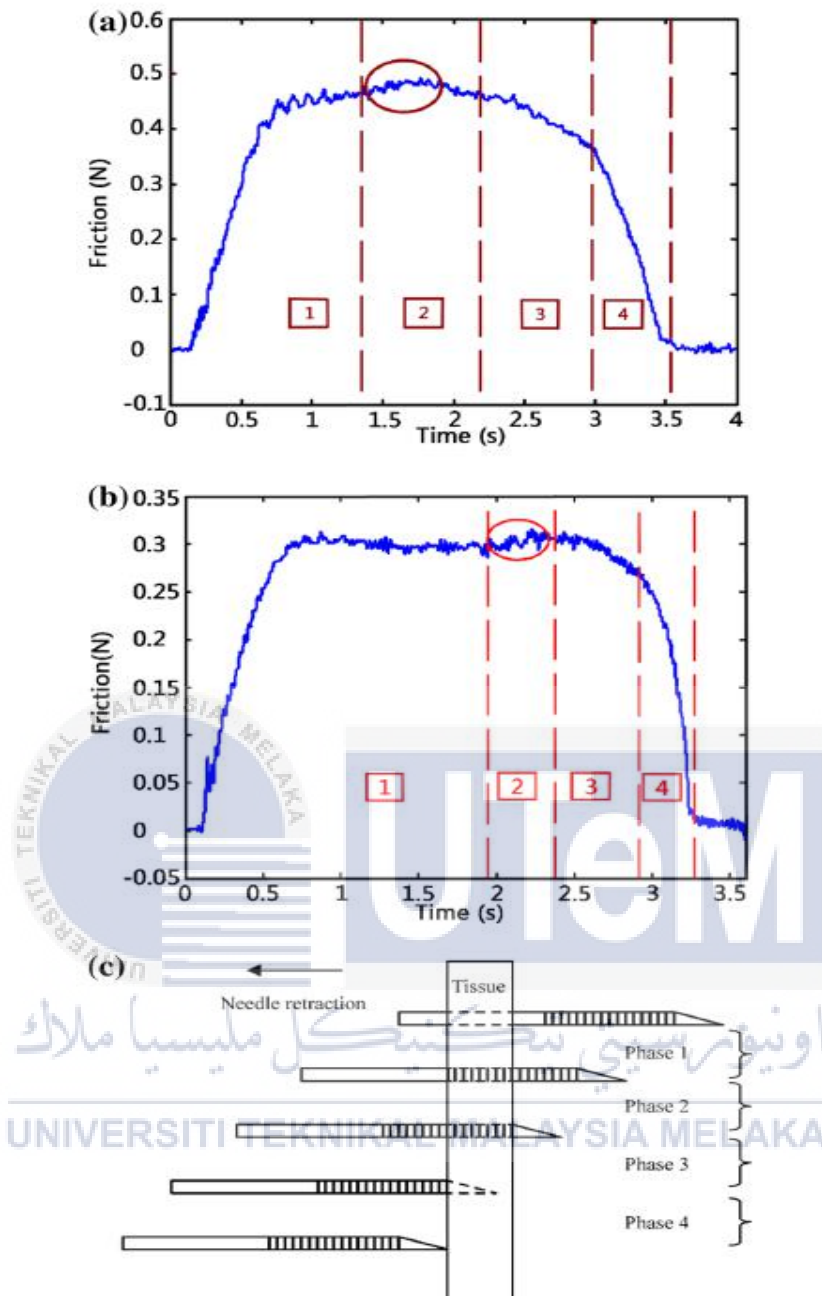


Figure 2.12: Friction force against time (a) for regular dimple (b) for blended dimple (c) respective phase (Wang et al., 2016)

## 2.4 Self-lubricating Material Properties

Self-lubricating material can be described as a material demonstration minimal friction and wear when sliding without having a separate source of solid or liquid lubricant. Current materials can be divided into materials that provide minimal friction and wear and materials that have an internal supply of lubrication (Lancaster, 1967).

Typical layer lattice solid lubricants like graphite and MoS<sub>2</sub> in powder and bonded coatings configuration is capable of functioning from 350°C to 400°C. Under ideal circumstances can be utilized at more elevated temperature for a little while. The elevated temperature polyimides have thermal capabilities similar to graphite and MoS<sub>2</sub> which can be easily utilized in graphite-fiber-reinforced configuration. In even elevated temperature, several soft oxides and fluorides continue to be self-lubricating till 900°C. Presently, these materials are utilized in the form of fused coatings that has thickness of 0.01 to 0.02 mm on metal substrates or lubricating element of metal matrix composites. They are produced from powder metallurgy techniques and plasma arc spraying. Hard coatings of several specified carbides, nitrides and oxides that function till 1000°C under sufficient adhesion to the material at all temperature are utilized for wear modulation. Thin MoS<sub>2</sub> ranging from 200-500nm thickness are extremely suitable for vacuum atmosphere but demonstrate restricted durability in reactive environment. Ion-plated layers on soft metals are capable lubricants especially in self-lubricating contact bearing (Sloney, 1982).

Self-lubricating solids can be categorized into non-replenishable films which is primarily utilized as thin and expendable film and replenishable films that is generated from a film transfer way from a self-lubricating composite to another surface. The second way can be then separated into 2 group. The first group is films generated from singular transfer mechanism that solely a composite and bearing pair is incorporated in producing friction and wear decreasing film on surfaces of the initially not lubricated component of the pair. The second group is a double transfer mechanism that the singular transferred, minimal shear strength composite layer from a bearing component that is then transferred to a another not lubricated bearing part that is fundamental inside the system (Gardos, 1982).

## 2.5 Palm Kernel Activated Carbon (PKAC)

### 2.5.1 Tribological properties of PKAC

In short, the results demonstrated that wear rate and friction coefficient of PKAC epoxy composite had lowered as the load exerted risen. Although, at greater load, friction coefficient rises a little and continue constant with load exerted. On top of that, several adhesive and grinding wear classification were known on the worn surfaces. As a whole, PKAC epoxy composite demonstrated special features as solid lubricant at small load in dry circumstance. (Chua et al, 2014)

PKAC is a scrap resulting from extraction of palm oil procedure. This scrap has carbon attributes and leftover oils that is a natural lubricant that has promising capability to be an authentic self-lubricating. It has been shown to be no prominent impact of sliding distance on coefficient of friction(COF), but the wear rate has risen a little. Nonetheless, once the working temperature has surpassed the crucial limit, both wear rate and COF soar promptly as sliding distance increases. Grinding, adhesive and crack generation which introduces delamination were recognized as primary wear mechanisms. In comparison with other synthetic and agricultural scrap based polymeric composite, PKAC is determined as a promising self-lubricating material functioning under 90°C (Tahir et al., 2016).

The most important variable which impacts coefficient of friction in PKAC epoxy composite is the weight percentage and working temperature plays the most key role for wear rate. The suggested statistical models have a range of 90 to 94 percentage reliability that is only applicable in plastic deformation phase. Those models can enable material design personnel prevent components from breaking down prematurely. (Tahir et al., 2017).

The outcomes demonstrated that coefficient of friction (COF) and wear rate rises as working temperature rises. Quick rise of COF can be observed after temperature surpass

90°C because of the heat from friction and breakdown of epoxy bond. Nonetheless, after 120°C, tribofilm is generated on the counter surface causes the COF to remain the same. Wear rate continue rising due to the thermally triggered phenomena that causes the decrement in hardness that lead to breakdown of epoxy element in the composite. Abrasive wear and crack phenomena that causes delamination wear were recognized as the primary wear mechanism (Tahir et al., 2015).

### **2.5.2 Adsorption property of PKAC**

The outcome of the study demonstrates that PKAC is a promising capable adsorbent for the adsorption of an elementary dye, BB9. Equilibrium data are properly illustrated by the Redlich–Peterson isotherm continued with the Langmuir and Freundlich models. The Langmuir monolayer saturation adsorption limits are 311.72 mg/g (Jumasiah et al., 2005).

The adsorption of methylene blue into PKAC was examined in this study. The adsorption progression followed a artificial 2nd order kinetic model. The outcome displayed that intra-particle diffusion is key to define the rate because adsorption mechanism is regulated through particle diffusion and not via film diffusion. It is also observed that the rate of adsorption is seen to risen with operating temperature which shows that more methylene blue was adsorbed at elevated temperature and portrayed that the adsorption process was an endothermic phenomenon (Abechi, 2011).

## CHAPTER 3

### METHODOLOGY

#### 3.1 Sample Fabrication

The materials utilized in this research to fabricate the samples were palm kernel activated carbon (PKAC) and high-density epoxy comprises of 105-B West System Epoxy Resin and 206-B West System Slow Hardener. Production of PKAC is classified and PKAC was supplied by manufacturer. The PKAC powder was crushed and sieved repeatedly until all its particles size were reduced to 250  $\mu\text{m}$ . The PKAC powder was weighted at 17.14g (60wt.%) and mixed with epoxy (resin to hardener ratio of 4:1) weighted at 11.43(40wt.%) in a beaker. The mixture was stirred with a spatula until a uniform color and texture is observed. The mold is coated with a layer of mold release wax and the mixture was deposited in the mold. The mixture undergone hot pressing with temperature of at 80°C and pressure of approximately 2.5 MPa for a duration of 10 minute and was cooled at room temperature for about 16 minutes prior to removal from mold. The disc specimen was allowed to cure for about a week at room temperature. The disc specimen was 37mm in radius and 5mm in thickness. The surface of the disc that was selected to for sliding test was polished. (M. Mohmad, M. F. B. Abdollah, N. Tamaldin, H. Amiruddin 2016)

### 3.2 Surface Roughness Measurements

Surface roughness of polished surface of the disc with a profilometer. The surface roughness was measured at 10 different points on the polished surface and ranges from 0.4  $\mu\text{m}$  to 0.7  $\mu\text{m}$ .

### 3.3 Laser Surface Texturing

The PKAC epoxy composite disc specimen is patterned using a CO<sub>2</sub> laser surface patterning machine with pore diameter of 1000  $\mu\text{m}$  with depth of 500  $\mu\text{m}$ , contact ratio value of 0.21 and area density of 19%. A total of 9 PKAC epoxy disc specimen were laser patterned. According to Murashima et al. (2016), the contact ratio,  $R_C$  was obtained with equation (3.1). Zhang et al (20145) reports that the area density,  $A_p$  can be determined with equation (3.2)

$$R_C = 1 - \frac{\pi r^2}{\ell^2} \quad (3.1)$$

$$A_p = \frac{\pi r^2}{16\ell^2} \quad (3.2)$$

where  $\ell$  is the distance between dimples and  $r$  is the radius of the pore that are shown in Figure 3.3.

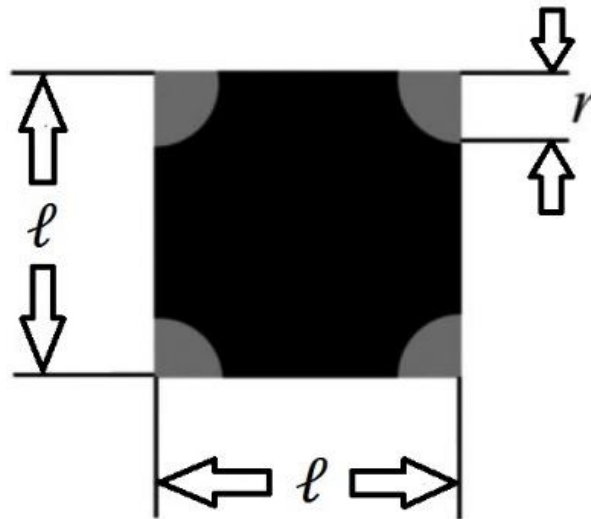


Figure 3.3: Structural parameter for patterned surface

### 3.4 Sliding Tests

Prior to the sliding tests, the carbon-chromium steel ball was cleaned in an ultrasonic bath immersed with hexane solution. The sliding experiments was performed with a ball-on-disc equipment in dry condition in room temperature. The elementary components and principals of ball-on-disc equipment is illustrated in Figure 3.4. The PKAC epoxy composite disc was first bolted on the rotating plate. Rotating duration, rotation speed, wear track diameter and applied load parameters was set on the equipment before beginning the test. Rotating duration which is derived from sliding distance,  $D_S$  of 1000m is constant in all the test can be obtain from the equation 3.5. The sliding tests are performed with different load of 5N, 10N and 15N and different speed of 100rpm, 150rpm and 200rpm on textured and non-textured PKAC disc respectively. Sliding test is conducted on SKD-II disc under 5N at 200rpm only.

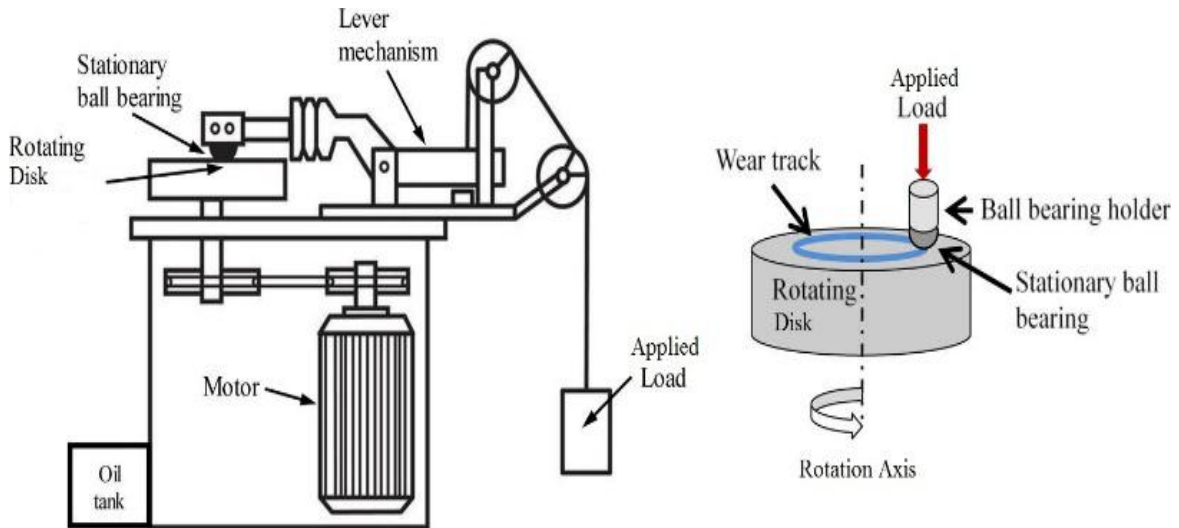


Figure 3.4: Elementary components and principal on ball-on-disk tribometer

$$D_s = 2\pi r_w N t \quad (3.5)$$

where  $r_w$  is the wear track radius,  $N$  is the rotation speed and  $t$  is the rotating duration

According to Mohmad et al. (2016), a mean coefficient of friction,  $\mu$  was obtained at the steady state region with the equation 3.6. The mean value was taken into consideration of the analysis.

$$\mu = \frac{F}{L} \quad (3.6)$$

where  $F$  is the frictional force in Newton(N) and  $L$  is the applied load in Newton(N)

### 3.5 Hardness Measurements

Hardness measurement were taken with Shore D Durometer on 3 different points of the textured and non-textured PKAC disc and SKD-II disc prior to the sliding test under load of 5N at 200rpm and is taken again on 3 different points of the wear track on the

PKAC discs and SKD-II disc after the sliding test. Average of hardness of both disc before and after sliding tests were considered in the analysis.

### 3.6 Microscopic Observation and Measurements

A microscope was then used to observe and analyze the morphology of wear tracks for both the ball bearing and discs. The wear track widths of the discs are also measured with the microscope at five different points. Average wear track widths are considered in the analysis.



## CHAPTER 4

### RESULTS AND DISCUSSIONS

#### 4.1 Physical-Mechanical properties

Mechanical properties of PKAC disc, ball bearing and SKD-II steel disc tabulated in Table 4.1.

Table 4.1: Mechanical properties of PKAC disc, ball bearing and SKD-II steel disc before sliding test under 5N at 200rpm

Properties	PKAC epoxy disc <sup>a</sup>	Carbon-chromium steel ball <sup>b</sup>	SKD-II steel disc <sup>b</sup>
Hardness, $H$ (GPa)	8.83	7.45	7.33
Density, $\rho$ (g/cm <sup>3</sup> )	1.4	7.81	7.67

<sup>a</sup>Properties are measured in the laboratory

<sup>b</sup>Properties are obtained from manufacturer

Table 4.2: Wear track hardness of different type of discs after sliding test under 5N at 200rpm

Properties	Textured PKAC epoxy disc <sup>a</sup>			Non-Textured PKAC epoxy disc			SKD-II steel disc		
	1	2	3	1	2	3	1	2	3
Hardness, $H$ (GPa)	7.453	7.455	7.451	7.450	7.453	7.457	7.340	7.320	7.330
	Average: 7.453			Average: 7.453			Average: 7.33		

Mohmad et al. (2017) reports that softening at wear track at PKAC epoxy disc is caused by the frictional heating that lower the hardness of the material. Hardness at wear track at SKD-II steel disc remain the same because of the higher melting point of the material which causes it to be unaffected by the frictional heating generated.

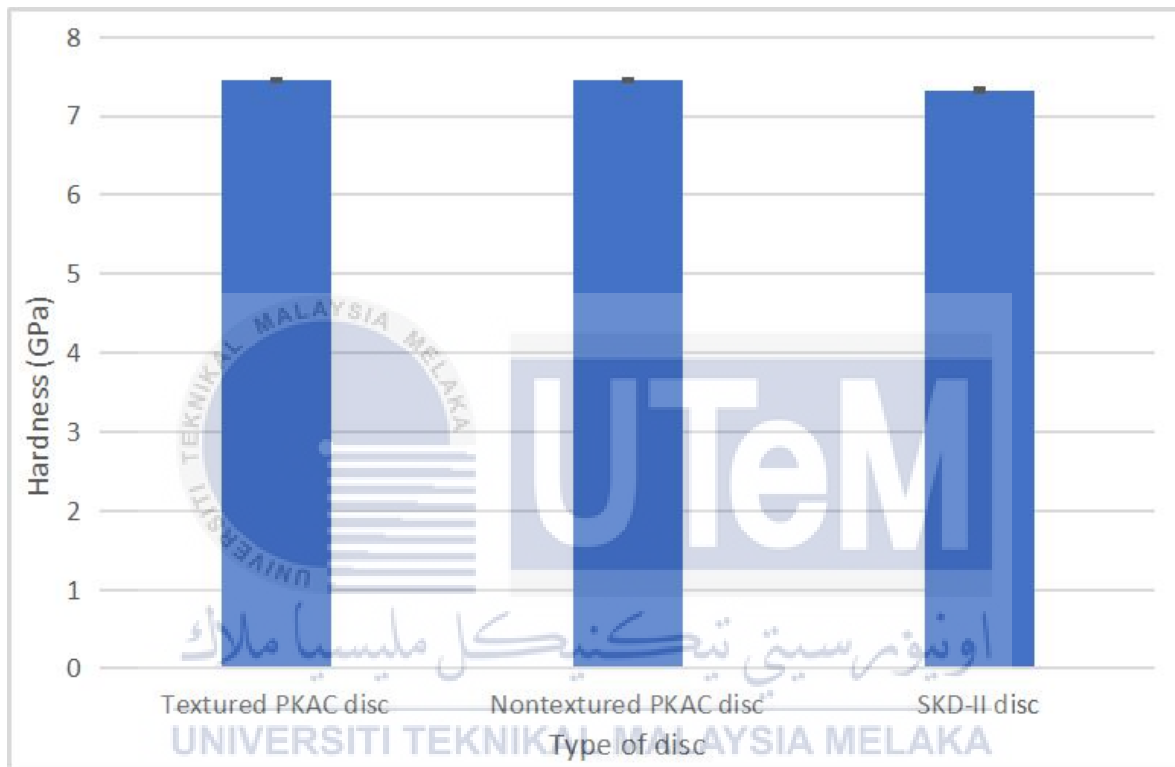


Figure 4.3 Hardness comparison between different type of discs

#### 4.2 Effect of load on the coefficient of friction

The coefficient of friction of disc from the sliding test is tabulated according to the tested parameters in Table 4.4 below.

Table 4.4: Tabulation of coefficient of friction based on their parameters

Speed(rpm) \ Load(N)	Textured PKAC disc			Non-textured PKAC disc			SKD-II disc
	5	10	15	5	10	15	5
200	0.1740	0.1630	0.1675	0.1870	0.1415	0.1414	0.53
150	0.1164	0.1527	0.1519	0.1217	0.1460	0.1506	
100	0.1420	0.1463	0.2159	0.1266	0.1365	0.1519	

Based on the trend lines plotted in Figure 4.5 and 4.6, PKAC material as a whole for textured and nontextured surface display trend of increasing coefficient of friction when applied load rises at low and moderate speed of 100rpm and 150rpm respectively. However, coefficient of friction reduces with load at high speed of 200rpm.

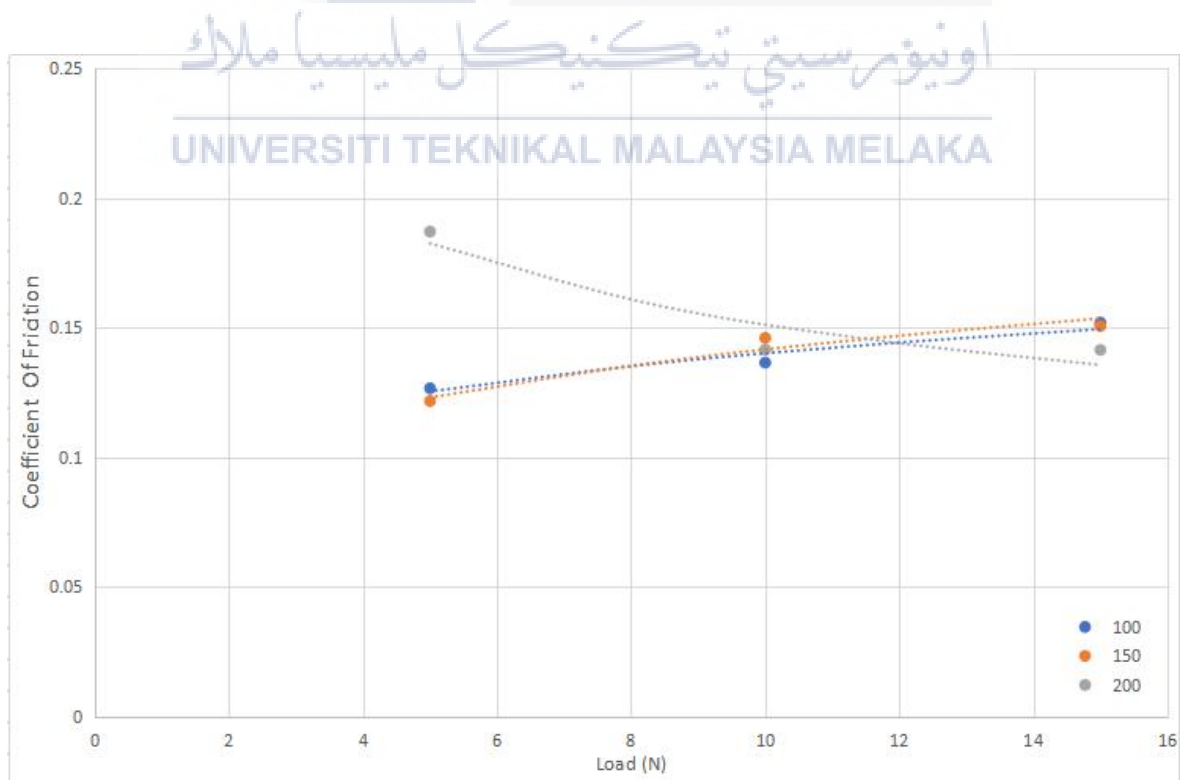


Figure 4.5: Coefficient of friction against load for non-textured disc

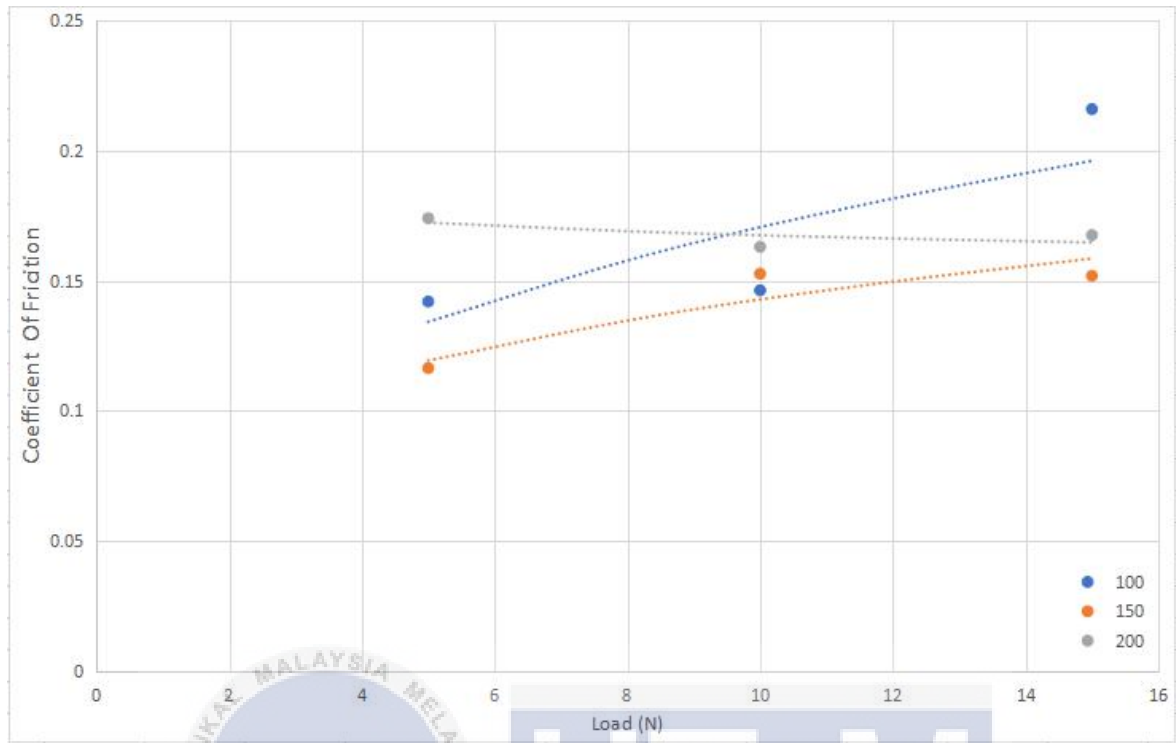


Figure 4.6: Coefficient of friction against load for textured disc

#### 4.3 Effect of sliding speed on PKAC-E disc

The coefficient of friction of disc from the sliding test is tabulated according to the tested parameters in Table 4.7 below

Table 4.7: Tabulation of coefficient of friction based on their parameters

Speed(rpm) \ Load(N)	Textured PKAC disc			Non-textured PKAC disc			SKD-II disc
	100	150	200	100	150	200	200
5	0.142	0.1164	0.1740	0.1266	0.1217	0.1870	0.53
10	0.1463	0.1527	0.1630	0.1365	0.1460	0.1415	
15	0.2159	0.1519	0.1675	0.1519	0.1415	0.1519	

Based on the trend lines plotted in Figure 4.8 and 4.9, PKAC material as a whole for textured and nontextured surface display trend of increasing coefficient of friction when sliding speed rises at low and moderate applied load of 5N and 10N respectively. However, coefficient of friction reduces with load at high speed of 15N. It can be seen that sliding speed affects coefficient of friction of PKAC similarly to load.

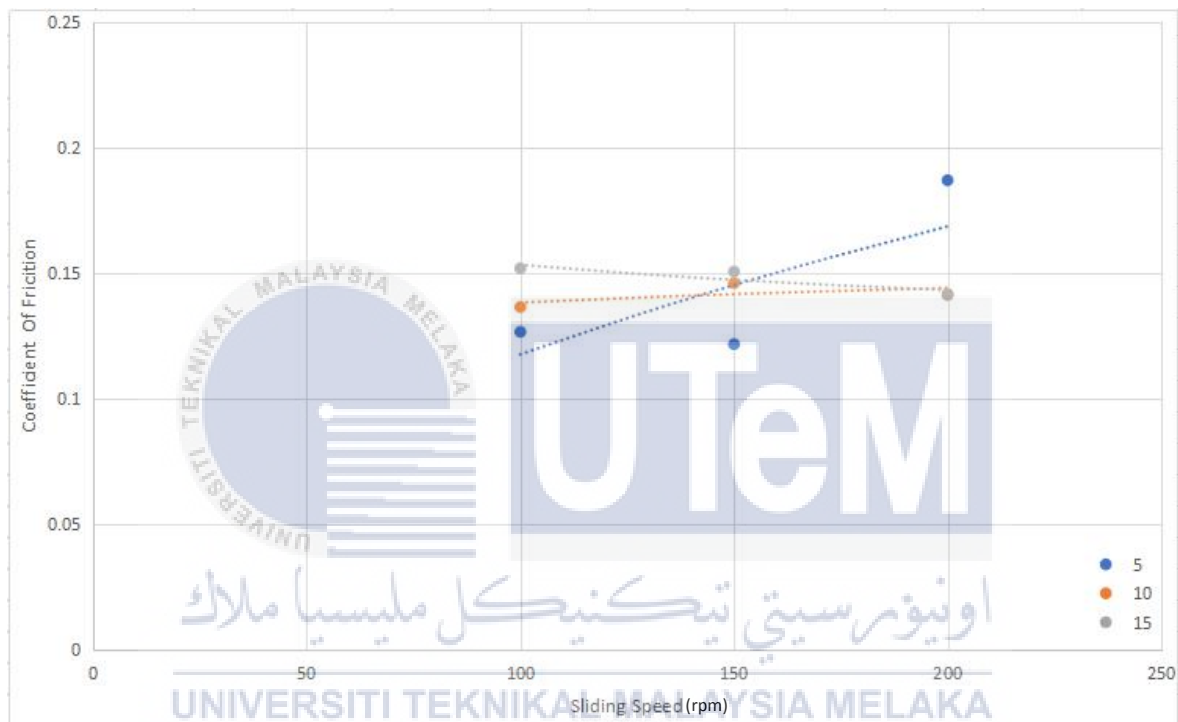


Figure 4.8: Coefficient of friction against sliding speed for non-textured disc

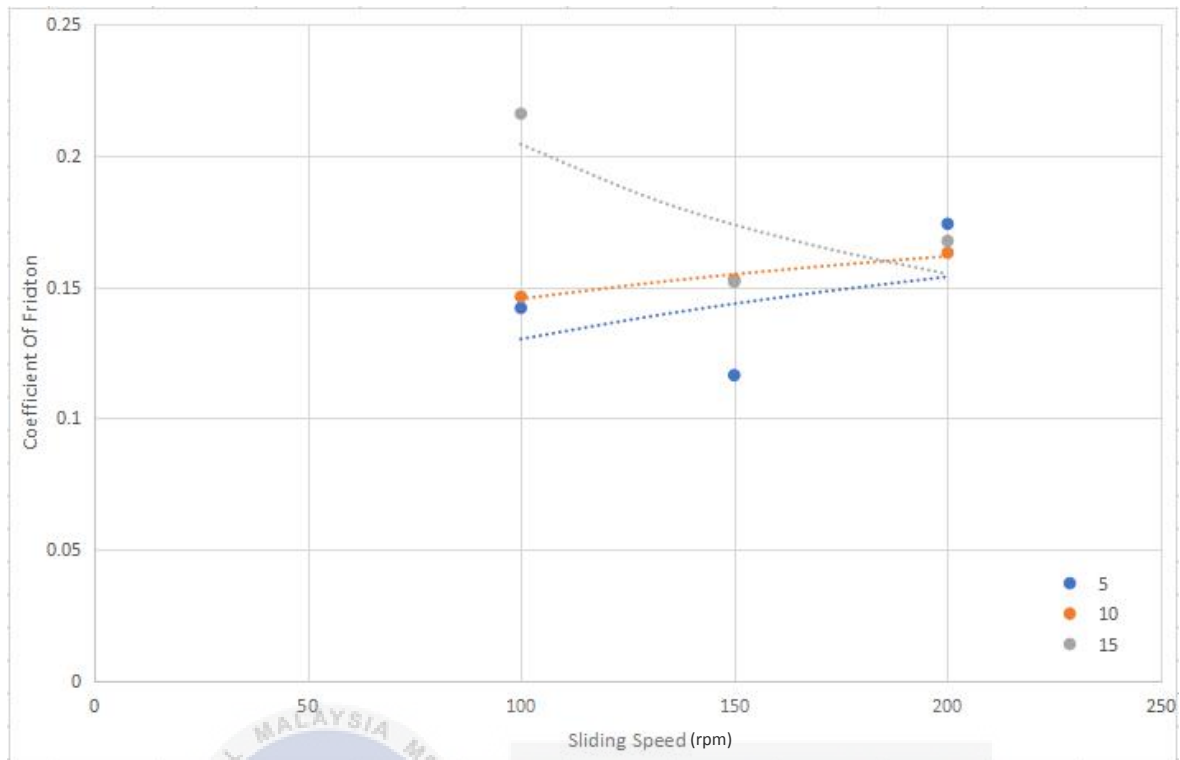


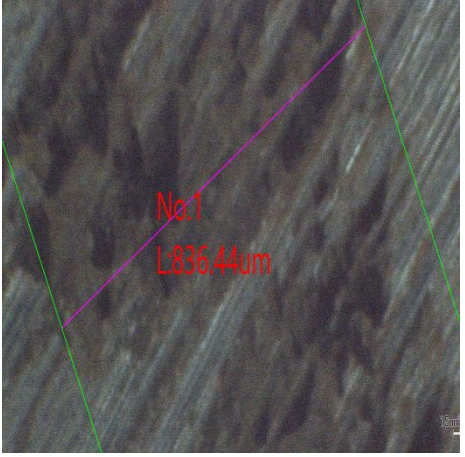
Figure 4.9: Coefficient of friction against sliding speed for textured disc

#### 4.4 Wear track morphology of disc and ball bearing analysis

##### 4.4.1 Wear track morphology of disc and ball bearing analysis for SKD-II disk

As seen in table 4.10, the average disc wear track width obtained for SKD-II disk is 877.568  $\mu\text{m}$ . No material transfer can be observed on the ball bearing wear track as seen in Table 4.9

Table 4.10: Tabulation of wear track morphology of ball bearing and disc of SKD-II disc

Parameters (Speed\Load)	Ball bearing wear track	Disc wear track
(200rpm\5N)		

#### 4.4.2 Wear track morphology of disc and ball bearing analysis for non-textured PKAC disk

The average width of wear track of non-textured PKAC-E disc under 5N at 200rpm obtained is 289.686  $\mu\text{m}$ . Slight carbon transfer in the form of black lines and rusting can be observed on the ball bearing wear track as shown in Table 4.11.

The average width of wear track of non-textured PKAC-E disc under 5N at 150 rpm obtained is 266.88  $\mu\text{m}$ . Moderate carbon transfer in the form of black lines can be observed on the ball bearing wear track as shown in Table 4.11.

The average width of wear track of non-textured PKAC-E disc under 5N at 100 rpm obtained is 240.454 $\mu\text{m}$ . A lot of carbon transfer in the form of black lines can be observed on the ball bearing wear track as shown in Table 4.11.

The average width of wear track of non-textured PKAC-E disc under 10N at 200 rpm obtained is 360.328  $\mu\text{m}$ . A lot of carbon transfer in the form of black lines can be observed on the ball bearing wear track as shown in Table 4.11.

The average width of wear track of non-textured PKAC-E disc under 10N at 150rpm obtained is 343.398 $\mu\text{m}$ . Moderate carbon transfer in the form of black lines can be observed on the ball bearing wear track as shown in Table 4.11.

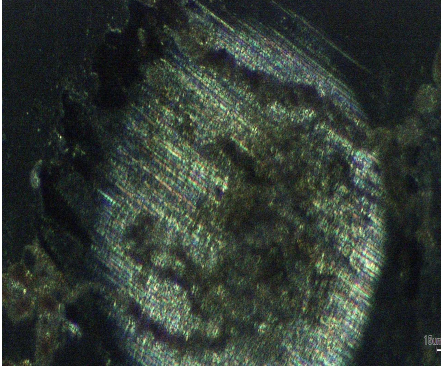
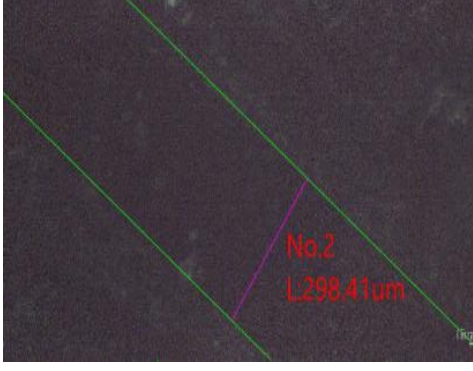
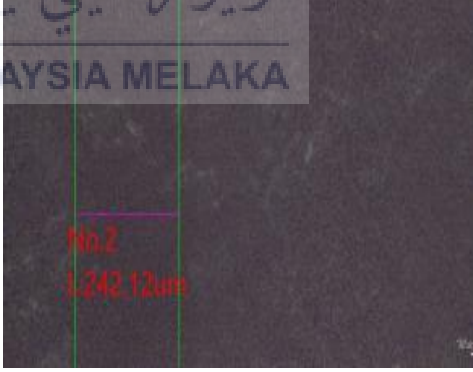
The average width of wear track of non-textured PKAC-E disc under 10N at 100rpm obtained is 310.724 $\mu\text{m}$ . Moderate carbon transfer in the form of black lines can be observed on the ball bearing wear track as shown in Table 4.11.

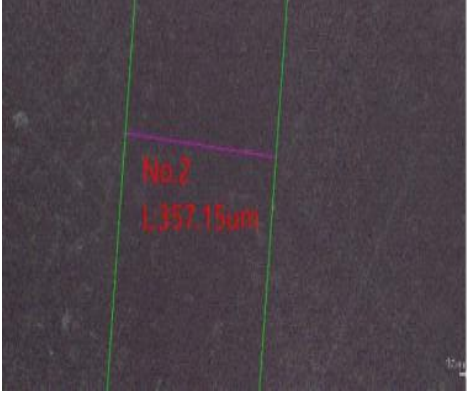
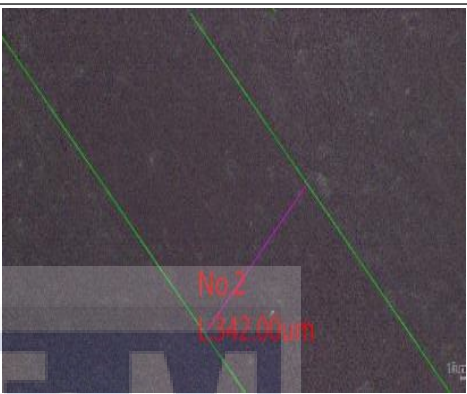
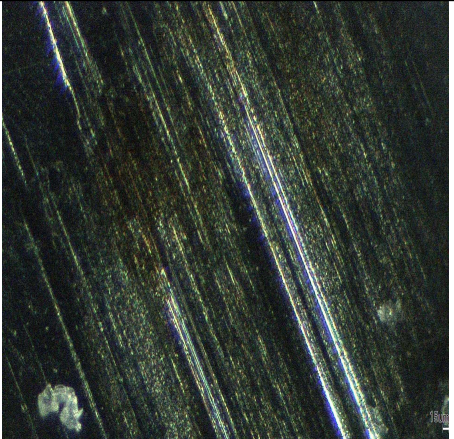
The average width of wear track of non-textured PKAC-E disc under 15N at 200rpm obtained is 427.372 $\mu\text{m}$ . A lot of carbon transfer in the form of black lines can be observed on the ball bearing wear track as shown in Table 4.11.

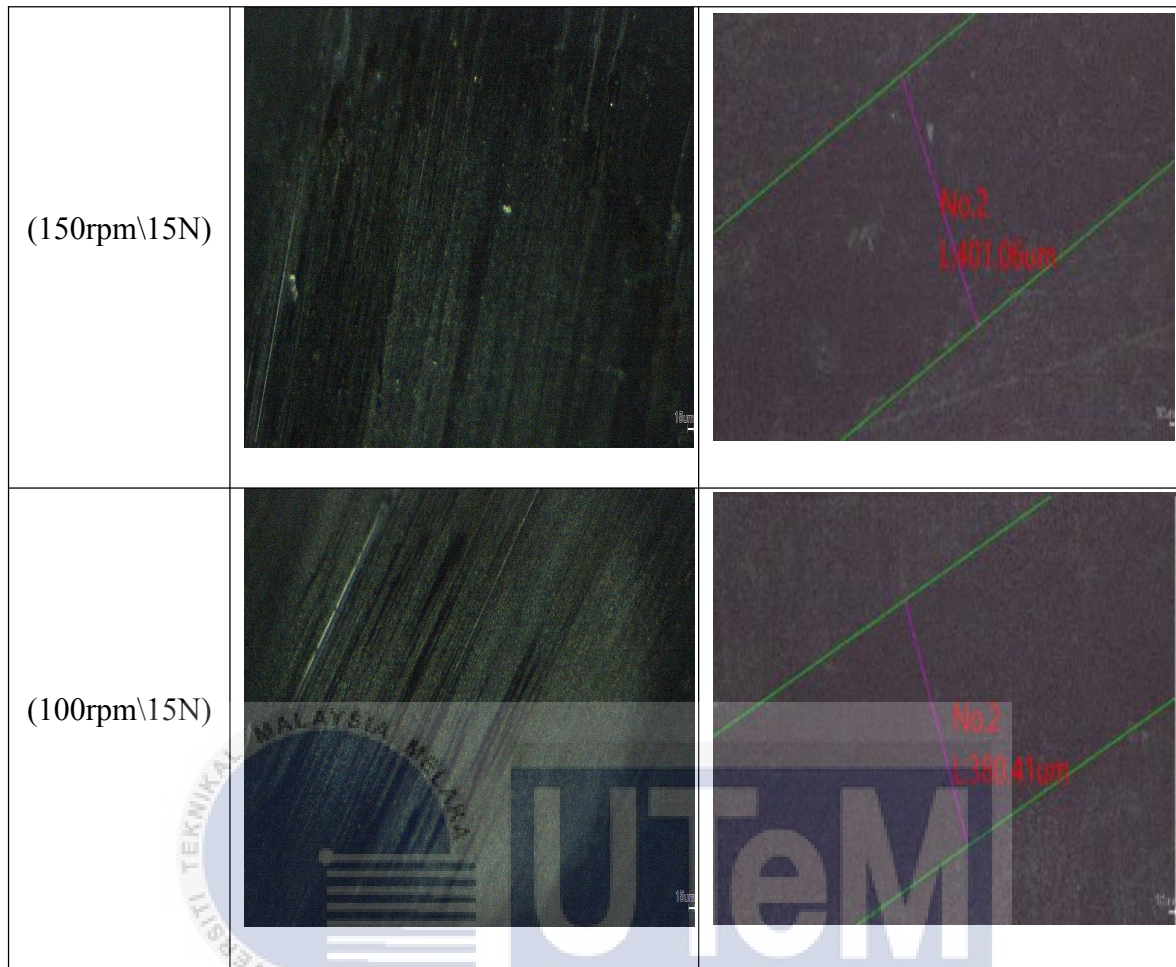
The average width of wear track of non-textured PKAC-E disc under 15N at 150 rpm obtained is 400.904 $\mu\text{m}$ . A lot of carbon transfer in the form of black lines can be observed on the ball bearing wear track as shown in Table 4.11.

The average width of wear track of non-textured PKAC-E disc under 15N at 100 rpm obtained is 379.87 $\mu\text{m}$ . Moderate carbon transfer in the form of black lines can be observed on the ball bearing wear track. as shown in Table 4.11.

Table 4.11: Tabulation of wear track morphology of ball bearing and disc of nontextured PKAC disc

Parameters (Speed\Load)	Ball bearing wear track	Disc wear track
(200rpm\5N)		
(150rpm\5N)		
(100rpm\5N)		

<p>(200rpm\10N)</p>		
<p>(150rpm\10N)</p>		
<p>(100rpm\10N)</p>		
<p>(200rpm\15N)</p>		



#### 4.4.3 Wear track morphology of disc and ball bearing analysis for textured PKAC disk

The average width of wear track of textured PKAC-E disc under 5N at 150 rpm obtained is 389.826 $\mu$ m. A lot of carbon transfer in the form of black lines can be observed on the ball bearing wear track as shown in Table 4.12.

The average width of wear track of textured PKAC-E disc under 5N at 200 rpm is 371.846 $\mu$ m. Moderate carbon transfer in the form of black lines can be observed on the ball bearing wear track in Table 4.12.

The average width of wear track of textured PKAC-E disc under 5N at 100 rpm obtained is 359.474 $\mu$ m. Slight carbon transfer in the form of black lines can be observed on the ball bearing wear track as shown in Table 4.12.

The average width of wear track of textured PKAC-E disc under 10N at 200 rpm obtained is 506.944 $\mu$ m. Moderate carbon transfer in the form of black lines can be observed on the ball bearing wear track as shown in Table 4.12.

The average width of wear track of textured PKAC-E disc under 10N at 150 rpm obtained is 420.84 $\mu$ m. Slight carbon transfer in the form of black lines can be observed on the ball bearing wear track as shown in Table 4.12.

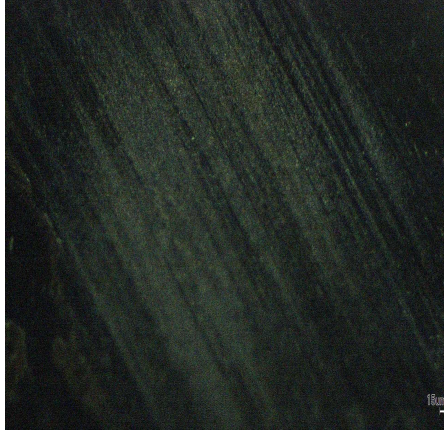
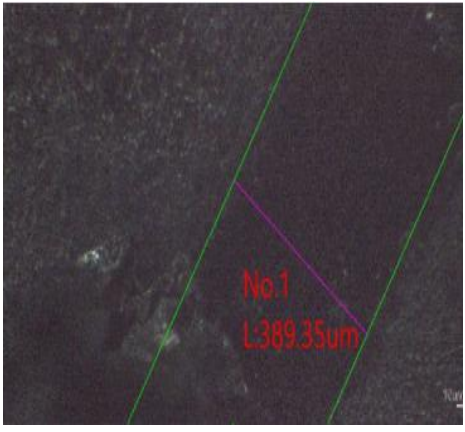
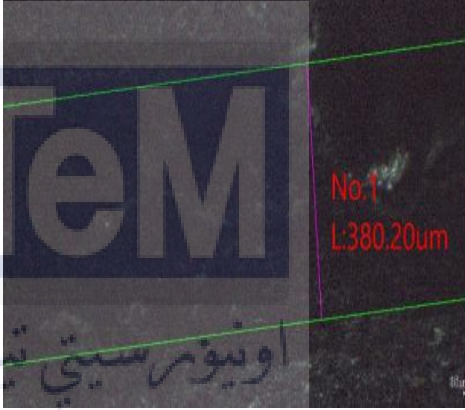
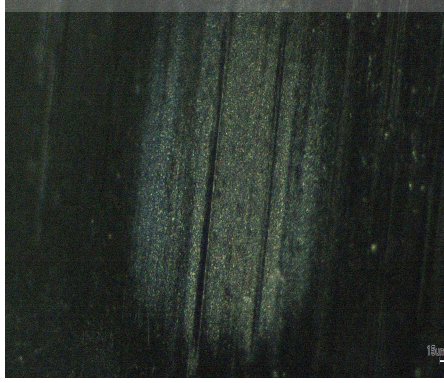
The average width of wear track of textured PKAC-E disc under 10N at 100 rpm are obtained is 409.282 $\mu$ m. Slight carbon transfer in the form of black lines can be observed on the ball bearing wear track. as shown in Table 4.12.

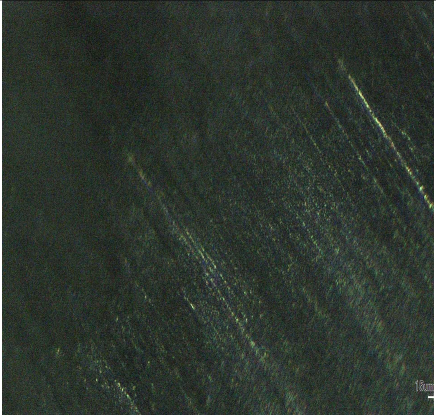
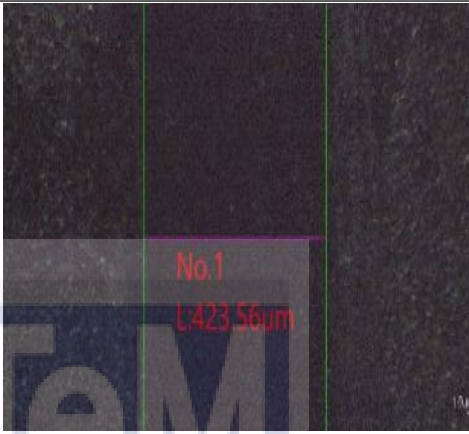
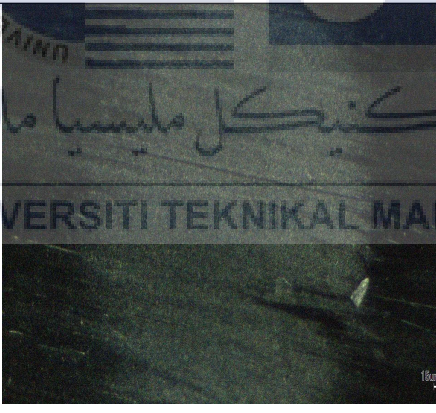
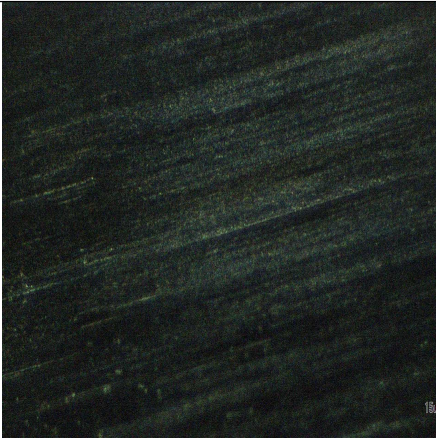
The average width of wear track of textured PKAC-E disc under 15N at 200 rpm obtained is 532.234 $\mu$ m. A lot of carbon transfer in the form of black lines can be observed on the ball bearing wear track as shown in Table 4.12

The average width of wear track of textured PKAC-E disc under 15N at 150 rpm obtained is 442.862 $\mu$ m. Moderate carbon transfer in the form of black lines can be observed on the ball bearing wear track. as shown in Table 4.12

The average width of wear track of non-textured PKAC-E disc under 15N at 100 rpm obtained is 443.838 $\mu$ m. Slight carbon transfer in the form of black lines can be observed on the ball bearing wear track as shown in Table 4.12.

Table 4.12: Tabulation of wear track morphology of ball bearing and disc of textured PKAC disc

Parameters (Speed\Load)	Ball bearing wear track	Disc wear track
(200rpm\5N)		
(150rpm/5N)		
(100rpm/5N)		

<p>(200rpm/10N)</p>		 <p>No.1 L:531.79um</p>
<p>(150rpm/10N)</p>		 <p>No.1 L:423.56um</p>
<p>(100rpm/10N)</p>		 <p>No.2 L:410.66um No.1 L:408.78um</p>
<p>(200rpm/15N)</p>		 <p>No.1 L:534.36um</p>

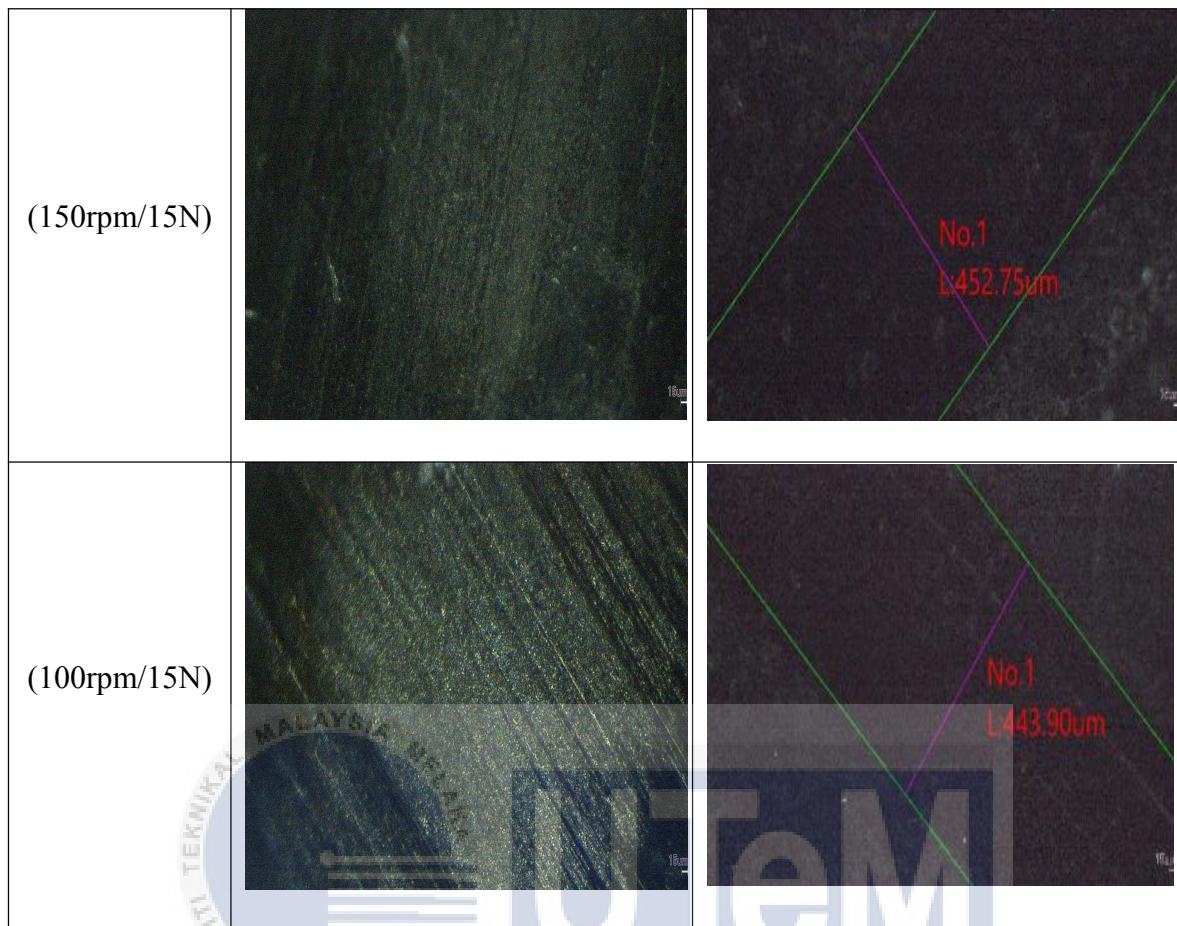


Table 4.13 tabulates the wear track width of different types of disc based on their tested parameters.

Table 4.13: Tabulation of wear track width of different types of disc in  $\mu\text{m}$  according to their tested parameters

Speed(rpm) Load(N)	Textured PKAC disc			Non-textured PKAC disc			SKD-II disc
	100	150	200	100	150	200	200
5	359.474	371.846	389.826	240.454	266.88	289.686	877.568
10	409.282	423.84	506.944	310.724	343.398	360.328	
15	443.838	442.862	532.234	379.87	400.904	427.372	

#### 4.5 Effect of surface texturization on coefficient of friction for PKAC-E disc

Based on Figure 4.14, it can be seen that at 100rpm, the coefficient of friction rises with load. However, nontextured disc produced lower coefficient of friction at all load compared to textured disc.

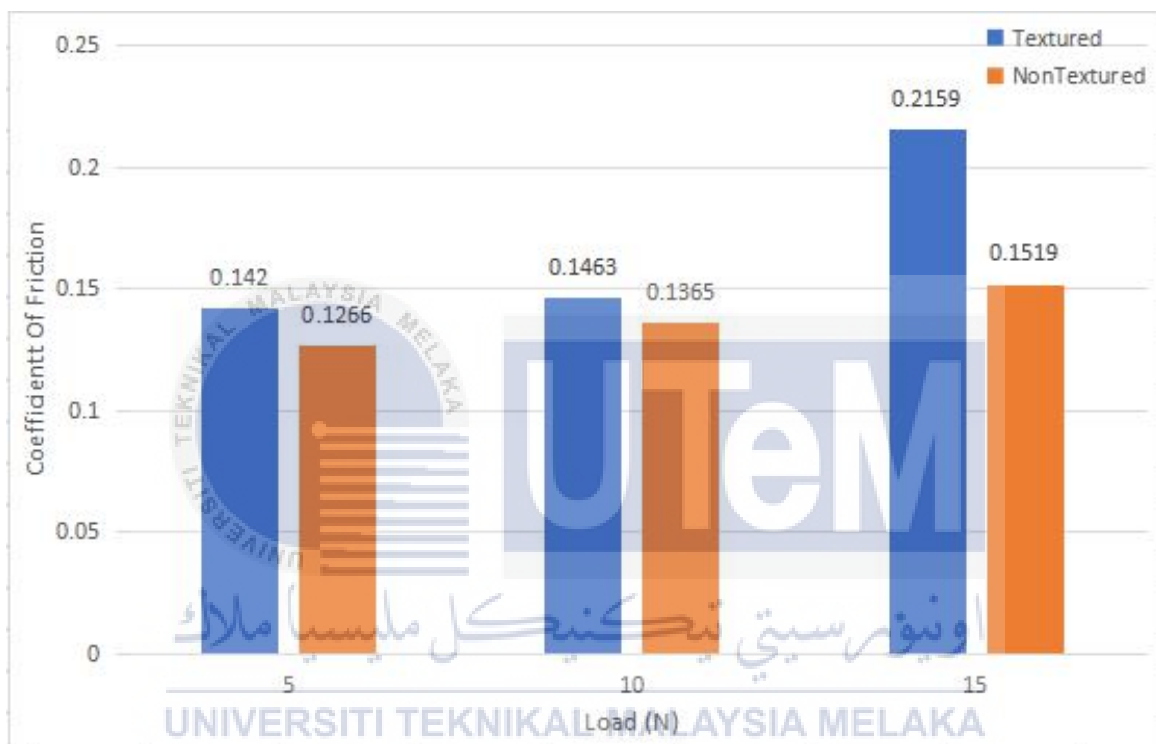


Figure 4.14: Coefficient of friction against load for 100rpm

Based on Figure 4.15, when the sliding speed is 150rpm, coefficient of friction is lower at moderate and high load which is 10N and 15N respectively for nontextured disc. However, under low load of 5N, textured disc produces a lower coefficient of friction than nontextured.



Figure 4.15: Coefficient of friction against load for 150rpm

Similar trend is also portrayed when the sliding speed is 200rpm as shown in Figure 4.16. Coefficient of friction is lower for textured disc for low load of 5N. However, coefficient of friction for textured disc is higher than nontextured when both disc is under 10N and 15N at 200rpm. Therefore, it is shown that surface texturization only manages to lower the coefficient of friction at low load of 5N at moderate and high speed of 150rpm and 200rpm.



Figure 4.16: Coefficient of friction against load for 200rpm

The varying trend of coefficient of friction (COF) for textured and non-textured disc is due to carbon transfer in the form black lines to the ball bearing contact surface. Under 5N of load and sliding speed of 200rpm, a lot of carbon in the form of black lines are transferred to the ball bearing in textured disc compared to non-textured disc as shown in Figure 4.17. Mohmad et al.(2017) reports that high carbon transfer from PKAC-E disc to ball bearing changes the contact patch from carbon-to-steel to carbon-to-carbon contact. This resulted in lower COF in nontextured disc compared to textured disc as there are more carbon-to-carbon contact in the non-textured disc.

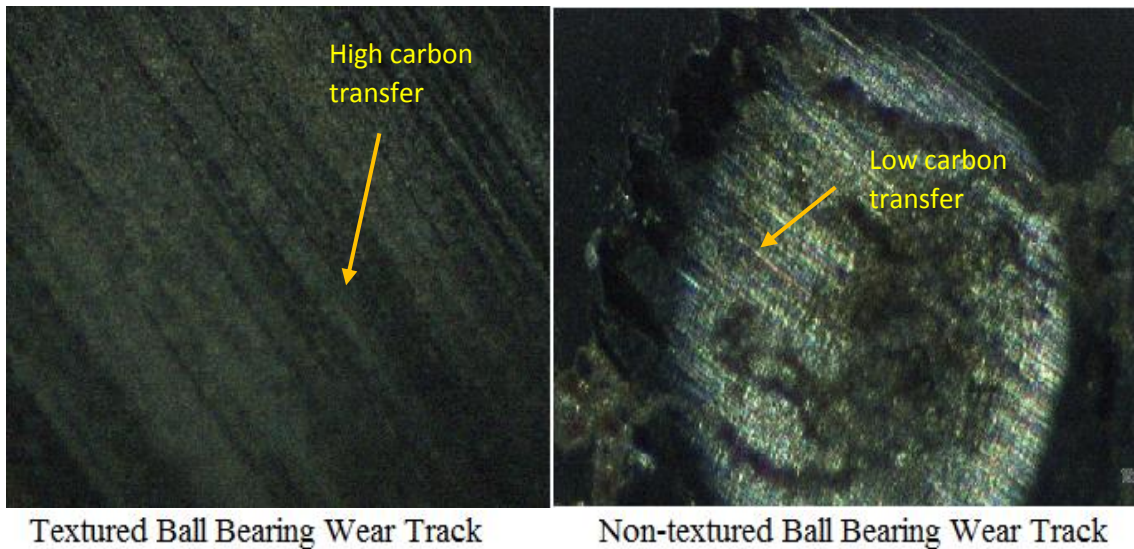


Figure 4.17: Carbon Transfer on Ball Bearing Surface Comparison for 5N at 200rpm

Under 5N of load and sliding speed of 150rpm, both ball bearing wear track display moderate carbon transfer to ball bearing as shown in Figure 4.18. This cause a small difference in COF in both disc of 0.0053. This is also similar when sliding speed is 150rpm and load is 15 N as shown in Figure 4.19 and the tiny difference in COF of both disc is 0.0013.

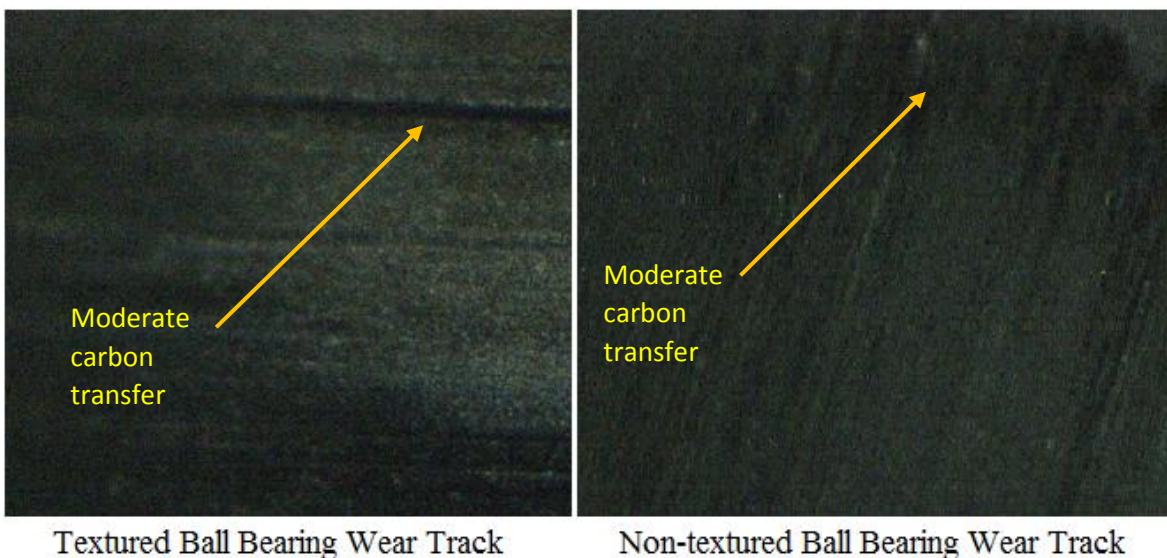
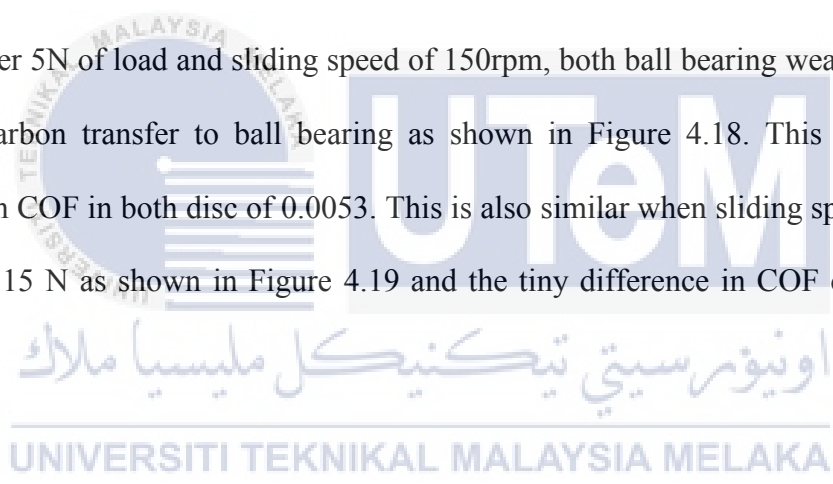


Figure 4.18: Carbon Transfer on Ball Bearing Surface Comparison for 5N at 150rpm

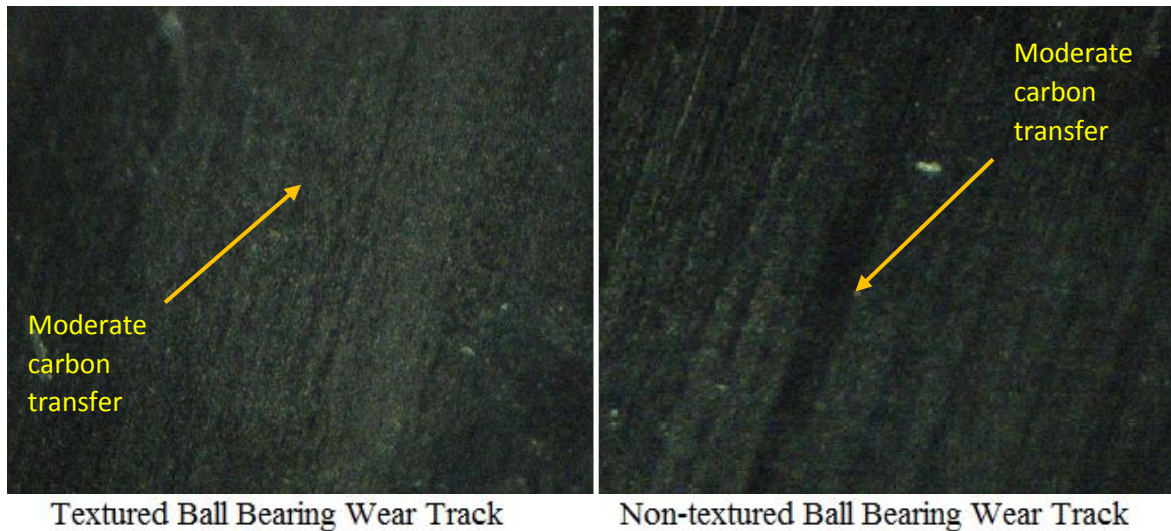


Figure 4.19: Carbon Transfer on Ball Bearing Surface Comparison for 15N at 150rpm

Under 5N of load and sliding speed of 100rpm, higher amount of carbon transferred to the ball bearing in non-textured disc compared to textured disc as shown in Figure 5.20. Resulting in more carbon-to-carbon contact which significantly lower the COF. This is also similar when the conditions are 10N and 200rpm, 10N and 150rpm, 10N and 100rpm, 15N and 200rpm and 15N and 100rpm as shown in Figure 4.21, 4.22, 4.23, 4.24 and 4.25. The lower penetration of carbon into ball bearing contact surface for textured disc is due to dimples that traps the carbon debris produced from wear compared to non-textured surface that allows carbon debris to accumulate on the surface as illustrated in Figure 4.26. The accumulated carbon debris then can penetrate the ball bearing contact surface to produce the carbon-to carbon contact patch.

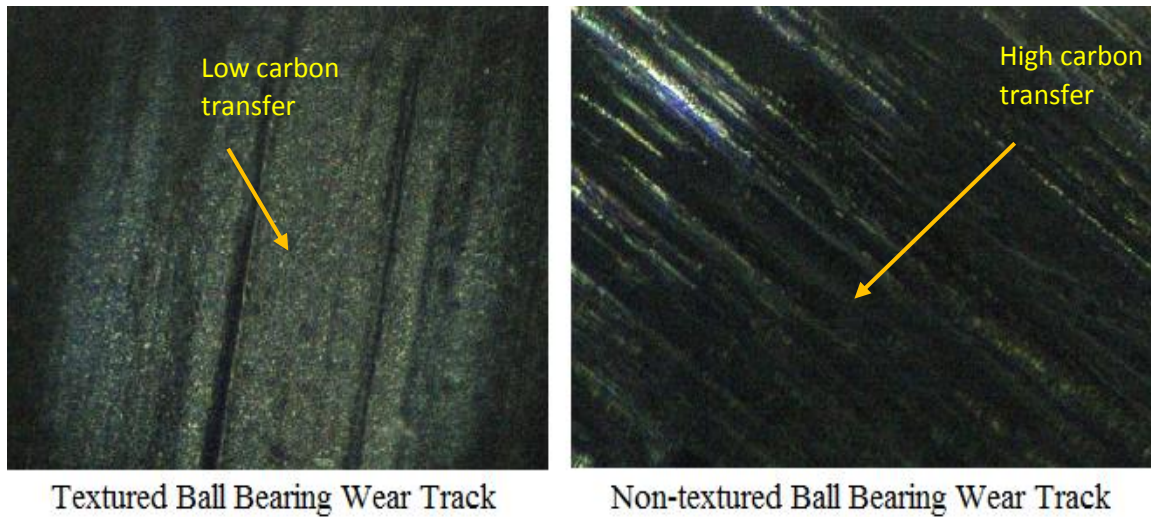


Figure 4.20: Carbon Transfer on Ball Bearing Surface Comparison for 5N at 100rpm

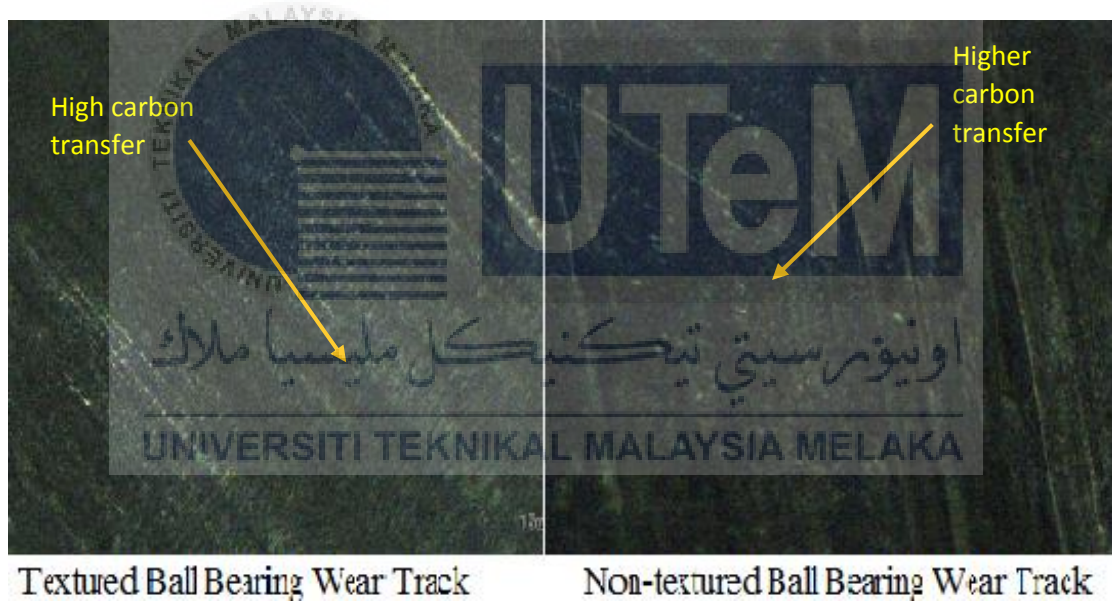


Figure 4.21: Carbon Transfer on Ball Bearing Surface Comparison for 10N at 200rpm

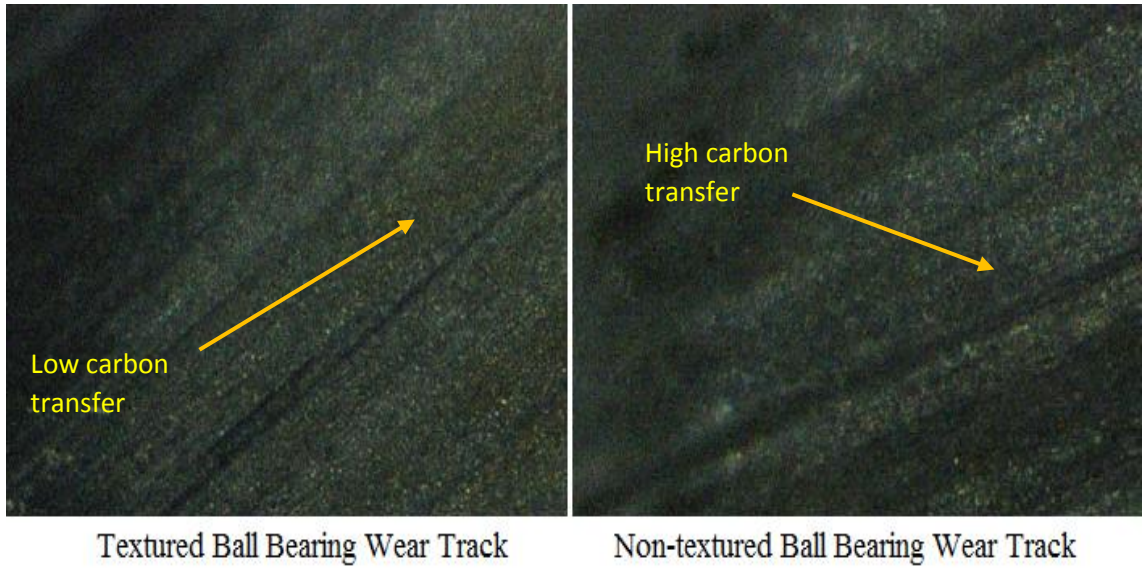


Figure 4.22: Carbon Transfer on Ball Bearing Surface Comparison for 10N at 150rpm

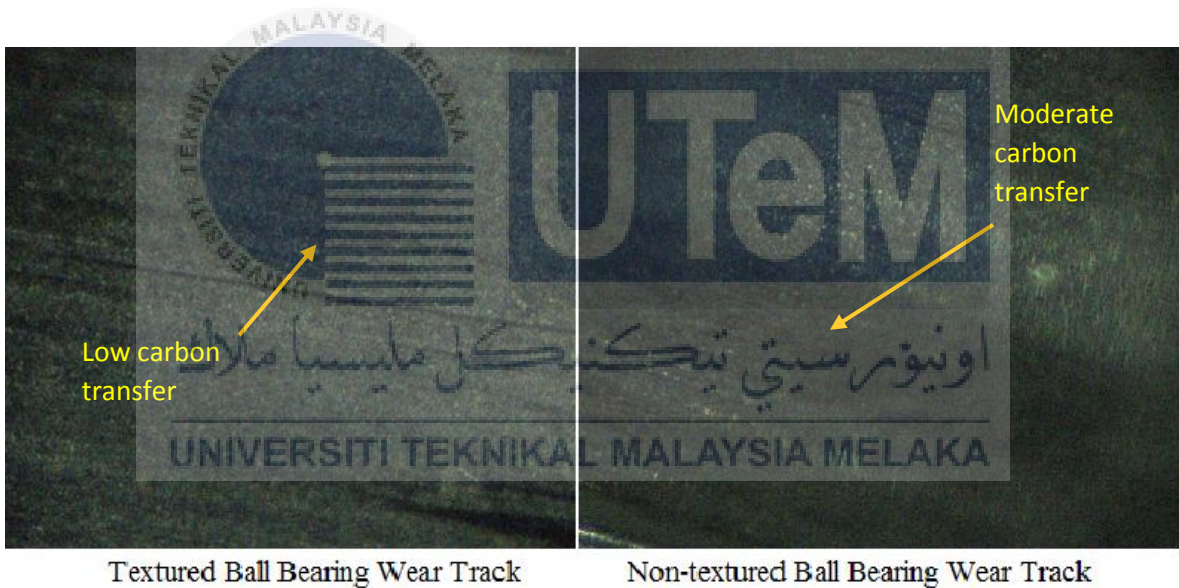


Figure 4.23: Carbon Transfer on Ball Bearing Surface Comparison for 10N at 150rpm

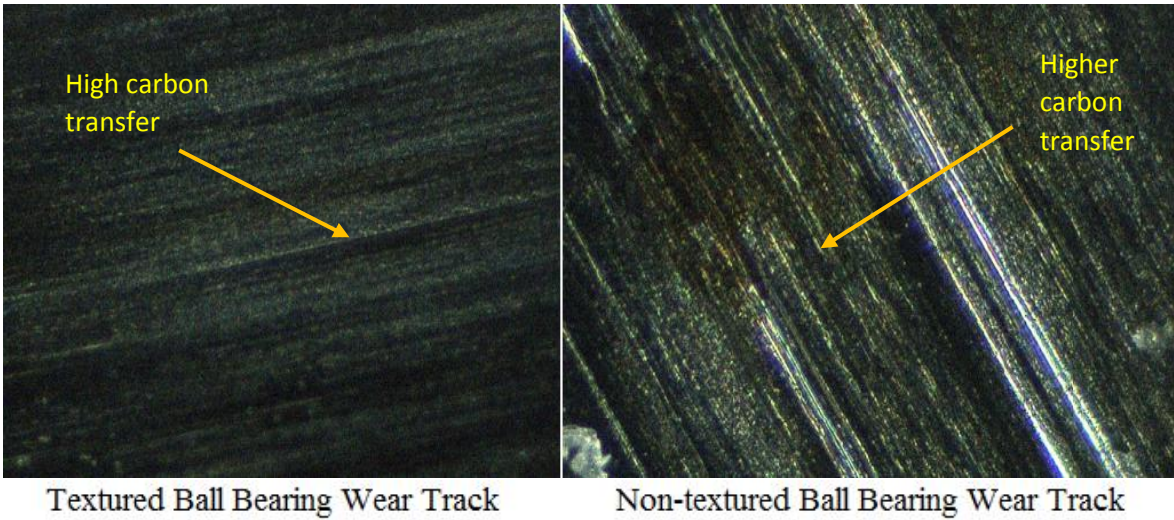


Figure 4.24: Carbon Transfer on Ball Bearing Surface Comparison for 15N at 200rpm



Figure 4.25 : Carbon Transfer on Ball Bearing Surface Comparison for 15N at 100rpm

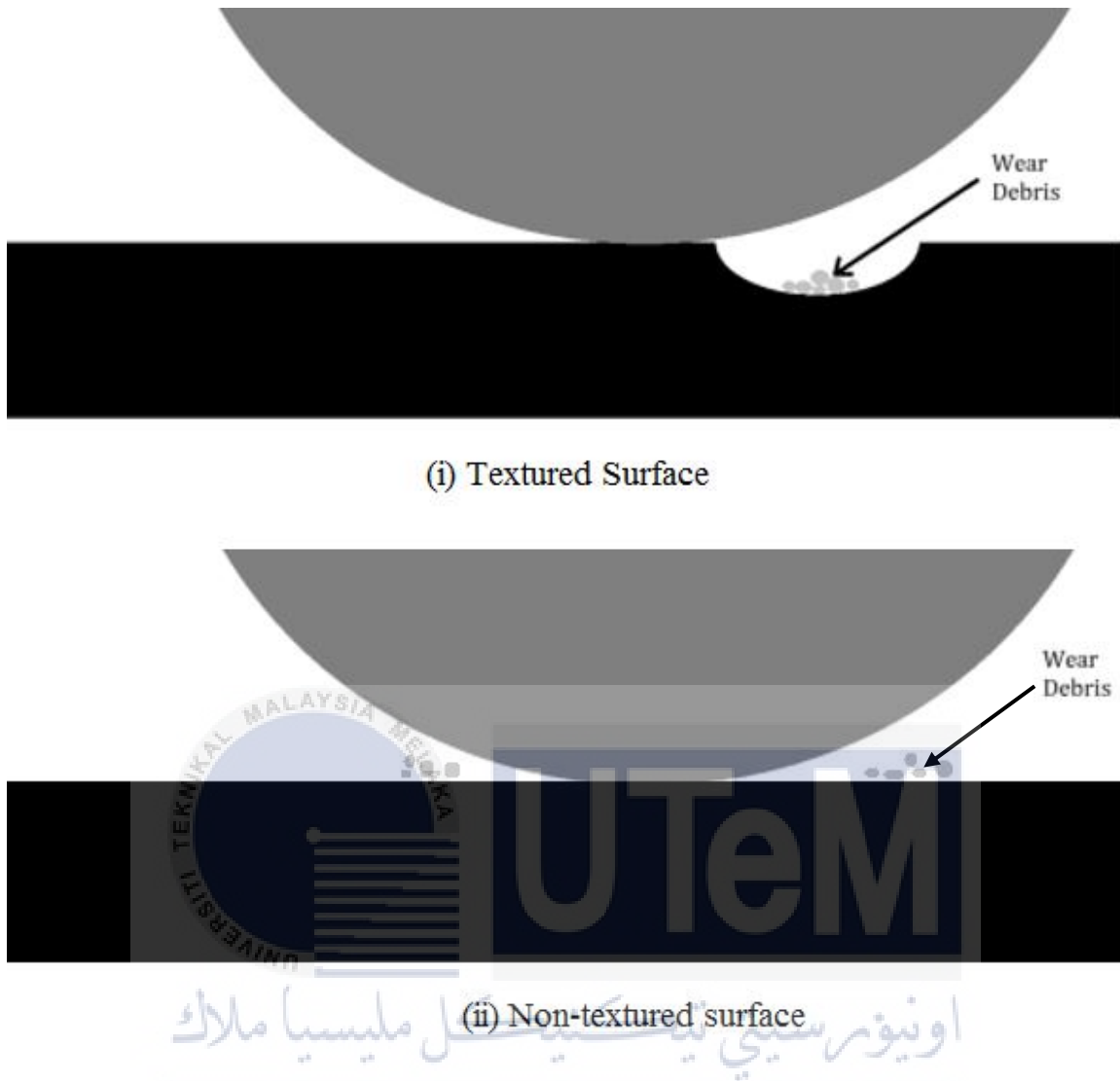


Figure 4.26: Trapping of Wear Debris on (i) Textured Surface (ii) Textured Surface

#### 4.6 Effect of surface texturization on wear of PKAC-E disc

The trend observed in Figure 4.27, 4.28 and 4.29 is wear track width increases with sliding speed and load for both textured and non-textured disc. However, textured disc exhibits larger wear track width than non-textured disc in any of the conditions tested. A larger wear track width will increase the wear of the disc and its corresponding contact surface. .

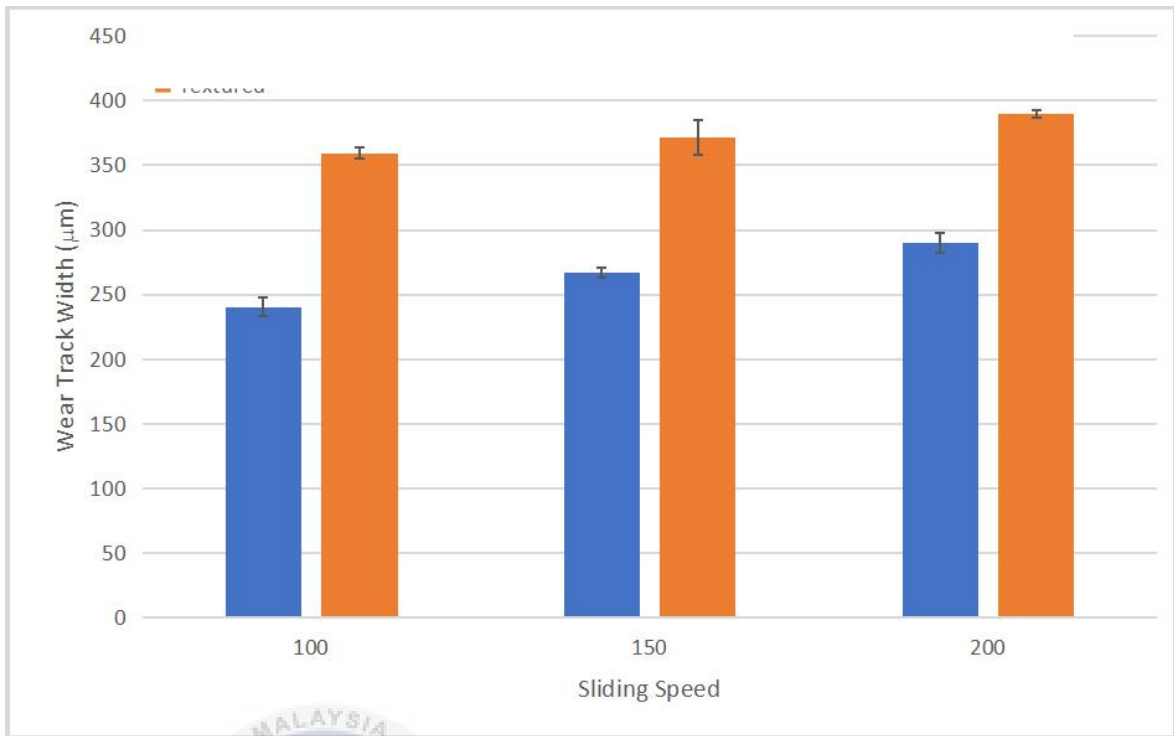


Figure 4.27: Disc Wear Track Width Against Sliding Speed for 5N

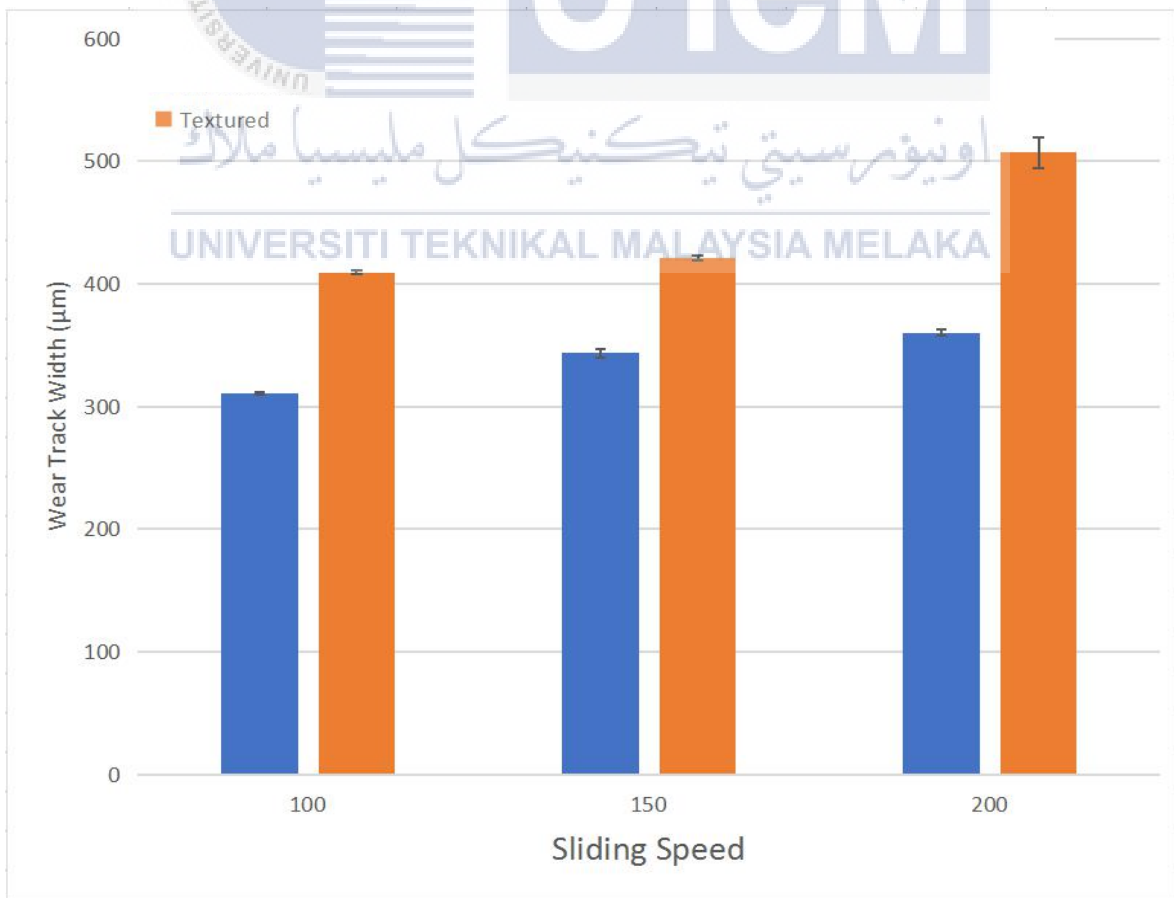


Figure 4.28: Disc Wear Track Width Against Sliding Speed for 10N

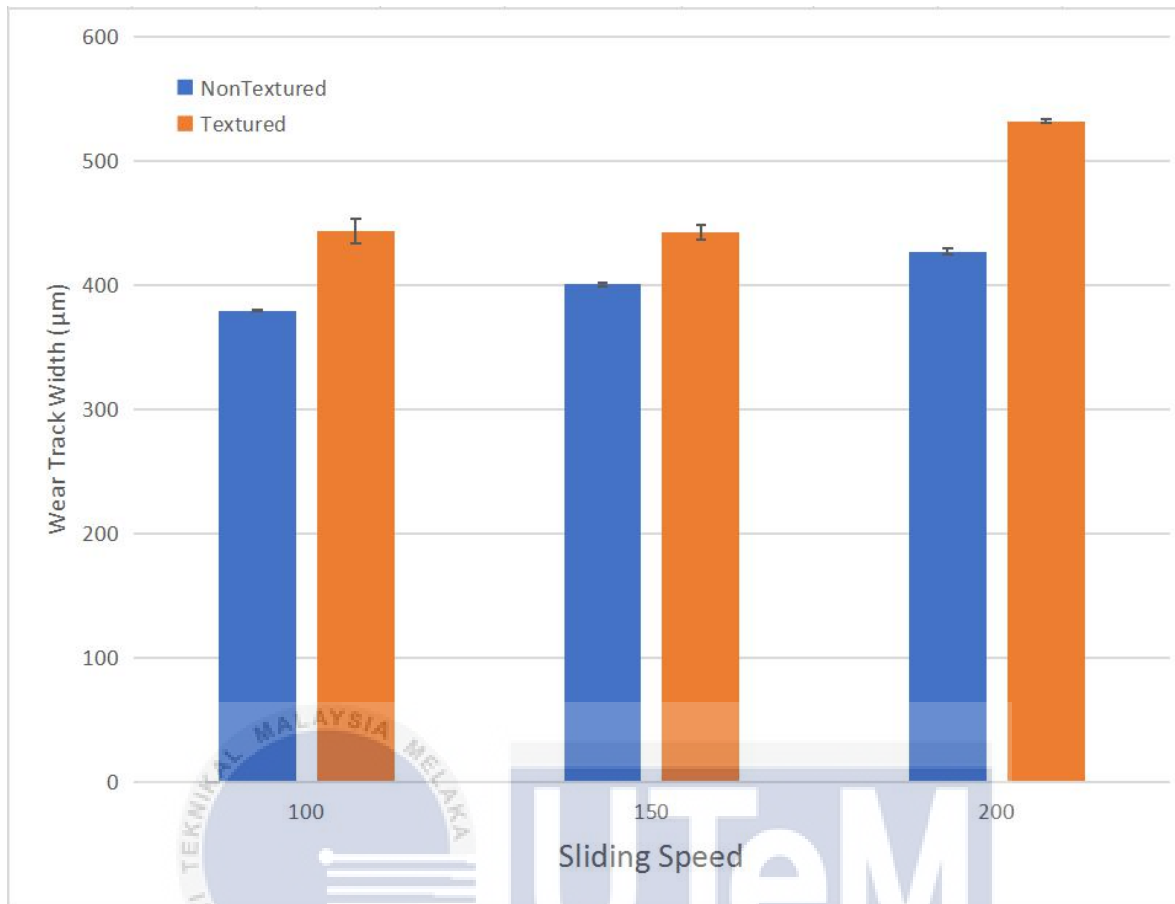


Figure 4.29: Disc Wear Track Width Against Sliding Speed for 15N

#### 4.7 Performance of SKD-II disc and PKAC-E disc as bearing material

The average steady state COF of textured and non-textured PKAC disc is lower than SKD-II disc at 200RPM under load of 5N. The average steady state COF achieved in textured and non-textured PKAC disc are 0.174 and 0.187 respectively while SKD-II achieved steady state COF of 0.53 as shown in Figure 4.30. This due to the carbon penetrating ball bearing phenomena that occur in PKAC-E disc changing the contact patch from carbon-to-steel to carbon-carbon which significantly lower the coefficient of friction. This carbon penetration phenomena is missing in SKD-II disc. However, PKAC-E disc will not have lifespan as a bearing material due to softening that occur on wear track. PKAC-E disc should have a nontextured surface to improve longevity due to its smaller

wear track width as shown in Figure 4.28. Softening does not occur to SKD-II disc but the significantly wider wear track on the SKD-II disc shows that longevity is also an issue for this material as shown in Figure 4.31.



Figure 4.30: Coefficient of Friction Comparison Between Different Type Of Discs under 5N at 200rpm

UNIVERSITI TEKNIKAL MALAYSIA MELAKA

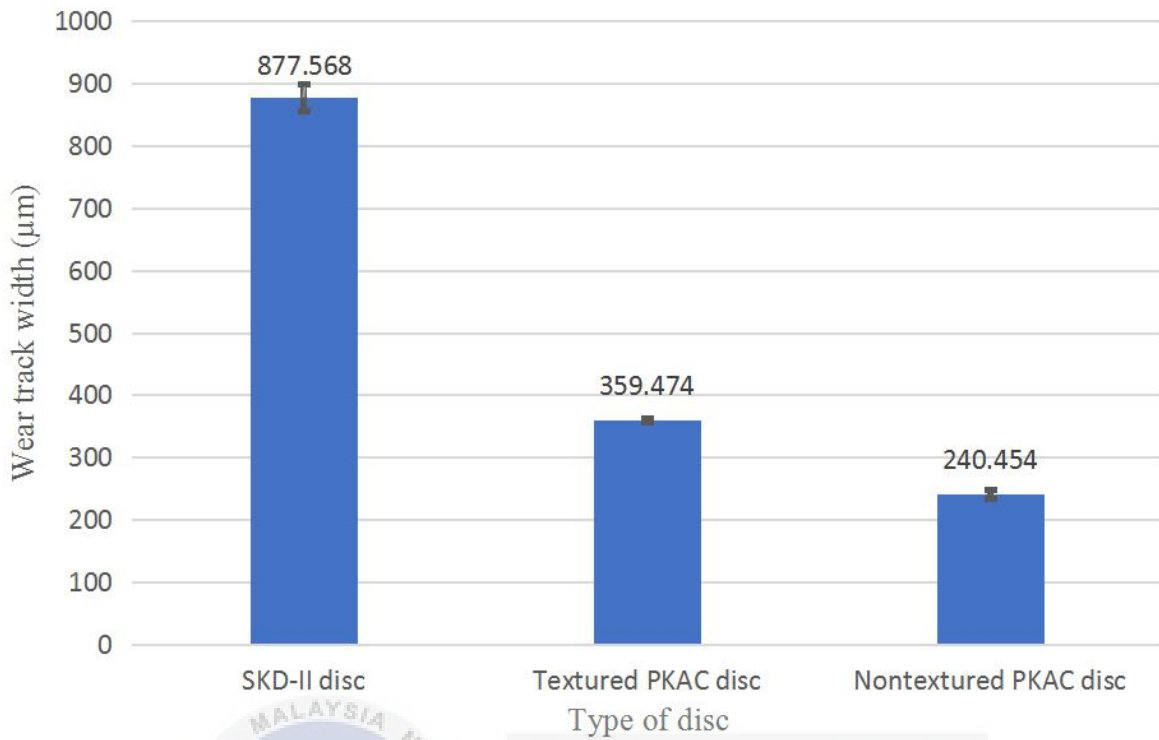


Figure 4.31: Wear track width comparison between different type of discs under 5N at 200rpm



## CHAPTER 5

### CONCLUSION AND RECOMMENDATIONS

#### 5.1 Conclusion

There are two main objectives in this project. They are to investigate the effect of load-speed on tribological performance of surface textured palm kernel activated carbon reinforced polymeric composite and to compare the performance of surface textured palm kernel activated carbon reinforced polymeric composite with conventional bearing material. In order to investigate the effect of load-speed on tribological performance of surface textured palm kernel activated carbon reinforced polymeric composite, three speed parameters and three load parameters are chosen. The speed parameters are 100rpm, 150rpm and 200rpm. The load parameters are 5N, 10N and 15N. The conventional bearing material chosen is SKD-II steel.

By running a ball on disk test with load of 5N at 200rpm on the textured PKAC-E disc, non-textured PKAC disc and the SKD-II steel disc, palm kernel activated carbon reinforced polymeric composite has demonstrated to be the superior bearing material whether with textured or flat surface as it generates a significantly lower average steady state coefficient of friction of 0.174 for textured surface and 0.187 for flat surface compared to SKD-II disc that produces average steady state coefficient of friction of 0.53. However, it was tested that PKAC-E material undergone softening at the wear track that reduces its hardness from 8.83 GPa to 7.453 GPa due to frictional heating. PKAC-E

material should have a nontextured surface to improve longevity due to its smaller wear track width. Softening does not occur to SKD-II disc but the significantly wider wear track on the SKD-II disc shows that longevity is also an issue for this material. Therefore, palm kernel activated carbon reinforced polymeric composite material is a superior bearing material.

As sliding speed increases, coefficient of friction increases for 5N and 10N but decreases for 15N. As load applied increase, coefficient of friction increases for 100rpm and 150rpm but decreases for 200rpm. PKAC-E material is suitable to be applied at high speed and load. Textured PKAC-E disc is suitable to be used as a bearing material under low load at high speed and has a shorter longevity. Non-textured PKAC disc is suitable to be used as bearing material under low load at low speed and under high load at high speed and has a longer longevity than textured surface.

## **5.2 Recommendation for future works**

In this study only, sliding speed of 100rpm 150rpm and 200rpm and applied load of 5N, 10N and 15N is tested. Higher applied load and sliding speed should be tested to further study the tribological performance of palm kernel activated carbon reinforced polymeric composite. Further study also should be conducted to improve the PKAC-E material physical properties such as melting point and hardness to enhance its capabilities as a bearing material.

## REFERENCES

- Abechi E.S, Gimba C.E, Uzairu A, & Kagbu J.A. (2011). Archives of Applied Science Research,. *Kinetics of adsorption of methylene blue onto activated carbon prepared from palm kernel shell*, 3(1), 154-164.
- Borghini, A., Gualtieri, E., Marchetto, D., Moretti, L., & Valeri, S. (2008). Tribological effects of surface texturing on nitriding steel for high-performance engine applications. *Wear*, 265(7-8), 1046-1051.
- Cannon, A. H., & King, W. P. (2009). Casting metal microstructures from a flexible and reusable mold. *Journal of Micromechanics and Microengineering*, 19(9), 095016.
- Costa, H., & Hutchings, I. (2009). Development of a maskless electrochemical texturing method. *Journal of Materials Processing Technology*, 209(8), 3869-3878.
- Costa, H., & Hutchings, I. (2014). Some innovative surface texturing techniques for tribological purposes. *Proceedings of the Institution of Mechanical Engineers, Part J: Journal of Engineering Tribology*, 229(4), 429-448.
- David C. Evans (1981). Self-lubricating bearings. *Industrial Lubrication and Tribology*, Vol. 33 Iss 4 pp. 132 – 138.

Dobrzański, L., & Drygała, A. (2007). Laser processing of multicrystalline silicon for texturization of solar cells. *Journal of Materials Processing Technology*, 191(1-3), 228-231.

Gardos, M. (1982). Self-lubricating composites for extreme environment applications. *Tribology International*, 15(5), 273-283.

Gawarkiewicz, R., & Wasilczuk, M. (2007). Wear measurements of self-lubricating bearing materials in small oscillatory movement. *Wear*, 263(1-6), 458-462.

Han, P., Kim, J., Ehmann, K. F., & Cao, J. (2013). Laser surface texturing of medical needles for friction control. *International Journal of Mechatronics and Manufacturing Systems*, 6(3), 215.

Ibatan, T., Uddin, M., & Chowdhury, M. (2015). Recent development on surface texturing in enhancing tribological performance of bearing sliders. *Surface and Coatings Technology*, 272, 102-120.

J. K. Lancaster. (1967). Composite self-lubricating bearing materials. *Lubrication and Wear Group*, 182(1), 33-54.

Jumasiah, A., Chuah, T., Gimbon, J., Choong, T., & Azni, I. (2005). Adsorption of basic dye onto palm kernel shell activated carbon: sorption equilibrium and kinetics studies. *Desalination*, 186(1-3), 57-64.

K. W. Chua, M.F.B. Abdollah, N.A. Mat Tahir, & H. Amiruddin. (2014). Jurnal tribologi  
2. *Potential of palm kernel activated carbon epoxy (PKAC-E) composite as solid lubricant: Effect of load on friction and wear properties*, 31-38.

Kogusu, S., Ishimatsu, T., Ougiya, Y., Yazawa, T., & Moromugi, S. (2008). Decoration of metal surface by dimples using ball-end milling process. *2008 IEEE International Conference on Industrial Technology*.

Kurella, A., & Dahotre, N. B. (2005). Review paper: Surface Modification for Bioimplants: The Role of Laser Surface Engineering. *Journal of Biomaterials Applications*, 20(1), 5-50.

L. M. Vilhena, M.Sedlac̆ek, B.Podgornik, J.Viz̆intin, A.Babnik, J.Moz̆ina. (2009). *Surface texturing by pulsed Nd:YAG laser*.

Mat Tahir, N. A., Abdollah, M. F., Hasan, R., & Amiruddin, H. (2016). The effect of sliding distance at different temperatures on the tribological properties of a palm kernel activated carbon–epoxy composite. *Tribology International*, 94, 352-359.

Mat Tahir, N. A., Abdollah, M. F., Hasan, R., Amiruddin, H., & Abdullah, M. I. (2017). Statistical models for predicting wear and friction coefficient of palm kernel activated carbon-epoxy composite using the ANOVA. *Industrial Lubrication and Tribology*, 69(5), 761-767.

Matsumura, T., & Takahashi, S. (2012). Micro dimple milling on cylinder surfaces. *Journal of Manufacturing Processes*, 14(2), 135-140.

Menezes P.L., Lovell M.R., Kabir M.A., Higgs C.F., Rohatgi P.K. (2012) Green Lubricants: Role of Additive Size. In: Nosonovsky M., Bhushan B. (eds) Green Tribology. Green Energy and Technology. Springer, Berlin, Heidelberg.

Mohmad, M., Abdollah, M. F., Tamaldin, N., & Amiruddin, H. (2017). The effect of dimple size on the tribological performances of a laser surface textured palm kernel activated carbon-epoxy composite. *Industrial Lubrication and Tribology*, 69(5), 768-774.

Mohmad, M., Abdollah, M. F., Tamaldin, N., & Amiruddin, H. (2017). Frictional characteristics of laser surface textured activated carbon composite derived from palm kernel. *The International Journal of Advanced Manufacturing Technology*, 95(5-8), 2943-2949.



Murashima, M., Umehara, N., & Kousaka, H. (2016). Effect of Nano-Texturing on Adhesion of Thermoplastic Resin against Textured Steel Plate. *Tribology Online*, 11(2), 159-167.

Qu, N., Chen, X., Li, H., & Zeng, Y. (2014). Electrochemical micromachining of micro-dimple arrays on cylindrical inner surfaces using a dry-film photoresist. *Chinese Journal of Aeronautics*, 27(4), 1030-1036.

Rajurkar, K., Zhu, D., McGeough, J., Kozak, J., & De Silva, A. (1999). New Developments in Electro-Chemical Machining. *CIRP Annals*, 48(2), 567-579.

Ronen, A., Etsion, I., & Kligerman, Y. (2001). Friction-Reducing Surface-Texturing in Reciprocating Automotive Components. *Tribology Transactions*, 44(3), 359-366.

Ryk, G., & Etsion, I. (2006). Testing piston rings with partial laser surface texturing for friction reduction. *Wear*, 261(7-8), 792-796.

Sedlaček, M., & Podgornik, B. (2017). Design and Tribological Performance of Textured Surfaces. *Materials Performance and Characterization*, 6(2), MPC20160022.

Sliney, H. (1982). Solid lubricant materials for high temperatures—a review. *Tribology International*, 15(5), 303-315.

Tahir, N. A., Abdollah, M. F., Hasan, R., & Amiruddin, H. (2015). The Effect of Temperature on the Tribological Properties of Palm Kernel Activated Carbon-Epoxy Composite. *Tribology Online*, 10(6), 428-433.

Voevodin, A., & Zabinski, J. (2006). Laser surface texturing for adaptive solid lubrication. *Wear*, 261(11-12), 1285-1292.

Wang, X., Han, P., Kang, M., & Ehmann, K. (2016). Surface-blended texturing of medical needles for friction reduction using a picosecond laser. *Applied Physics A*, 122(4).

Zhang, Y., Zhang, X., & Matsoukas, G. (2015). Numerical study of surface texturing for improving tribological properties of ultra-high molecular weight polyethylene. *Biosurface and Biotribology*, 1(4), 270-277.



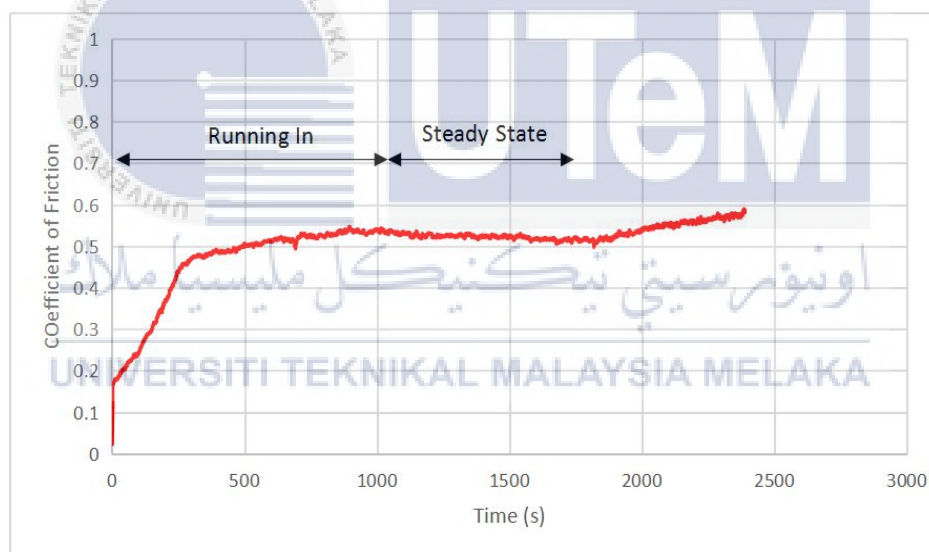
## APPENDIX A

### Data of Sliding Tests

#### Data of SKD-II Disc Sliding Test

Steady COF: 1037s-1910.313s

Average COF for the disc is tabulated is 0.53

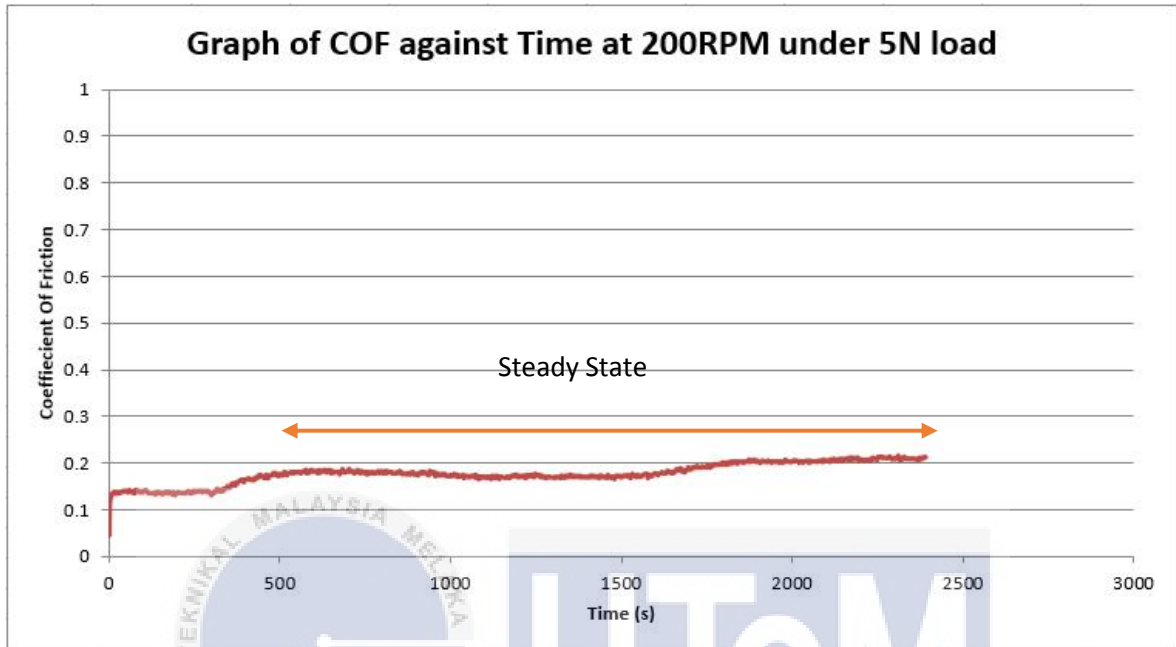


COF against time(s) for SKD-II steel disc under 5N load at 200RPM

### Data of Non-Textured PKAC-E Disc Sliding Test

Steady COF: 650.594s

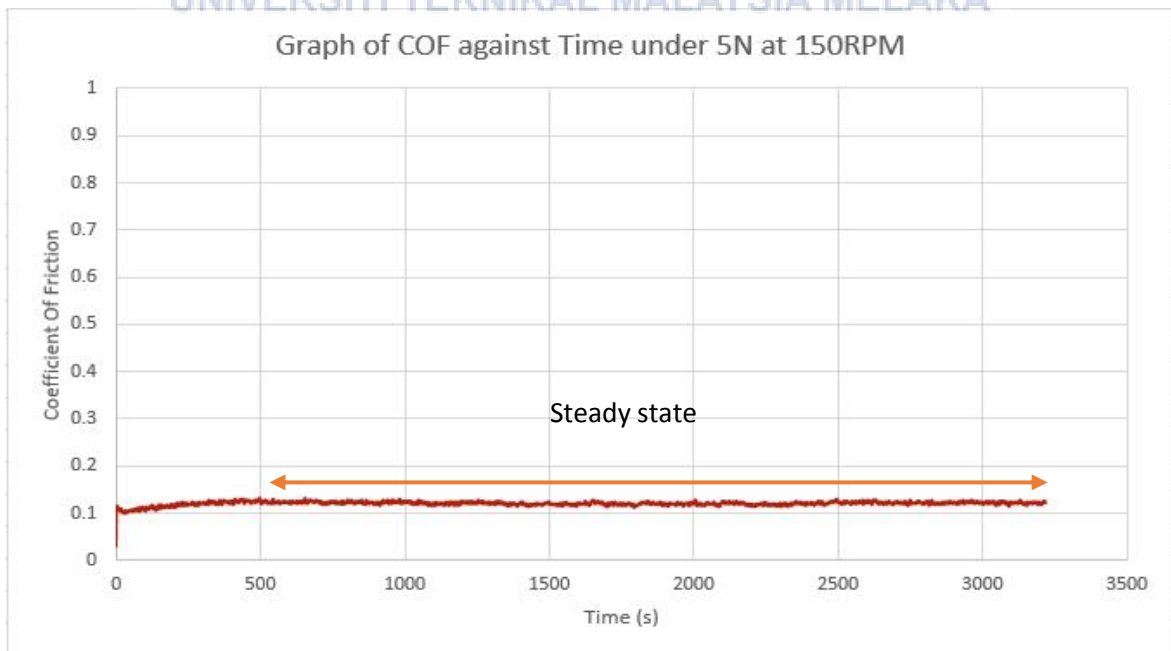
Average COF is 0.187



COF against time(s) for non-textured PKAC-E disc under 5N at 200RPM

Steady COF: start from 500.219s

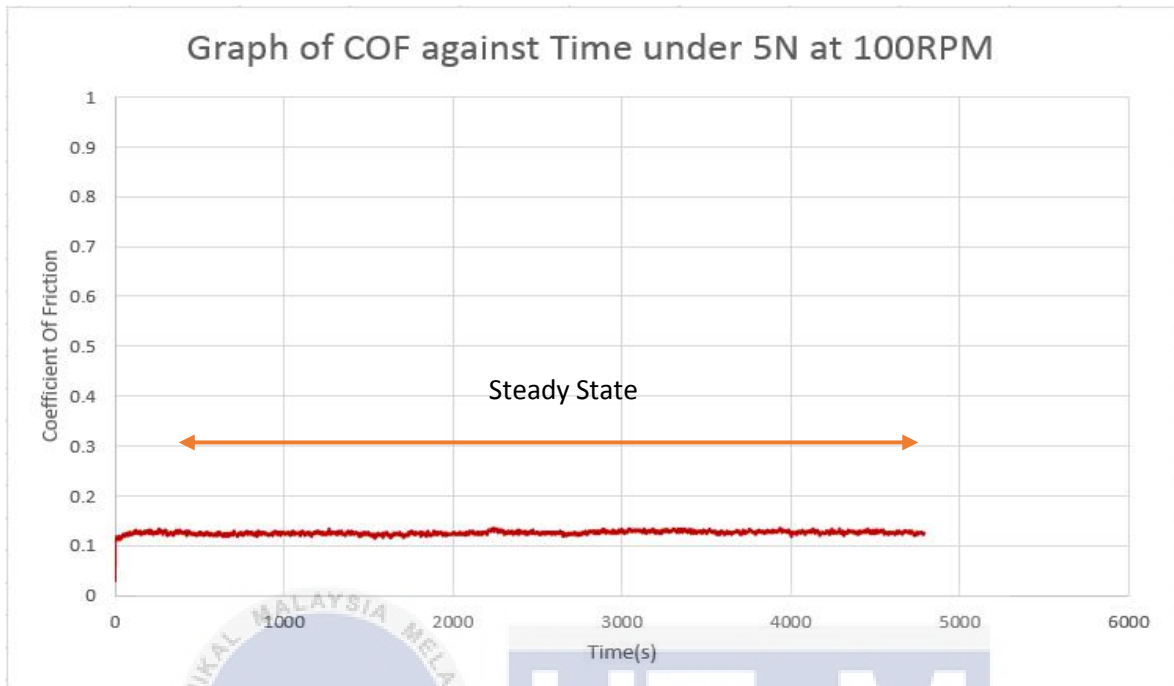
Average COF is 0.1217



COF against time(s) for non-textured PKAC-E disc under 5N at 150RPM

Steady COF: start from 280.188s

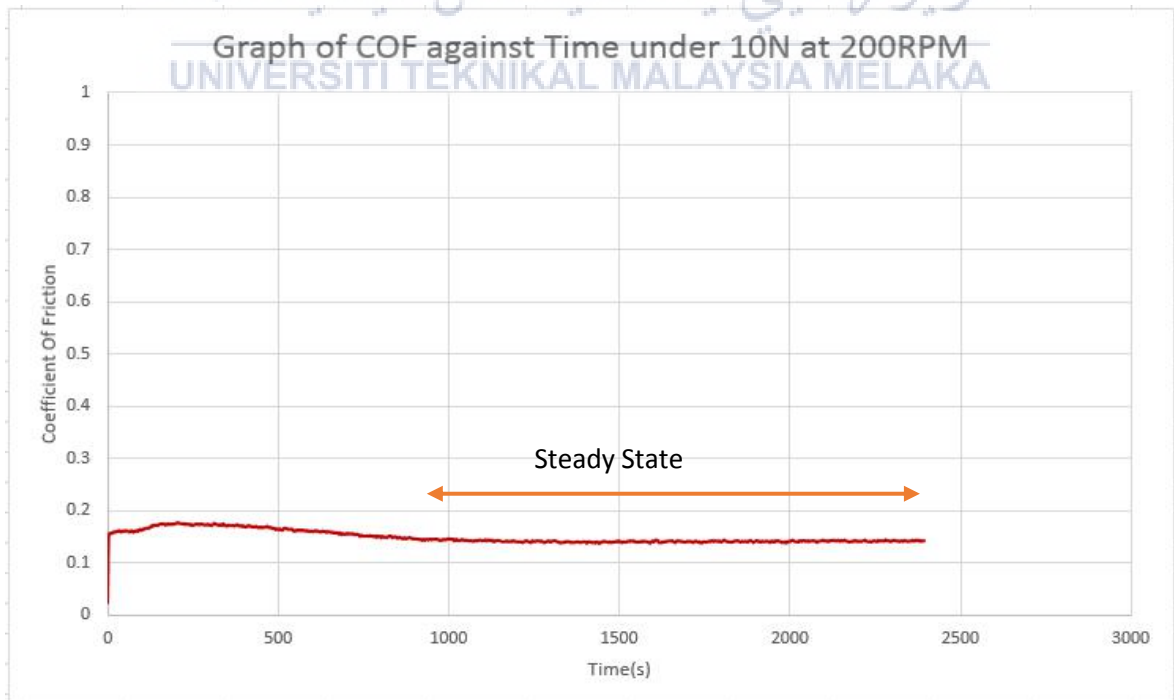
Average COF is 0.1266.



COF against time(s) for non-textured PKAC-E disc under 5N at 100RPM

Steady COF: start from 920.016s

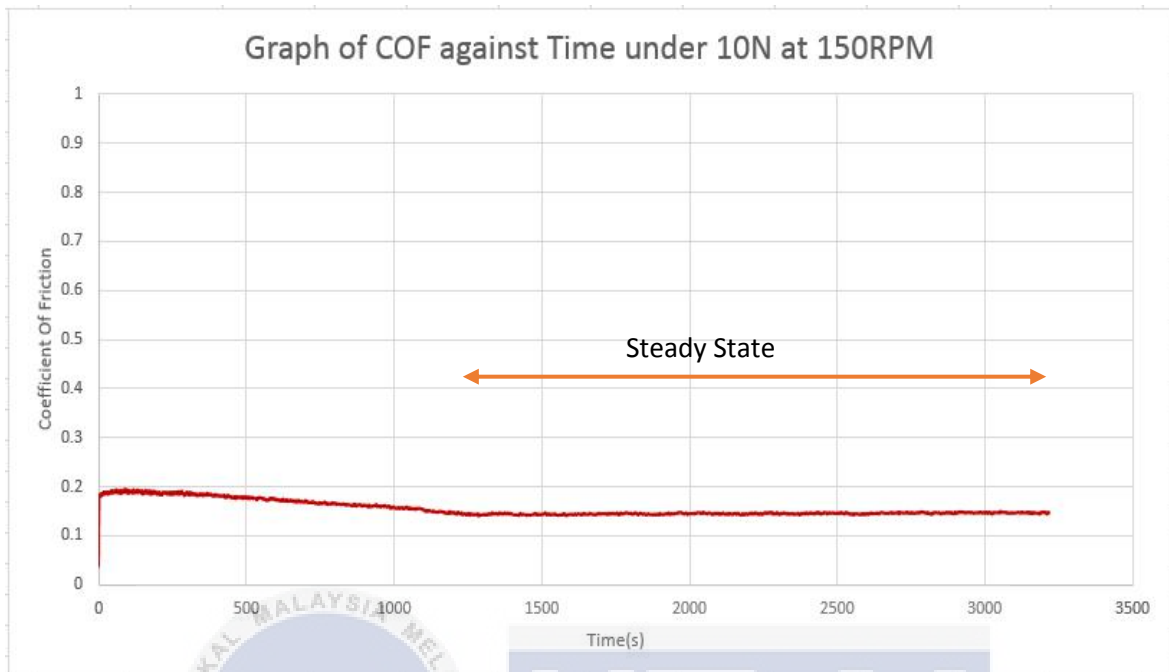
Average COF is 0.1415.



COF against time(s) for non-textured PKAC-E disc under 10N at 200RPM

Steady COF: startin from 1257s

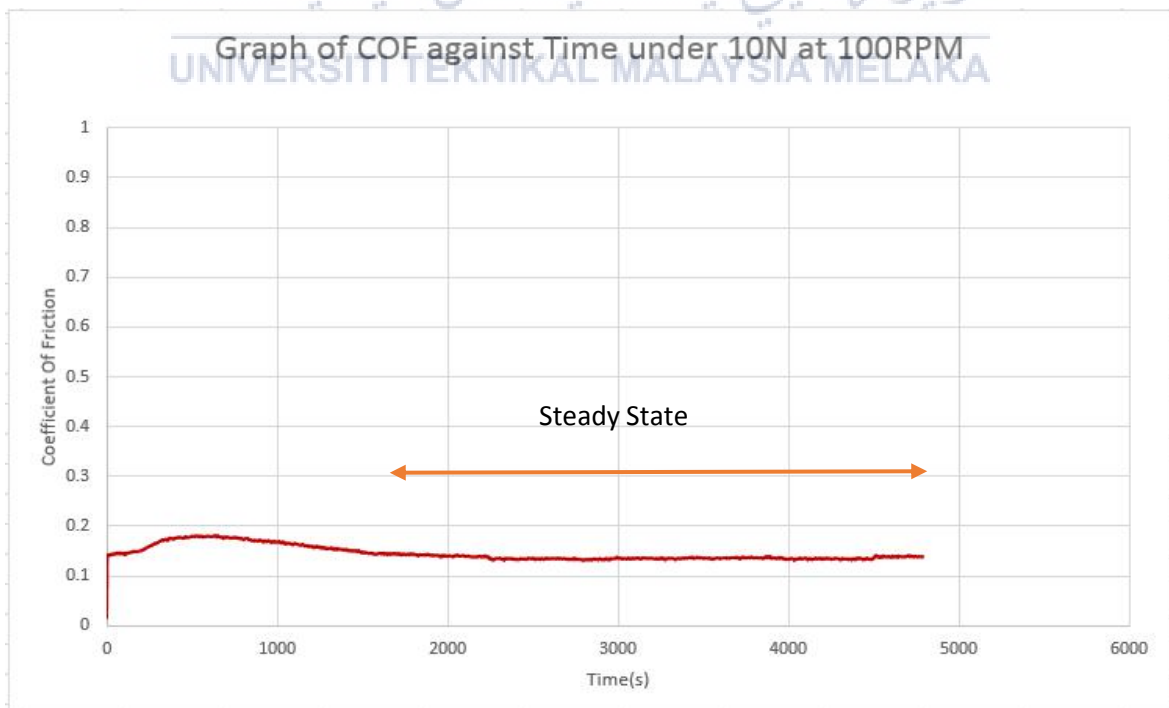
Average COF is 0.1460.



COF against time(s) for non-textured PKAC-E disc under 10N at 150RPM

Steady COF: start from 1588.781s

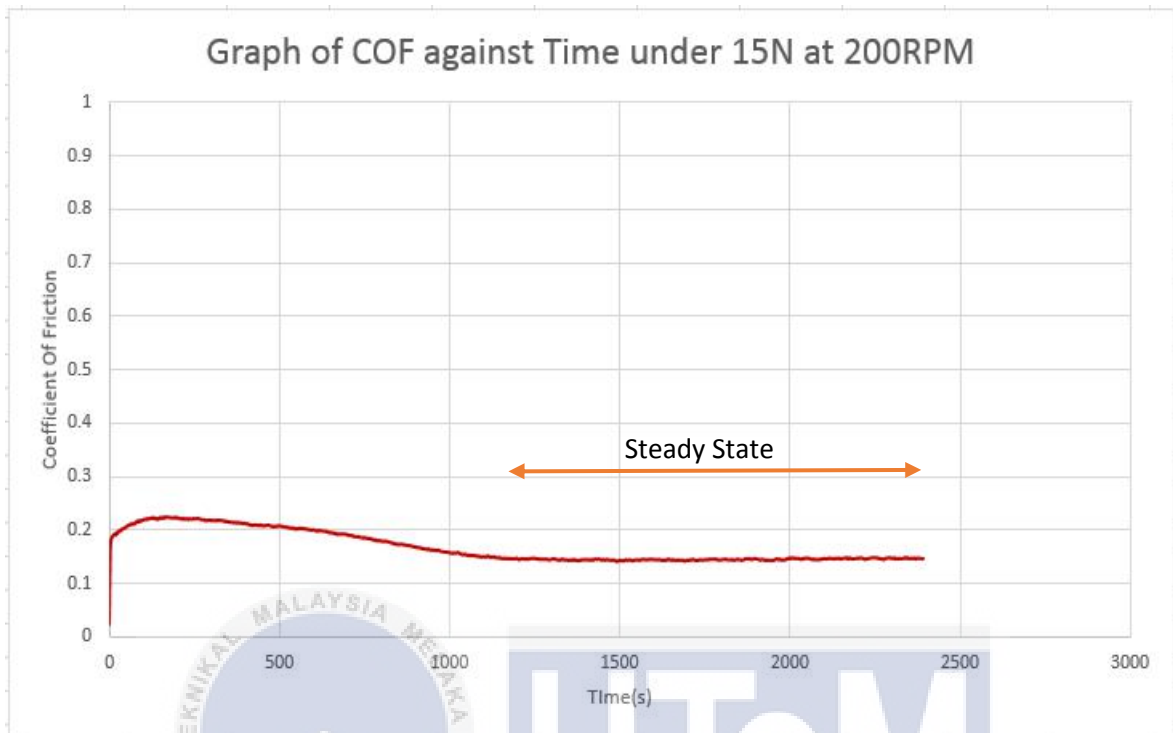
Average COF is 0.1365



COF against time(s) for non-textured PKAC-E disc under 10N at 100RPM

Steady COF: start from 1084s

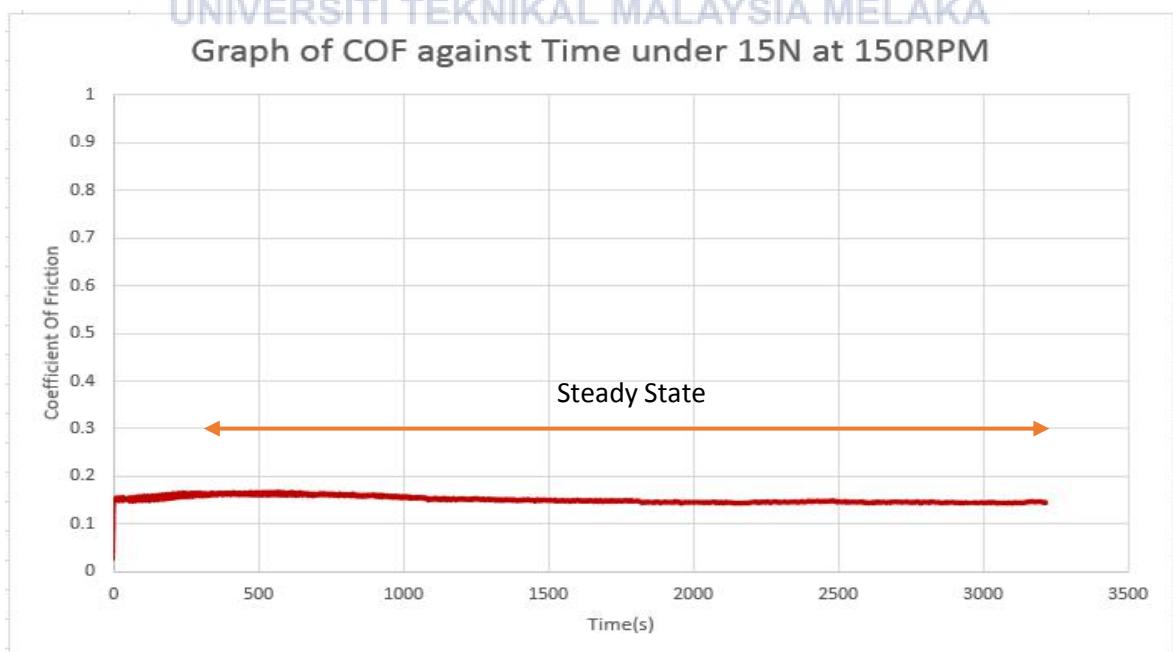
Average COF is 0.1414.



COF against time(s) for non-textured PKAC-E disc under 15N at 200RPM

Steady COF: start from 215.625s

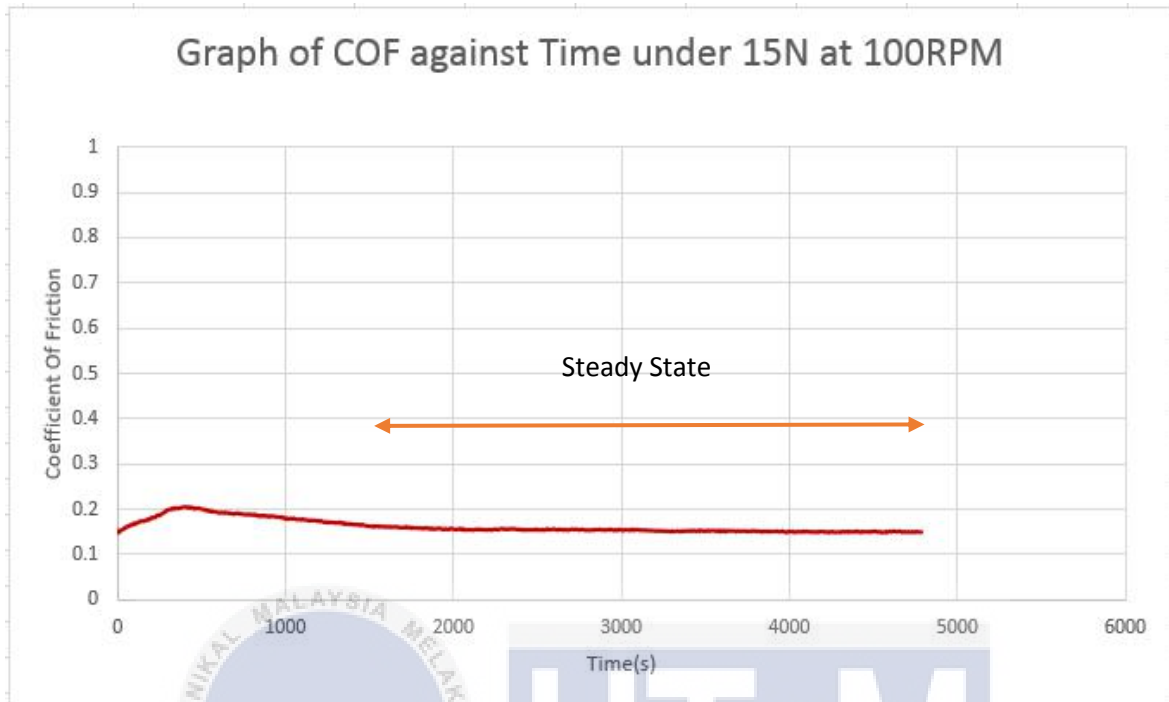
Average COF is 0.1506



COF against time(s) for non-textured PKAC-E disc under 15N at 150RPM

Steady COF: start from 1524.5s

Average COF is 0.1519

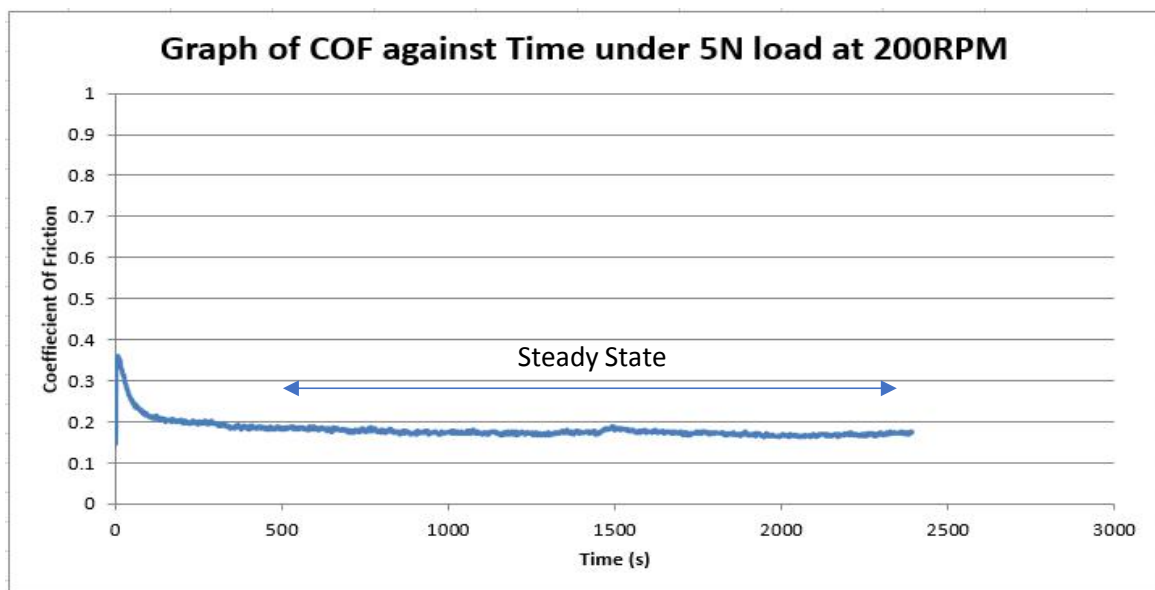


COF against time(s) for non-textured PKAC-E disc under 15N at 100RPM

#### Data of Textured PKAC-E Disc Sliding Test

Steady COF: start from 500s

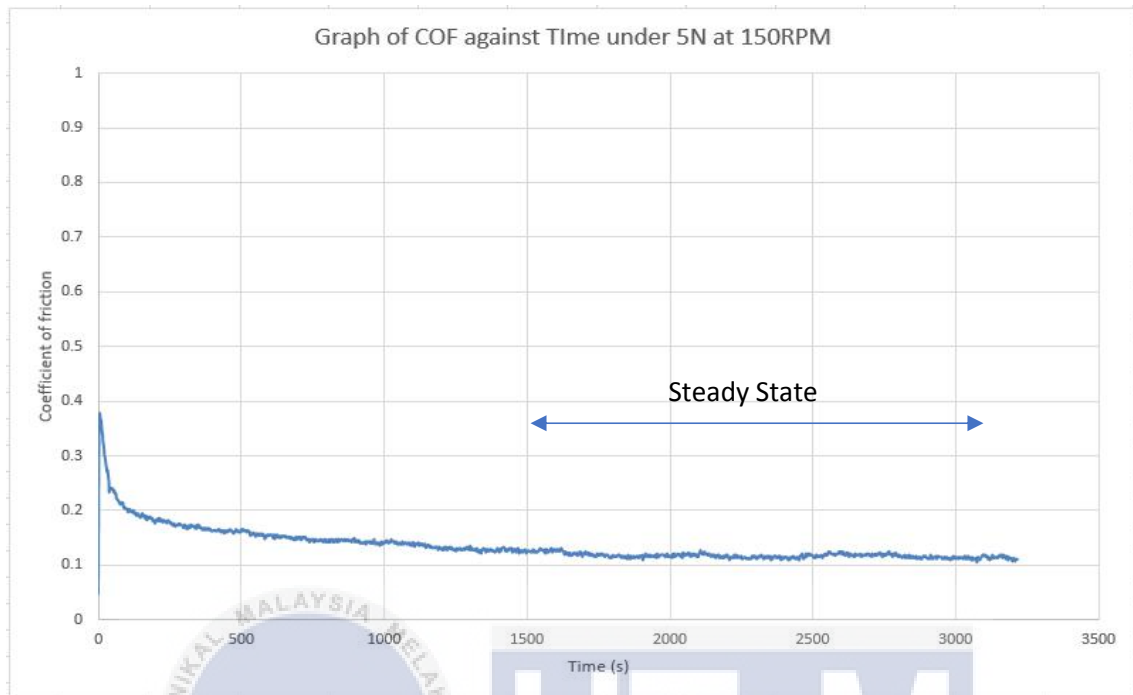
Average COF is 0.174.



COF against time(s) for textured PKAC-E disc under 5N at 200RPM

Steady COF :start from 1500s

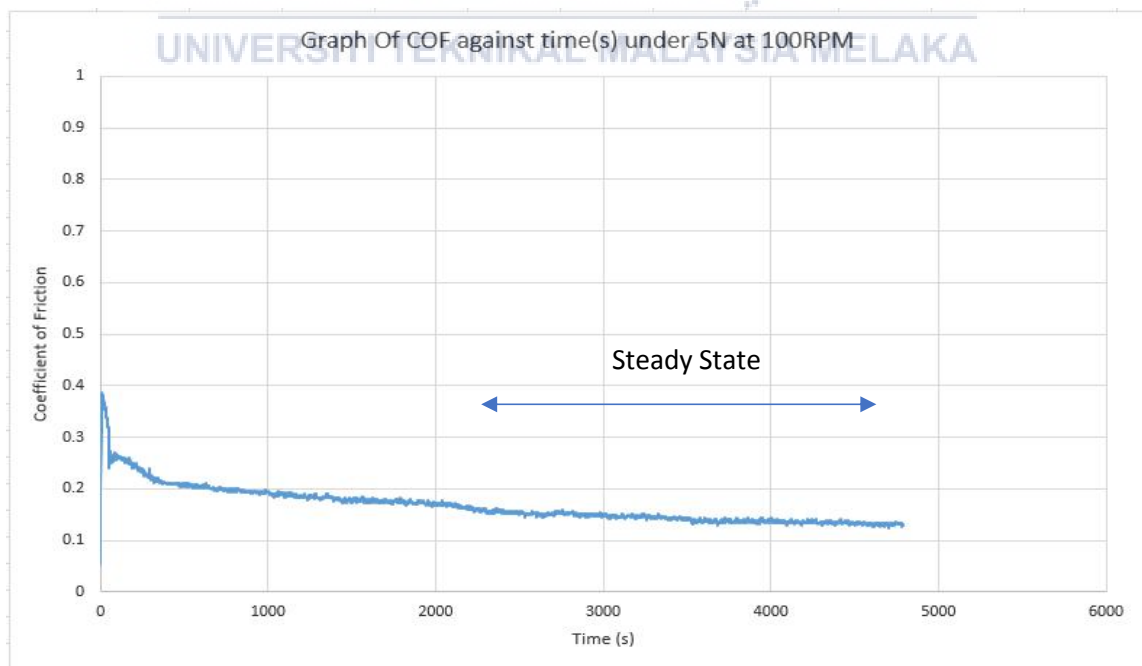
Average COF is 0.1164



COF against time(s) for textured PKAC-E disc under 5N at 150RPM

Steady COF: start from 2290s

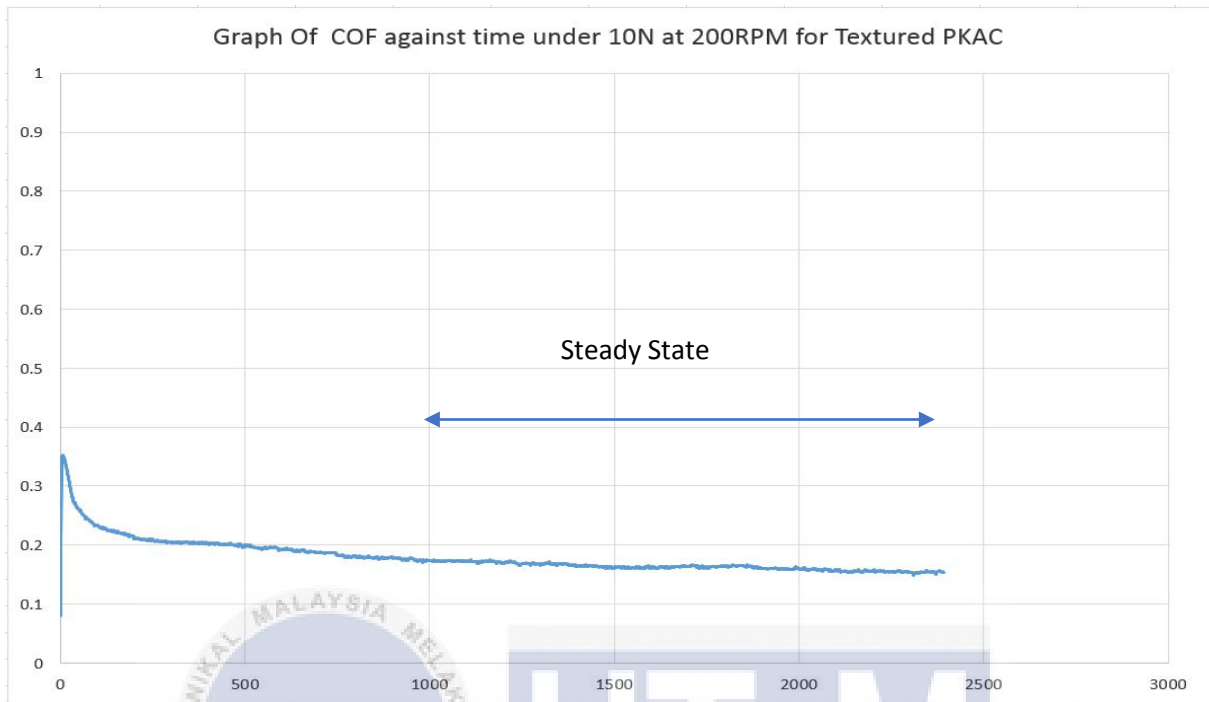
Average COF is 0.1420



COF against time(s) for textured PKAC-E disc under 5N at 100RPM

Steady COF: start from 1000s

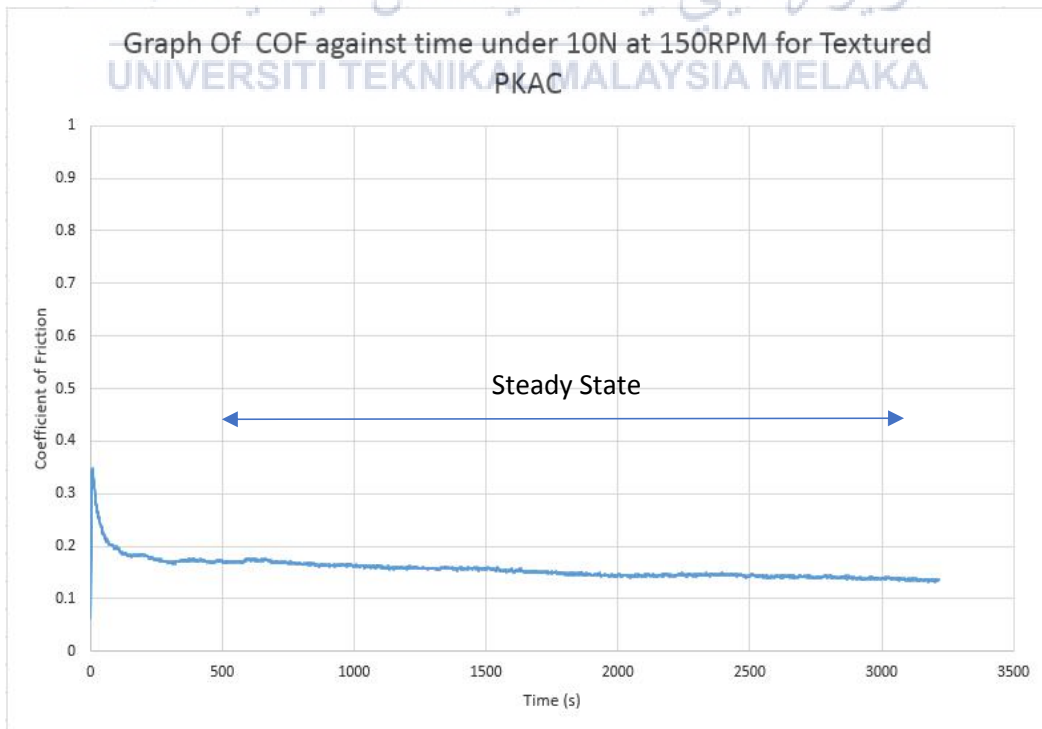
Average COF is 0.1630



COF against time(s) for textured PKAC-E disc under 10N at 200RPM

Steady COF : start from 319.25s

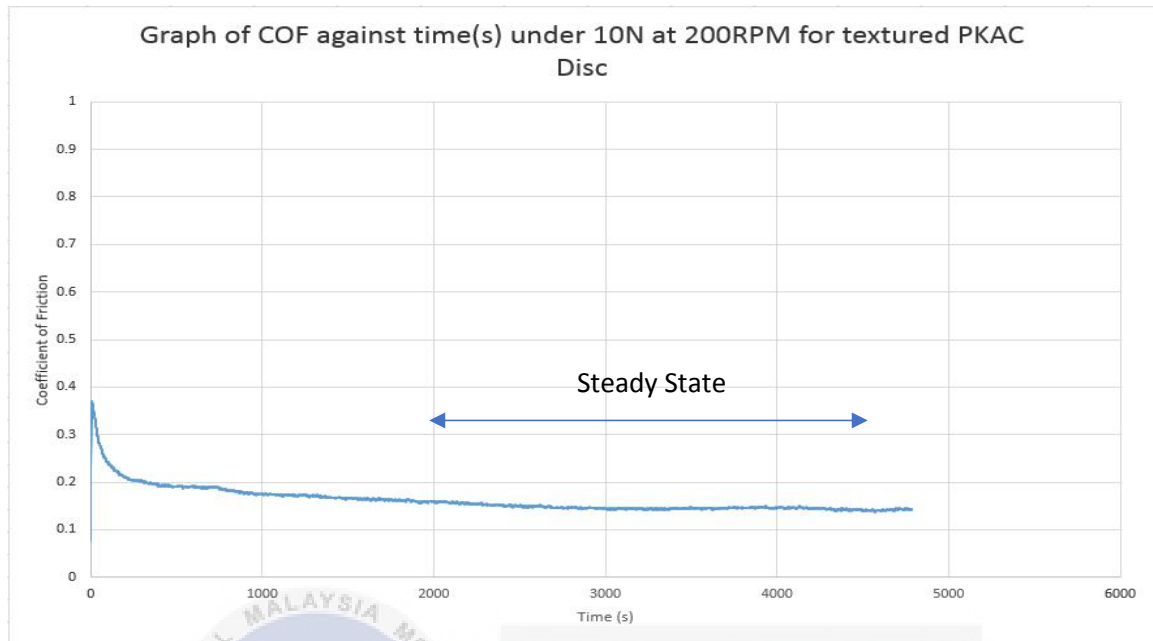
Average COF is 0.1527.



COF against time(s) for textured PKAC-E disc under 10N at 150RPM

Steady COF: start from 2000.859s

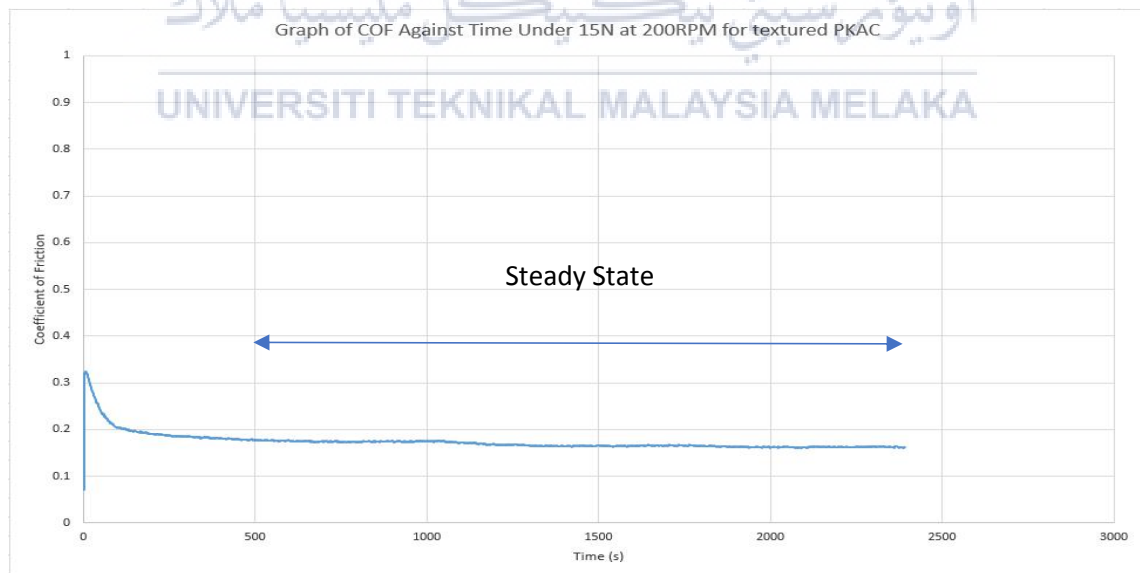
Average COF is 0.1463



COF against time(s) for textured PKAC-E disc under 10N at 100RPM

Steady COF: start from 477.47s

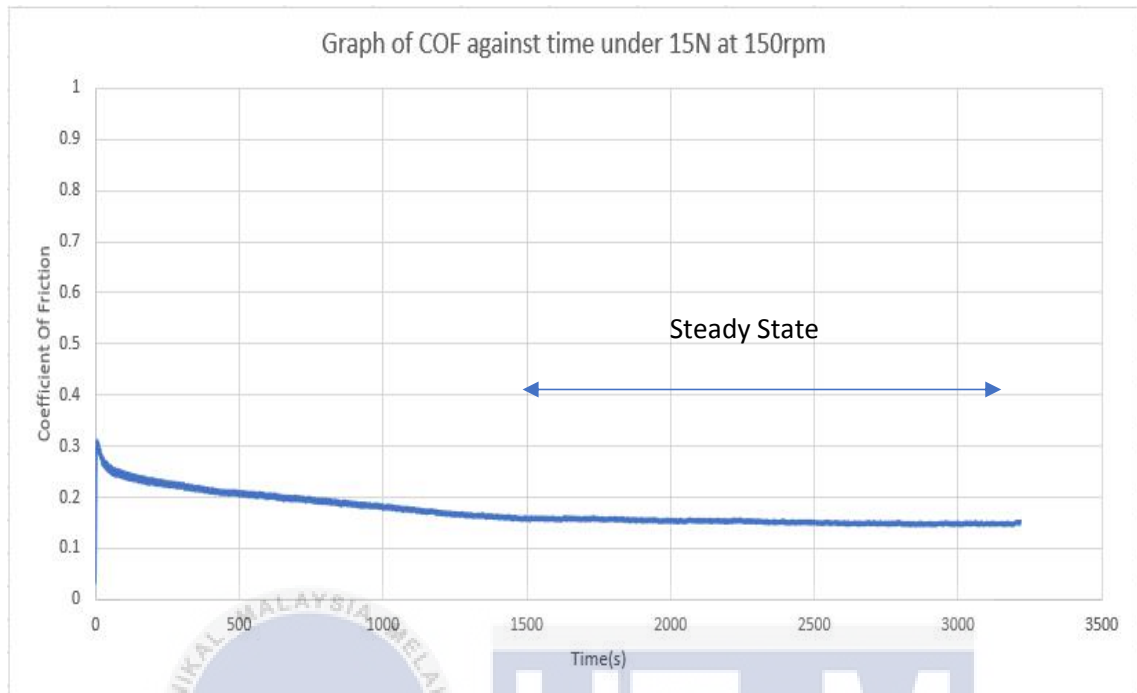
Average COF is 0.1675



COF against time(s) for textured PKAC-E disc under 15N at 200RPM

Steady COF: start from 1446.672s

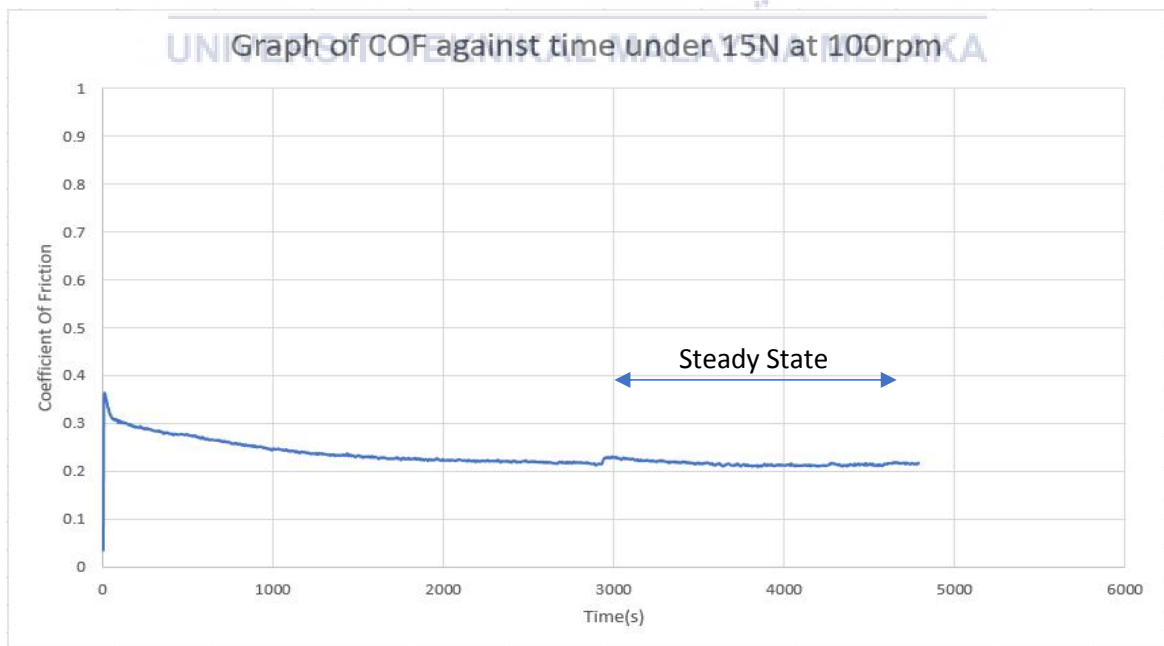
Average COF is 0.1519



COF against time(s) for textured PKAC-E disc under 15N at 150RPM

Steady COF: start from 3000.047s for the PKAC disc

Average COF is 0.2159



Graph of COF against time(s) for textured PKAC-E disc under 15N at 150RPM

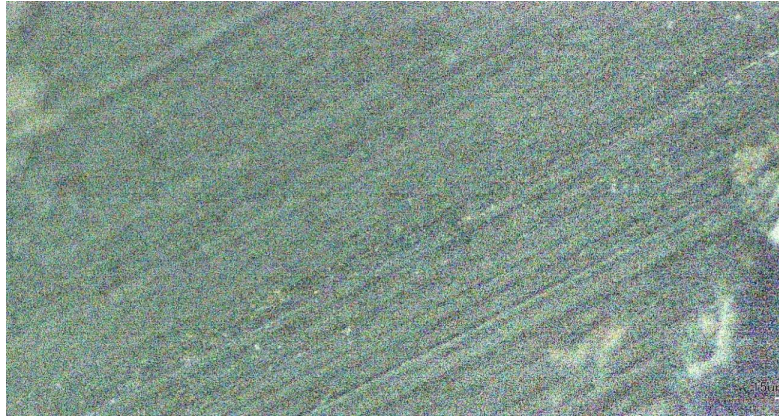
## APPENDIX B

### Microscopic wear track images at ball bearing and disk

### Microscopic wear track images at ball bearing and disk for SKD--II steel disc

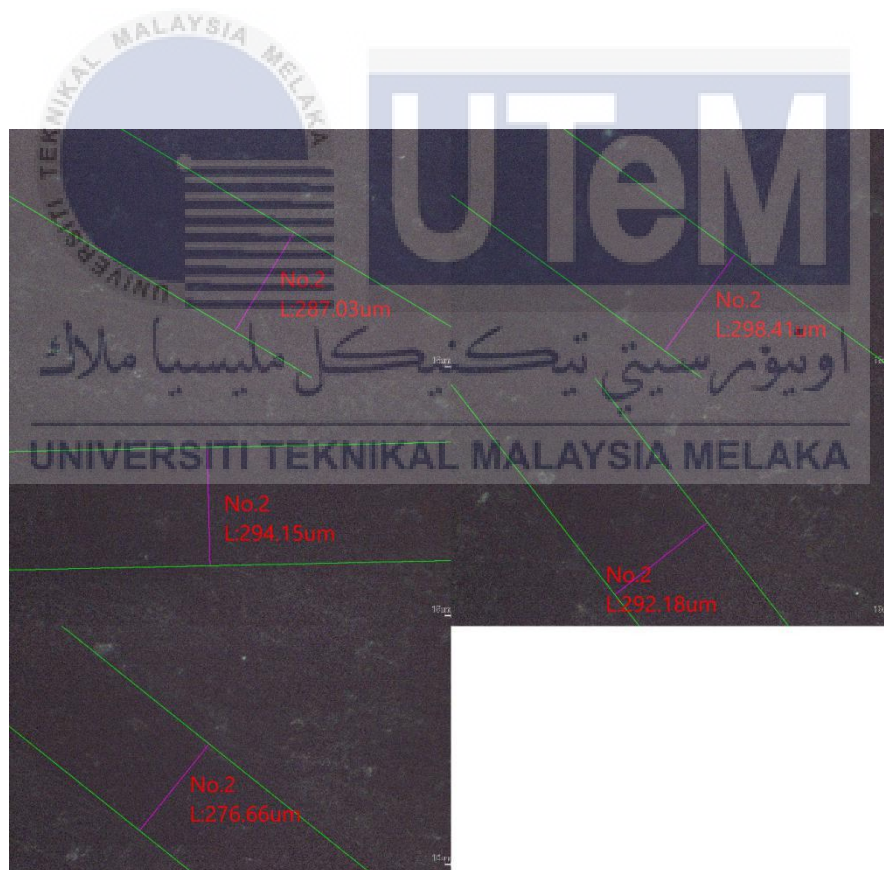


Microscopic disc wear tracks for SKD-II disc under 5N at 200rpm

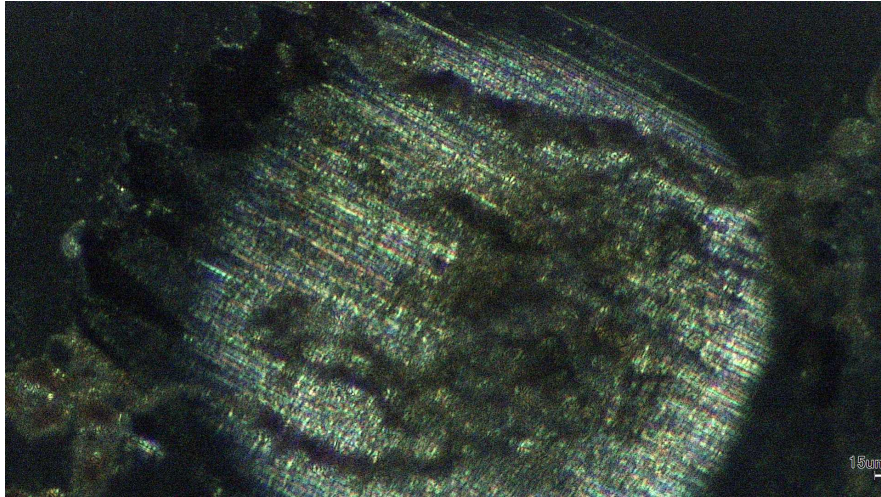


Microscopic ball bearing wear track for SKD-II disc under 5N at 200rpm

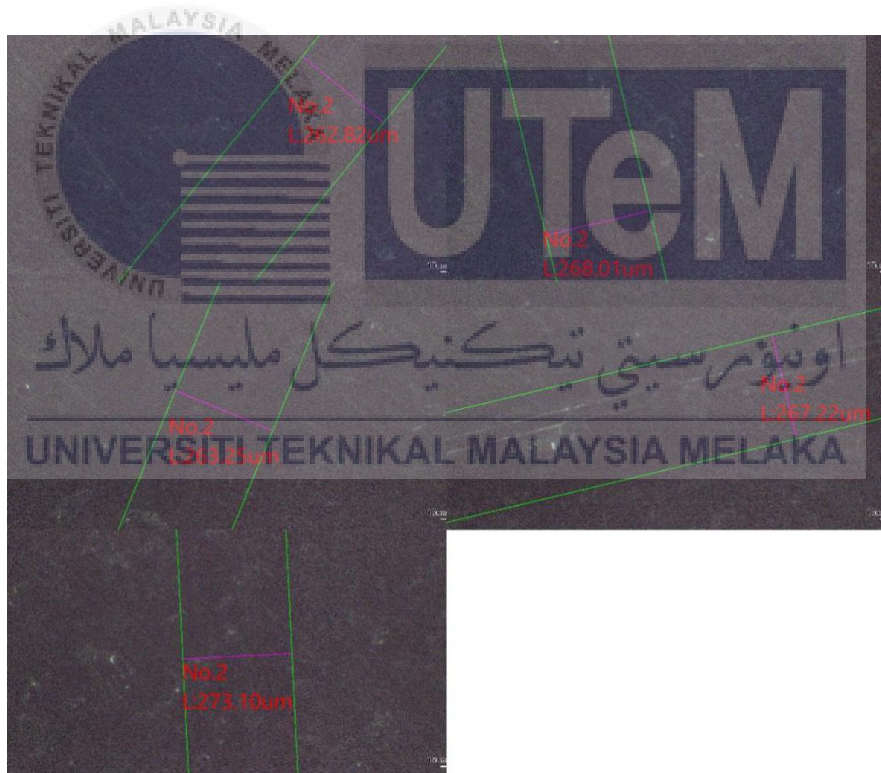
**Microscopic wear track images at ball bearing and disk for non-textured PKAC-E disc**



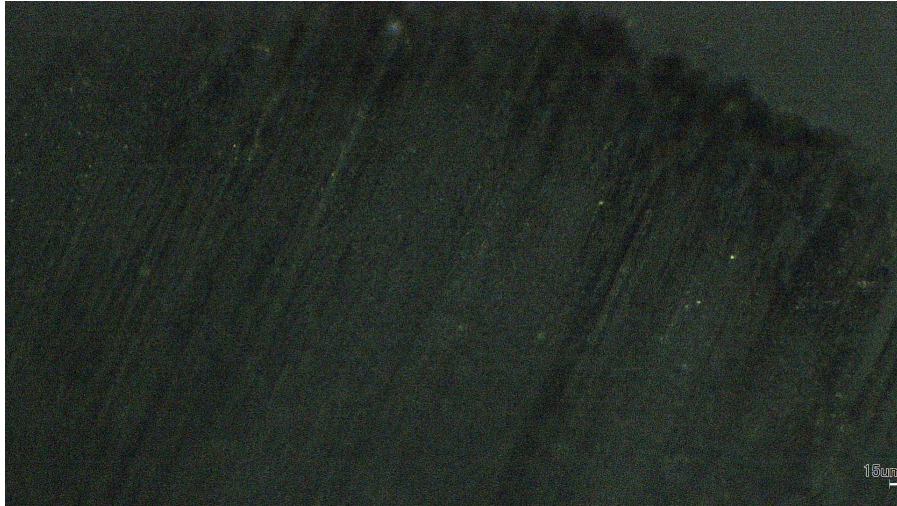
Microscopic disc wear track for non-textured PKAC-E disc under 5N at 200rpm



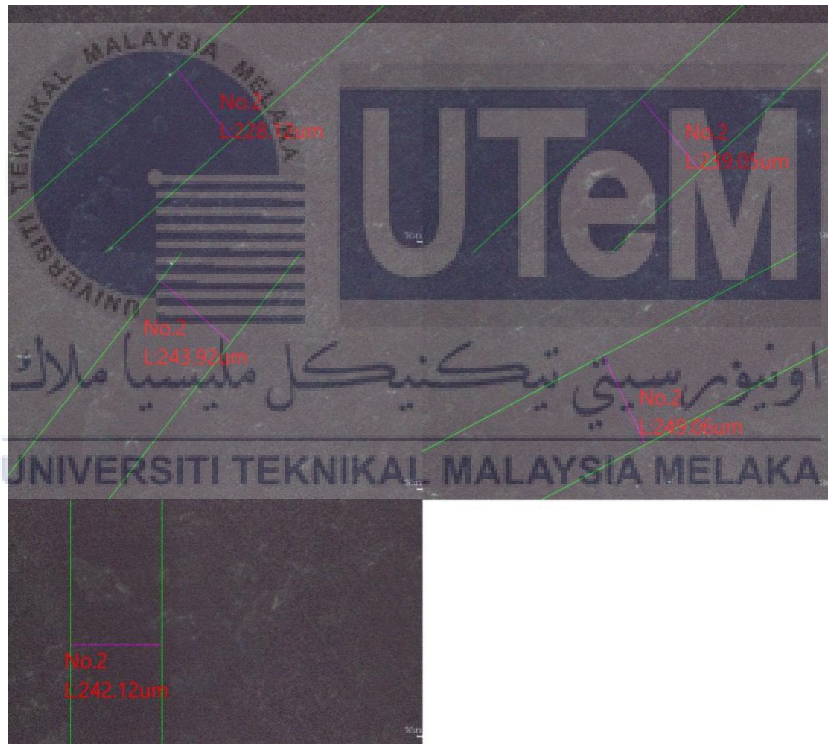
Microscopic ball bearing wear track for non-textured PKAC-E disc under 5N at 200rpm



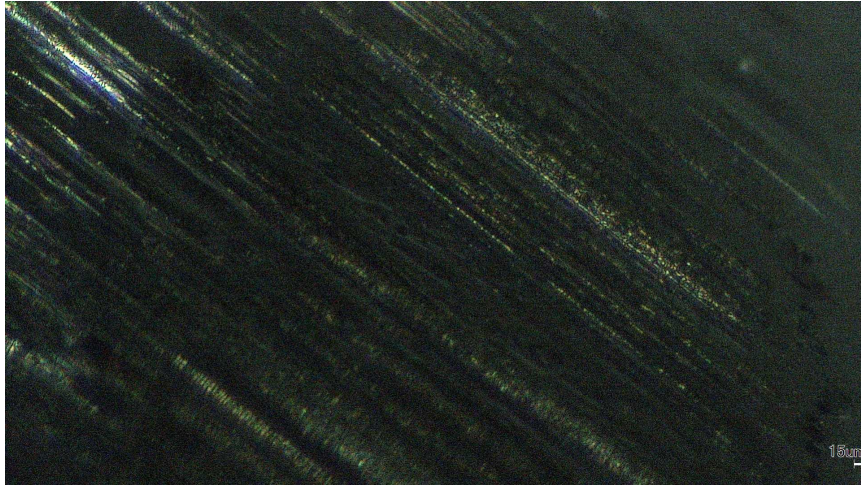
Microscopic disc wear track for non-textured PKAC-E disc under 5N at 150rpm



Microscopic ball bearing wear track for non-textured PKAC-E disc under 5N at 150rpm



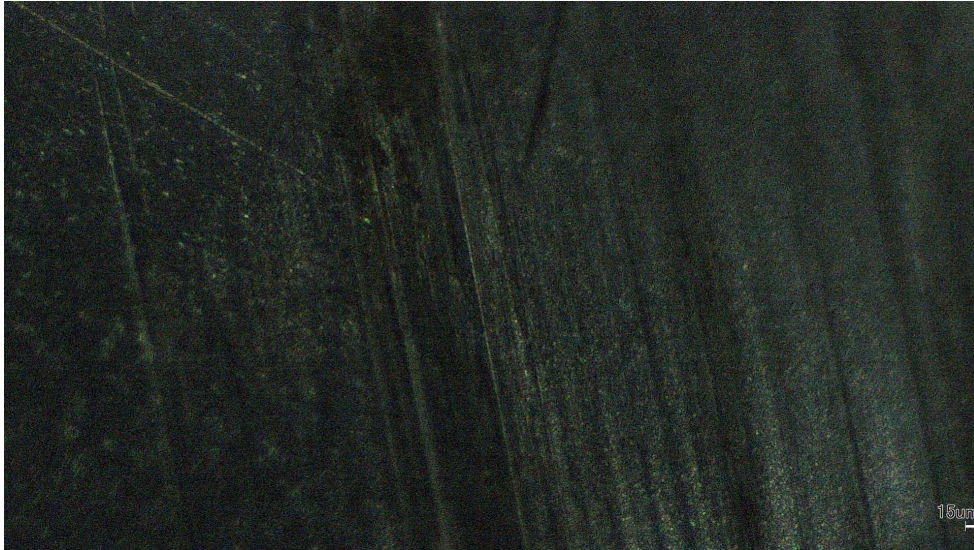
Microscopic disc wear track for non-textured PKAC-E disc under 5N at 100rpm



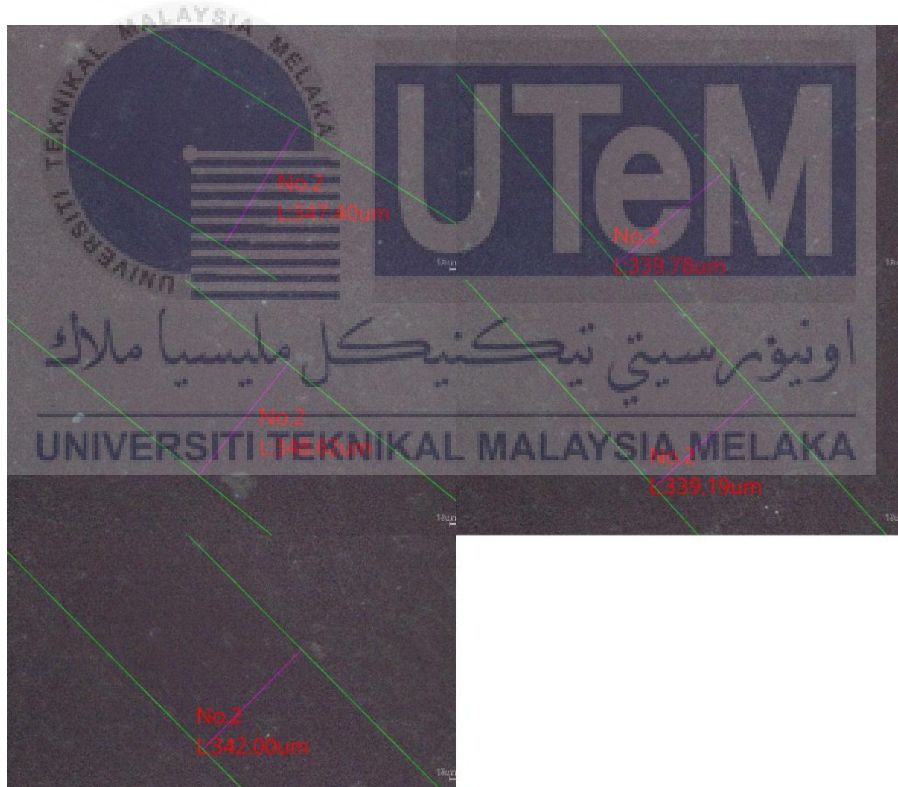
Microscopic ball bearing wear track for non-textured PKAC-E disc under 5N at 100rpm



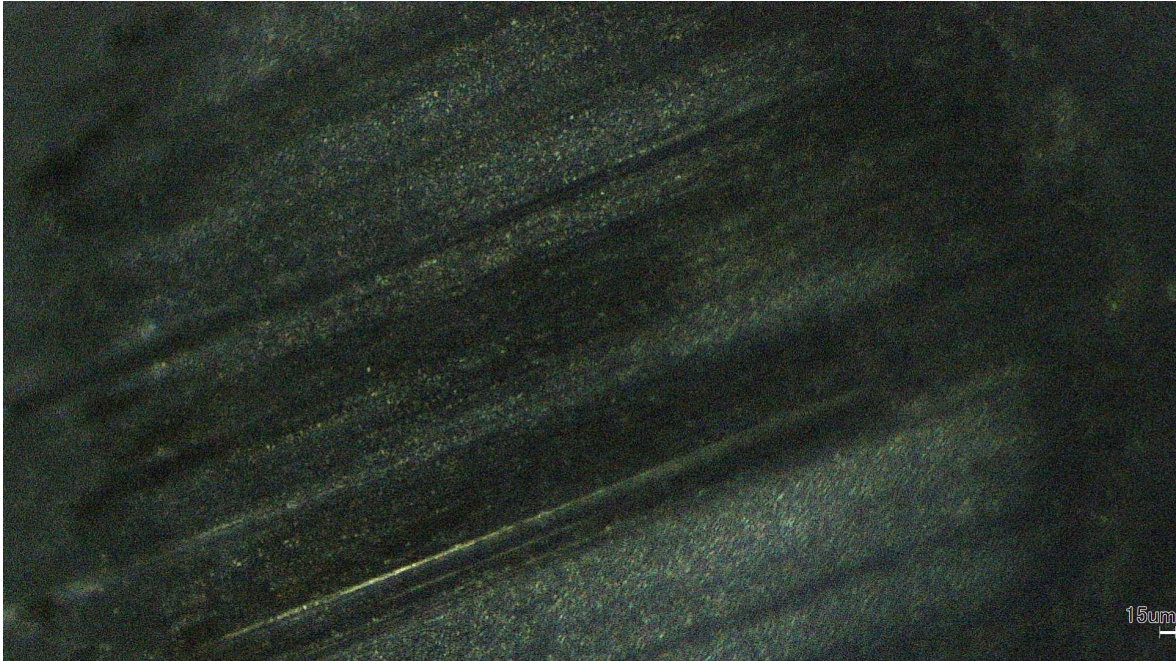
Microscopic disc wear track for non-textured PKAC-E disc under 10N at 200rpm



Microscopic ball bearing wear track for non-textured PKAC-E disc under 10N at 200rpm



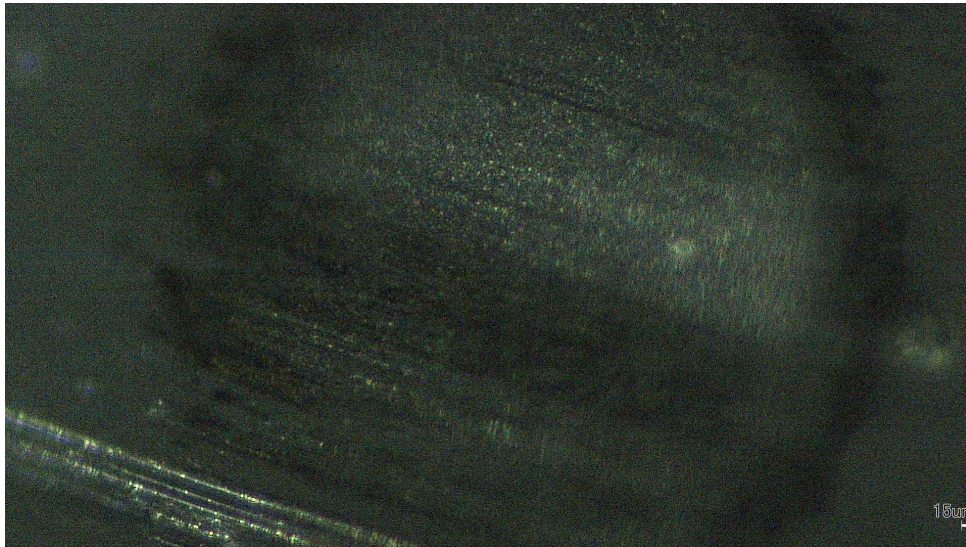
Microscopic disc wear track for non-textured PKAC-E disc under 10N at 150rpm



Microscopic ball bearing wear track for non-textured PKAC-E disc under 10N at 150rpm



Microscopic disc wear track for non-textured PKAC-E disc under 10N at 100rpm



Microscopic ball bearing wear track for non-textured PKAC-E disc under 10N at 100rpm



Microscopic disc wear track for non-textured PKAC-E disc under 15N at 200rpm

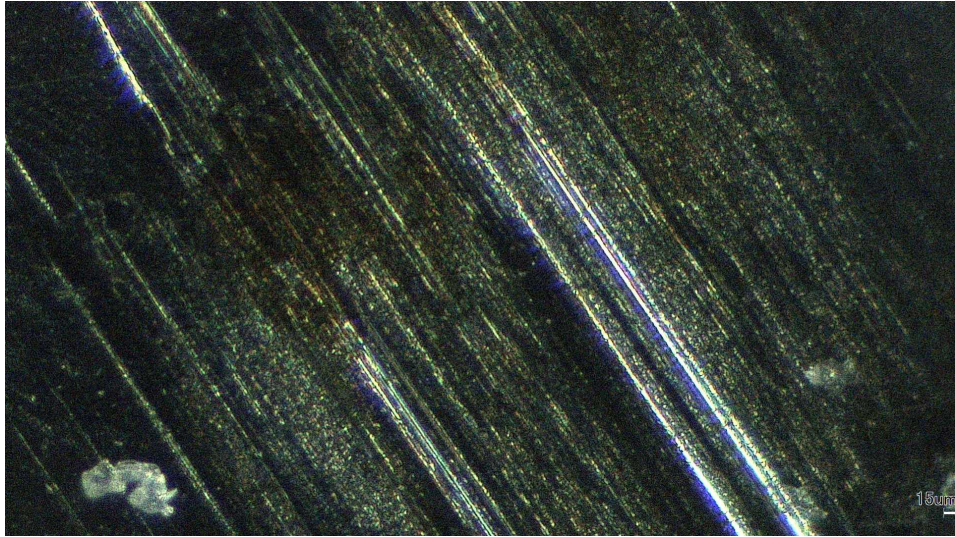
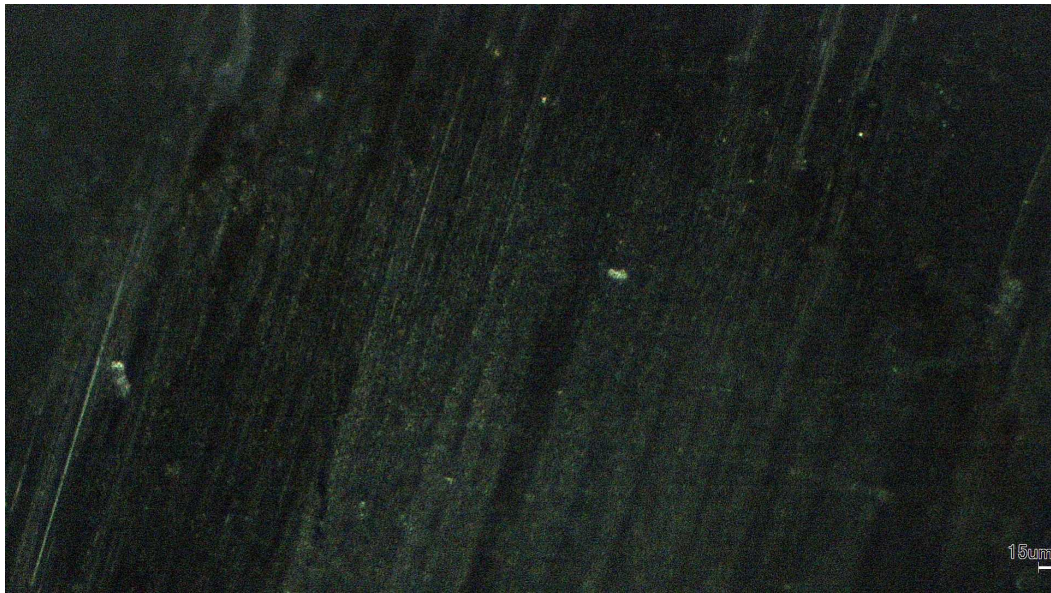


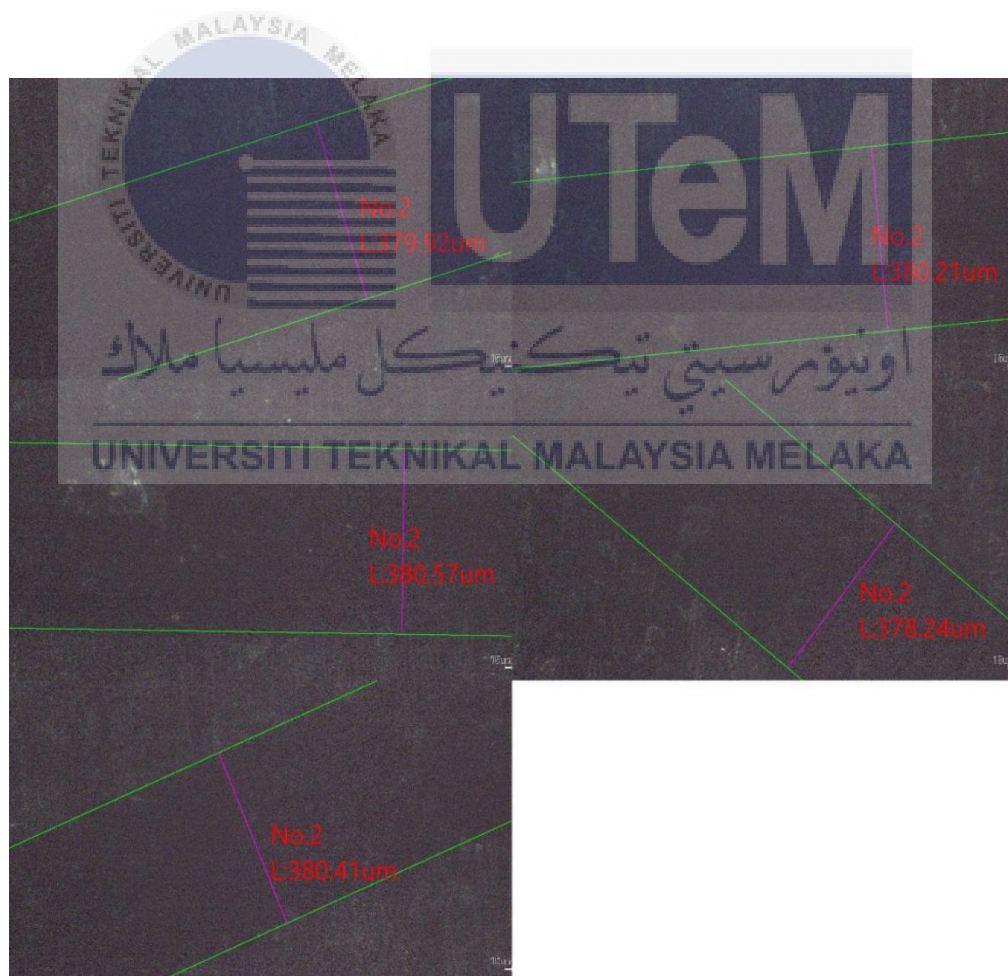
Figure 4.36: Microscopic ball bearing wear track for non-textured PKAC-E disc under 15N at 200rpm



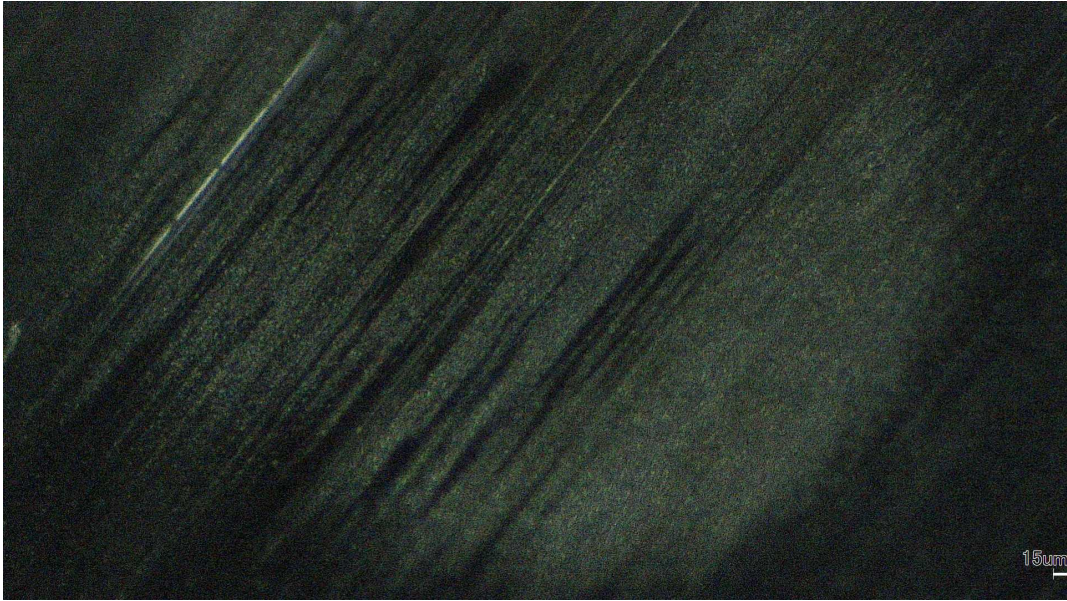
Microscopic disc wear track for non-textured PKAC-E disc under 15N at 150rpm



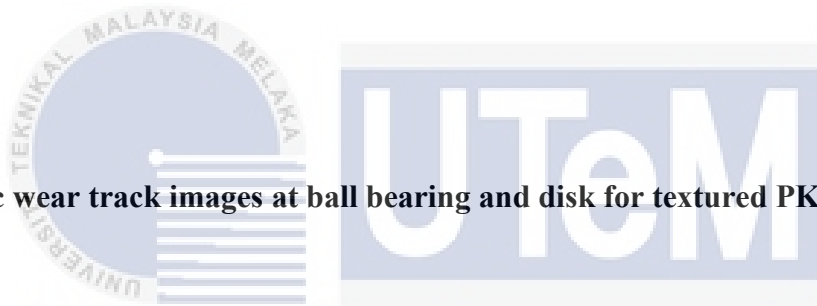
Microscopic ball bearing wear track for non-textured PKAC-E disc under 15N at 150rpm



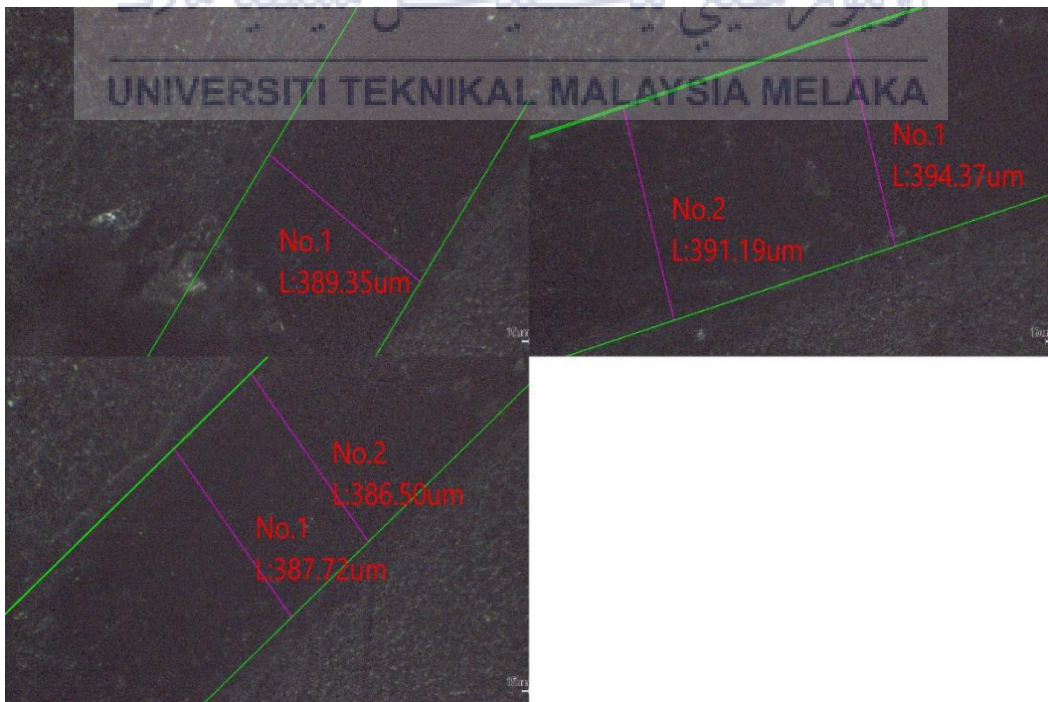
Microscopic disc wear track for non-textured PKAC-E disc under 15N at 100rpm



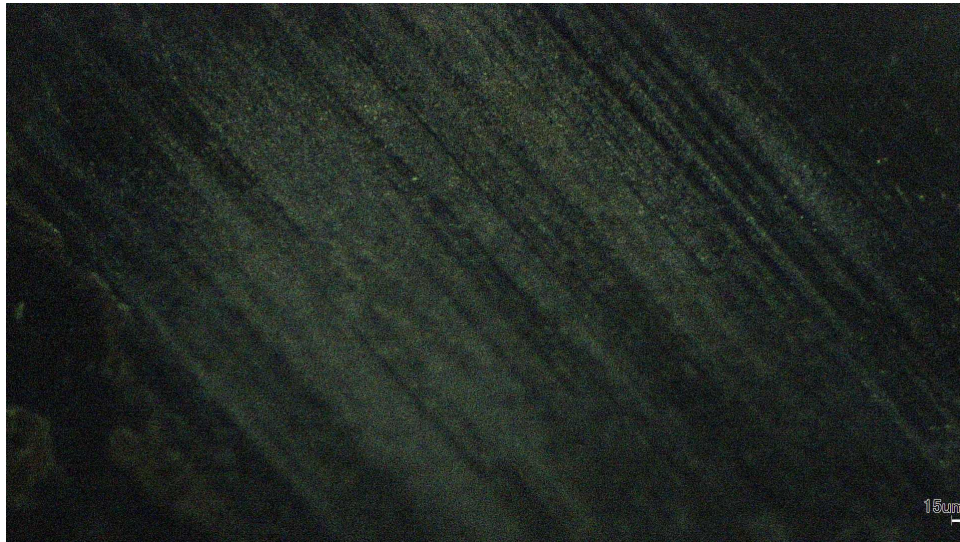
Microscopic ball bearing wear track for non-textured PKAC-E disc under 15N at 100rpm



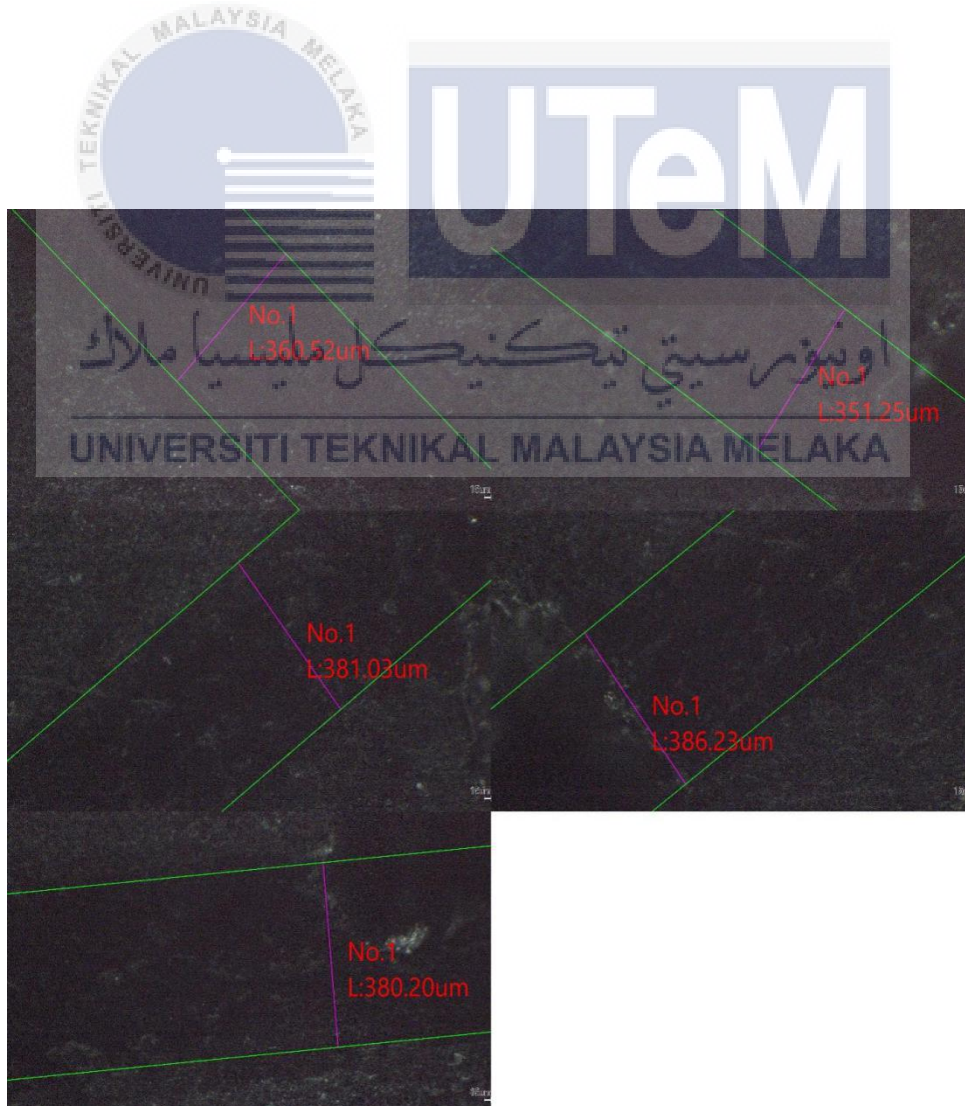
Microscopic wear track images at ball bearing and disk for textured PKAC-E disc



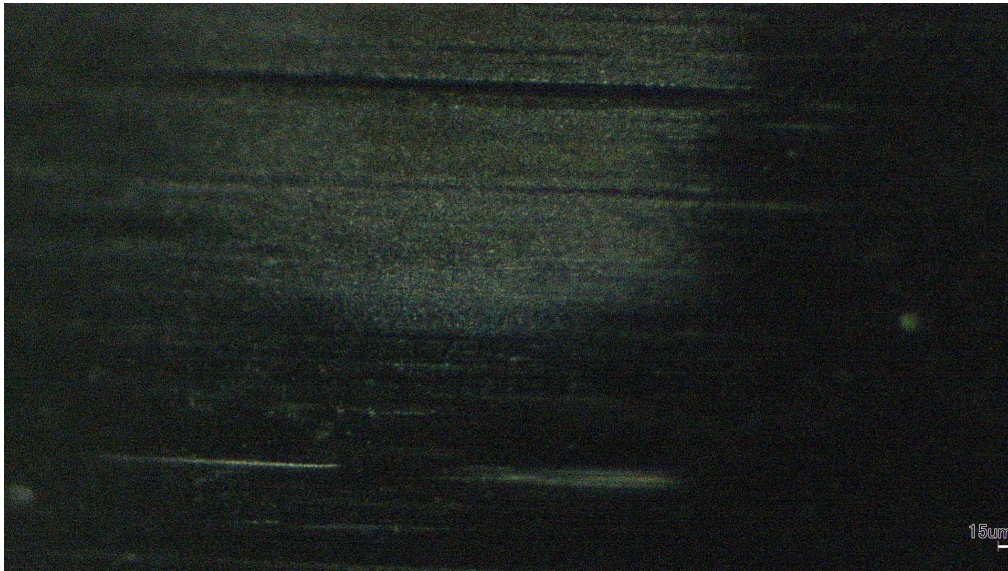
Microscopic disc wear track for textured PKAC-E disc under 5N at 200rpm



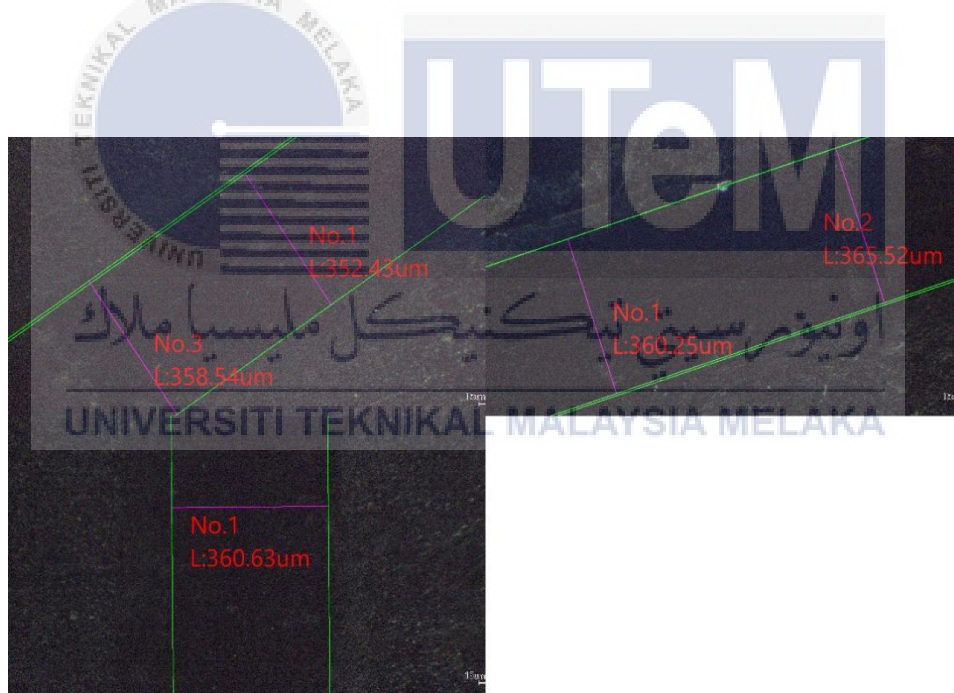
Microscopic ball bearing wear track for non-textured PKAC-E disc under 5N at 200rpm



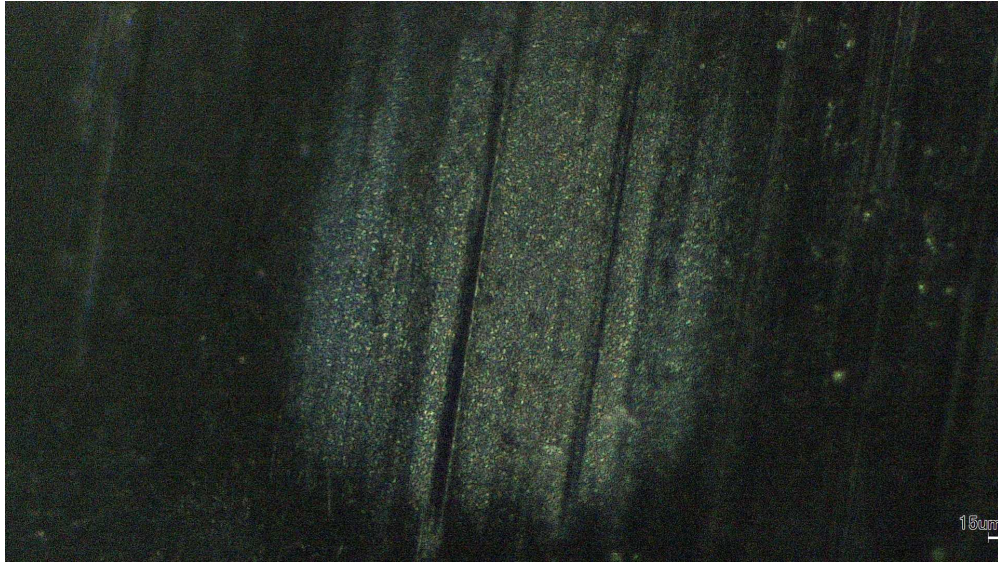
Microscopic disc wear track for textured PKAC-E disc under 5N at 150rpm



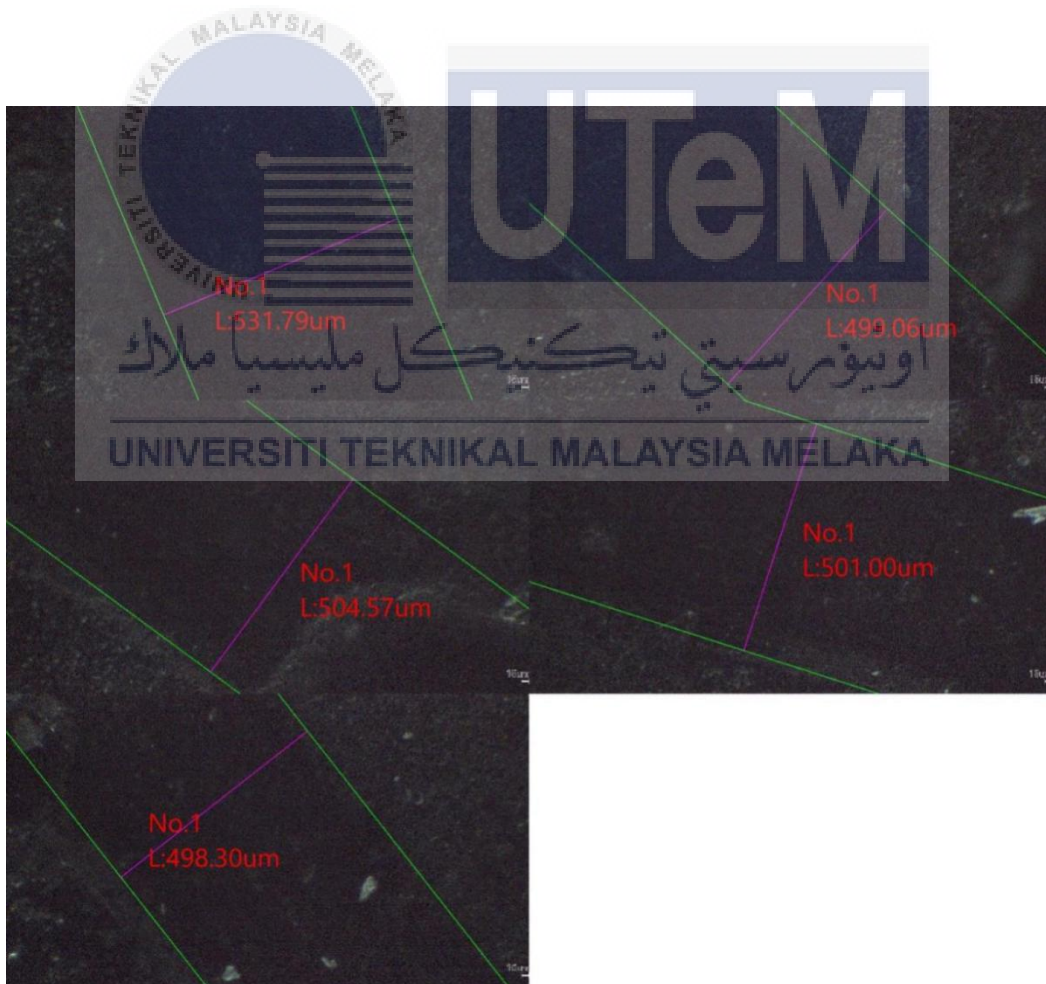
Microscopic ball bearing wear track for textured PKAC-E disc under 5N at 150rpm



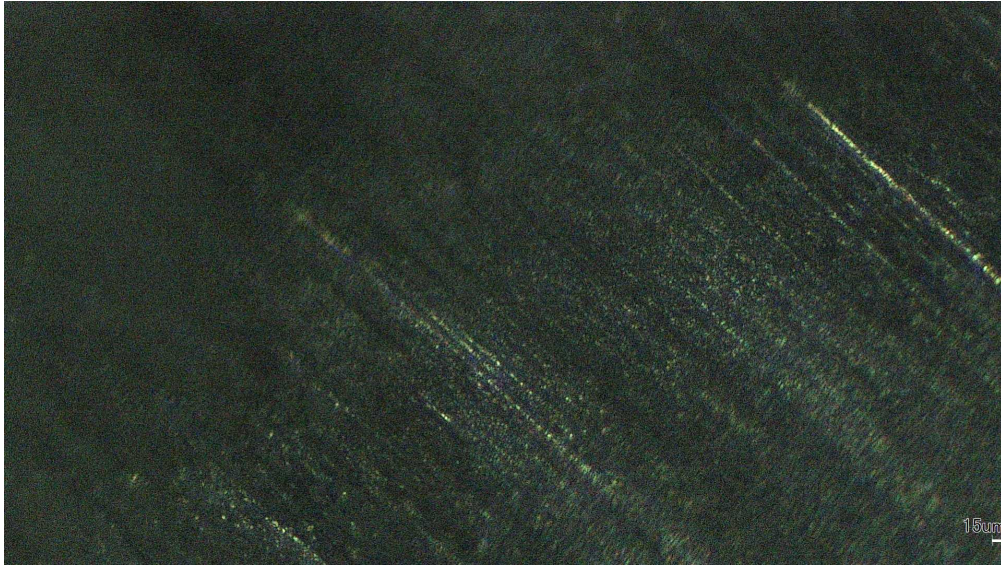
Microscopic disc wear track for textured PKAC-E disc under 5N at 100rpm



Microscopic ball bearing wear track for textured PKAC-E disc under 5N at 100rpm



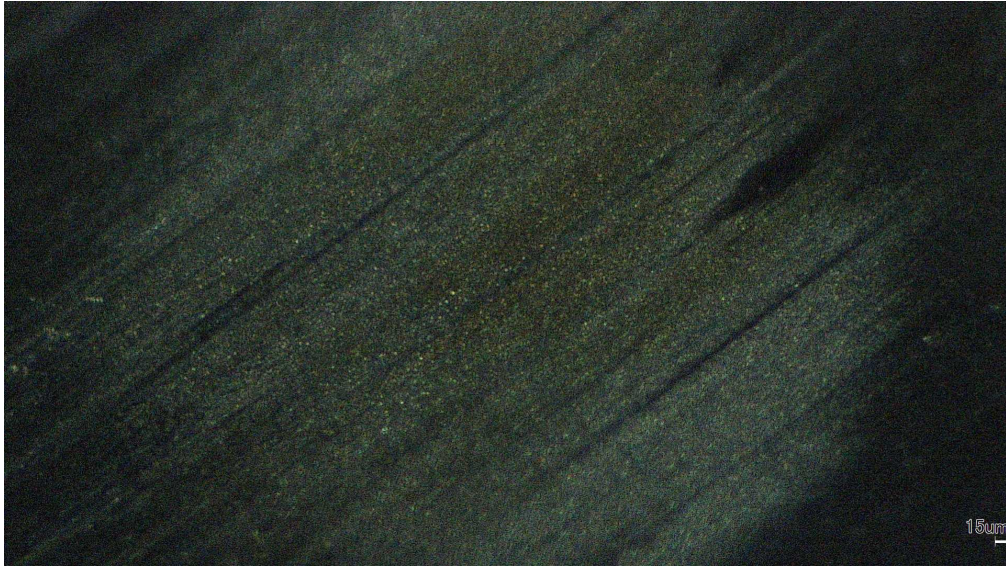
Microscopic disc wear track for textured PKAC-E disc under 10N at 200rpm



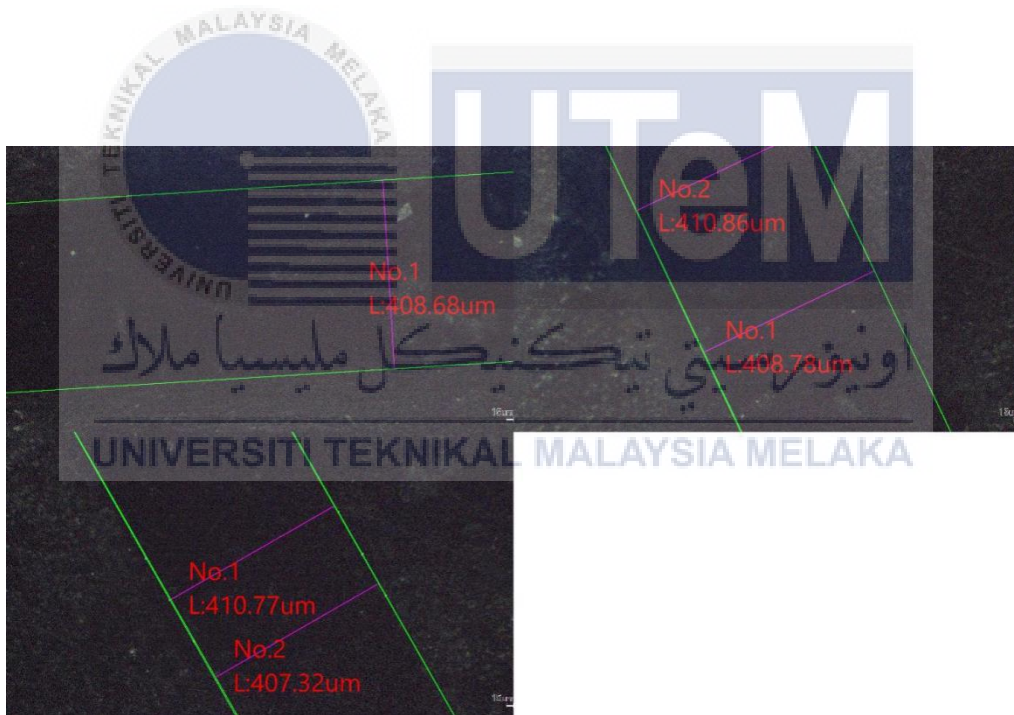
Microscopic ball bearing wear track for textured PKAC-E disc under 10N at 200rpm



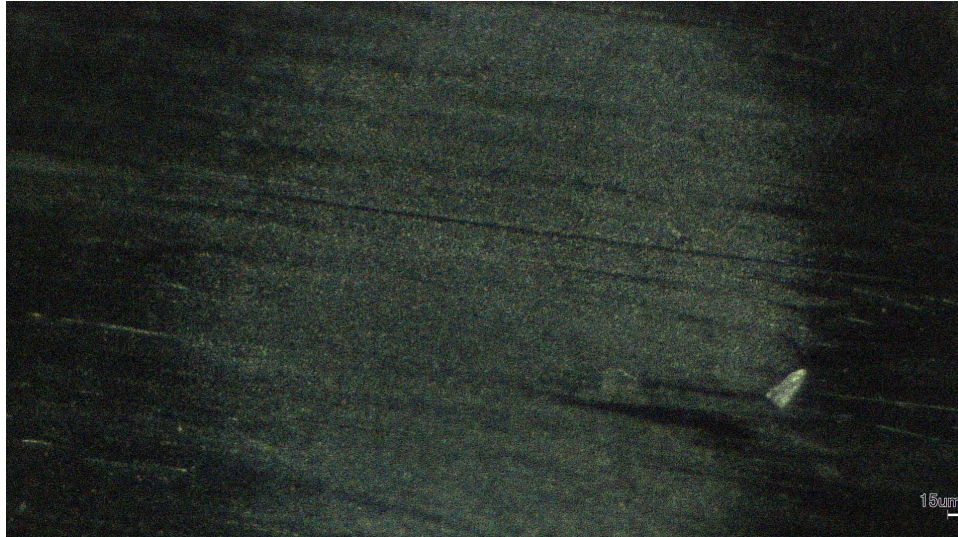
Microscopic disc wear track for textured PKAC-E disc under 10N at 150rpm



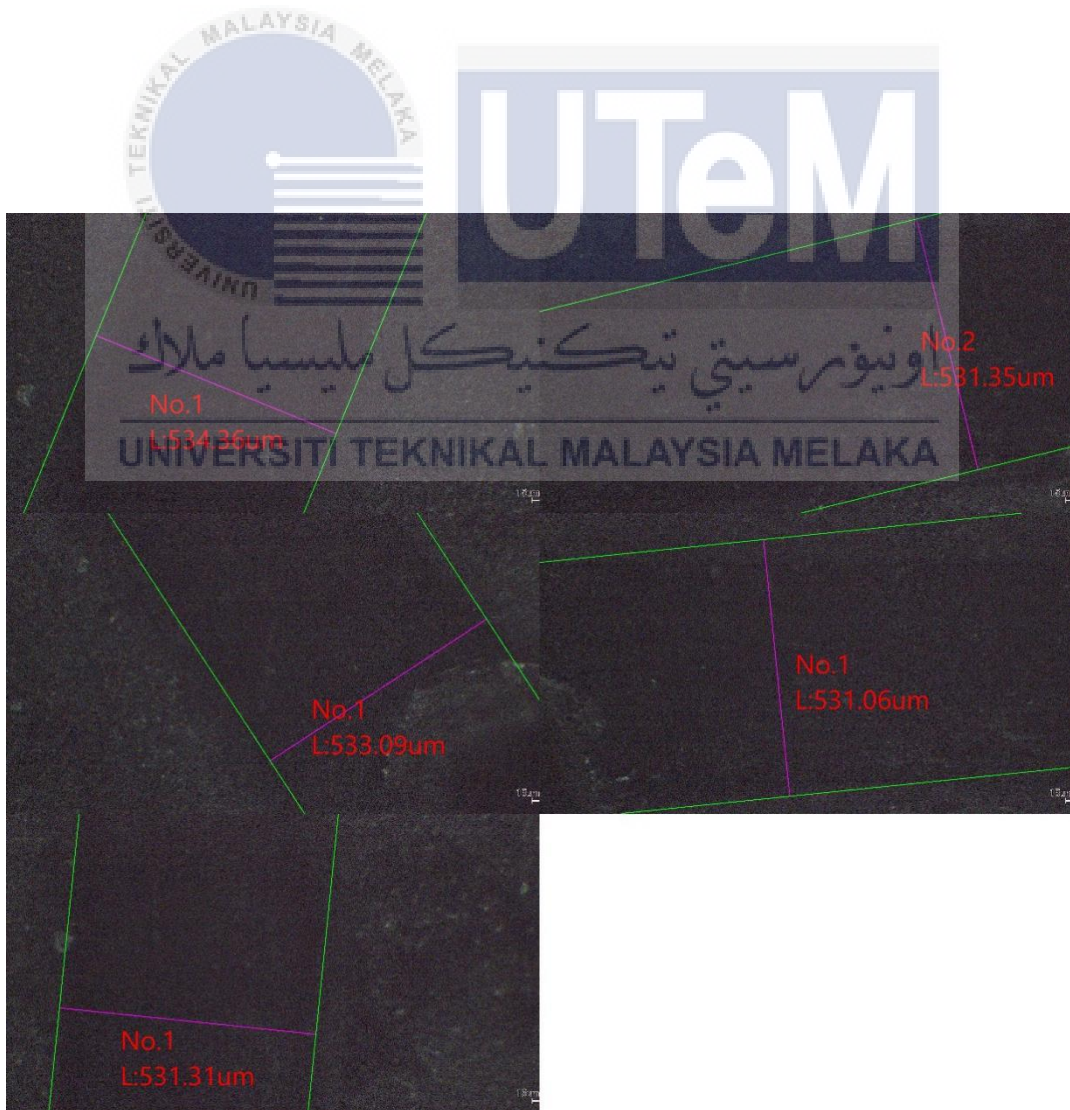
Microscopic ball bearing wear track for textured PKAC-E disc under 10N at 150rpm



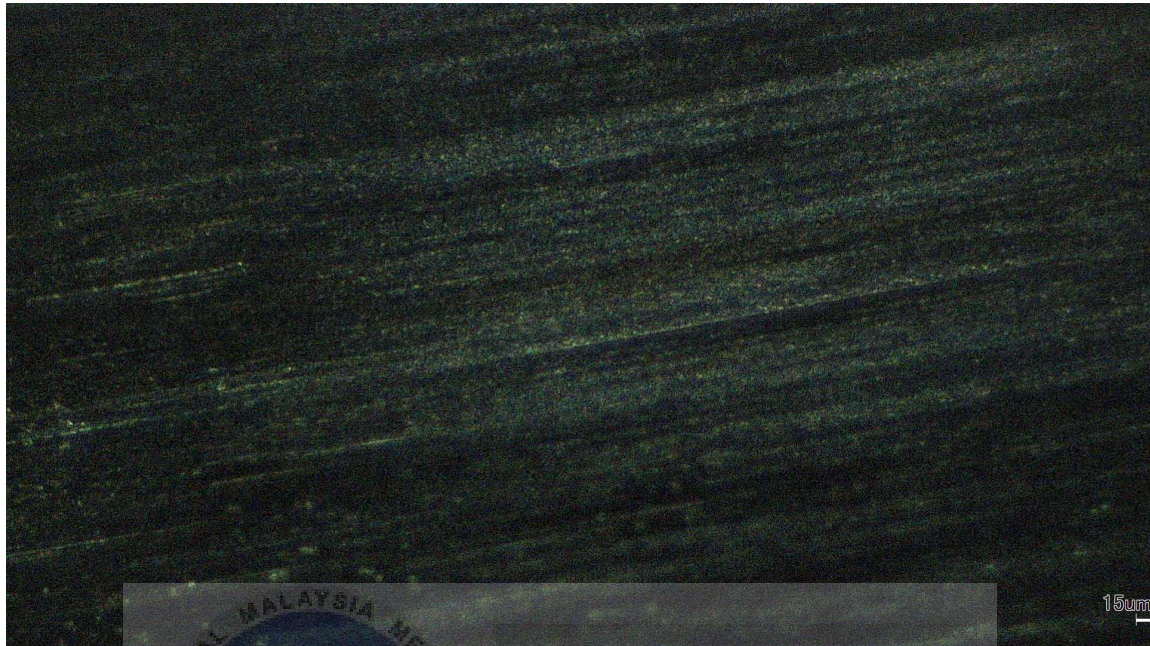
Microscopic disc wear track for textured PKAC-E disc under 10N at 100rpm



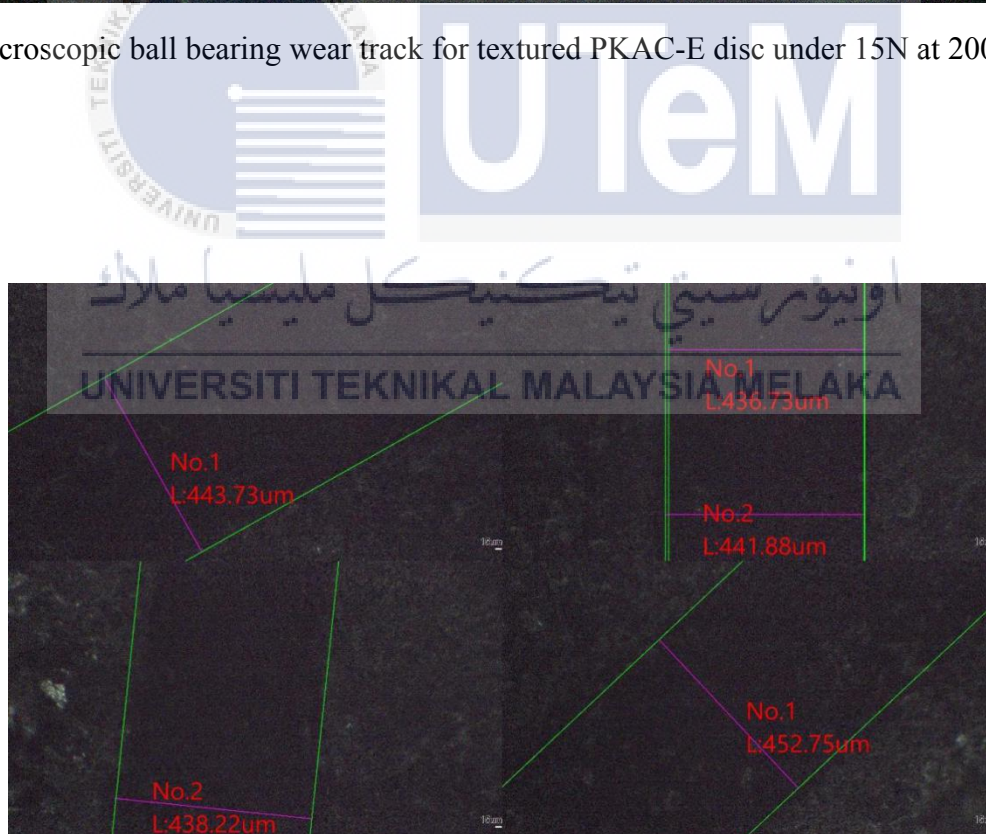
Microscopic ball bearing wear track for textured PKAC-E disc under 10N at 100rpm



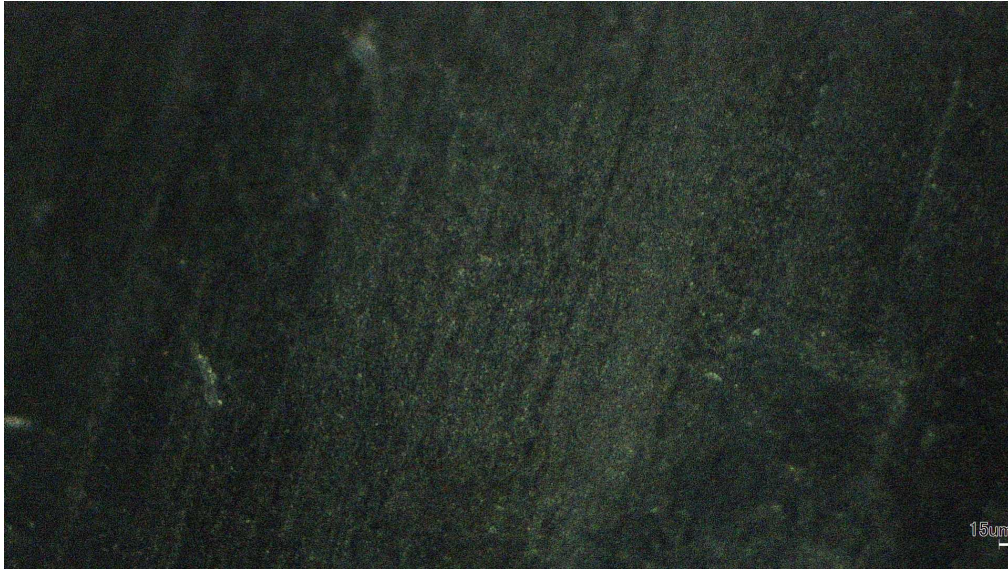
Microscopic disc wear track for textured PKAC-E disc under 15N at 200rpm



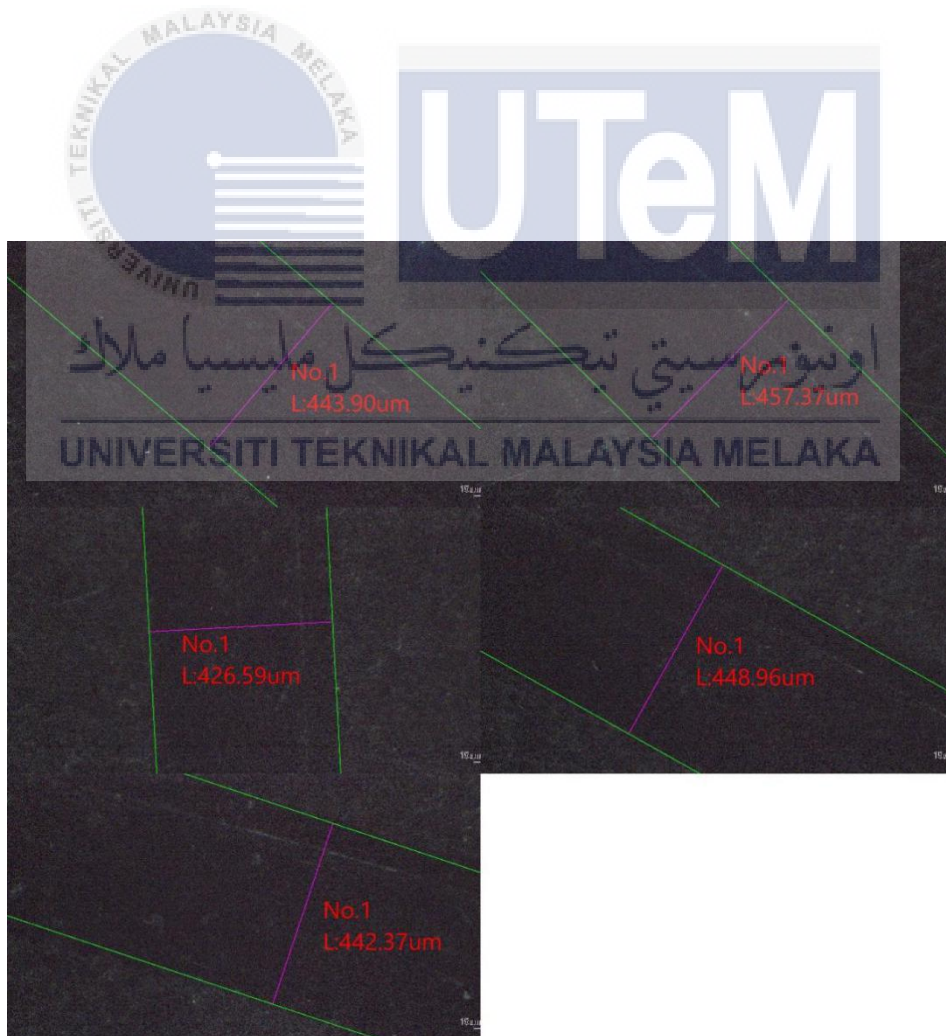
Microscopic ball bearing wear track for textured PKAC-E disc under 15N at 200rpm



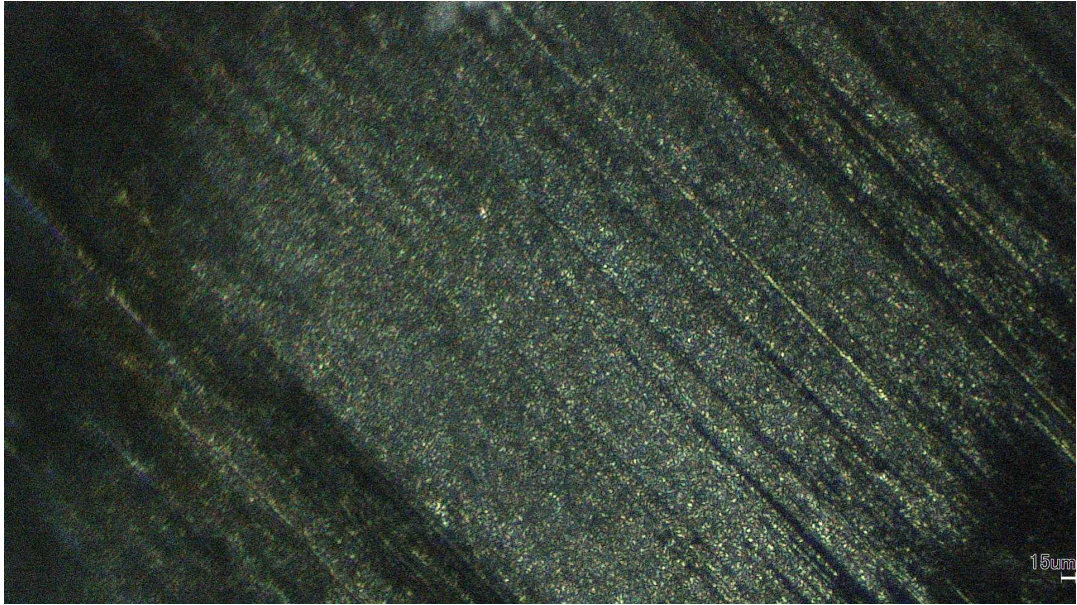
Microscopic disc wear track for textured PKAC-E disc under 15N at 150rpm



Microscopic ball bearing wear track for textured PKAC-E disc under 15N at 150rpm



Microscopic disc wear track for textured PKAC-E disc under 15N at 100rpm



Microscopic ball bearing wear track for textured PKAC-E disc under 15N at 100rpm

